AN INVESTIGATION ON THE IMPACT OF ANTENNA ARRAY GEOMETRY ON BEAMFORMING USER CAPACITY

by

Joseph Yi-Lin Chou

A thesis submitted to the
Department of Electrical and Computer Engineering
in conformity with the requirements
for the degree of Master of Science (Engineering)

Queen's University
Kingston, Ontario, Canada
March, 2002

Abstract

The world has seen explosive growth in the wireless communication area in recent years, with the number of users worldwide set to top one billion in the near future. In this ever-crowding world, wireless service providers must constantly strive to achieve greater system capacities to handle the ever-increasing demands on their systems, while keeping the infrastructure costs down. One of the ways a base station can increase the number of users it can serve is through the utilization of Space Division Multiple Access (SDMA) methods using base station antenna arrays. In this investigation we compare four antenna array geometries in a variety of scenarios in the quest to find the array geometry that maximizes the system user capacity.

We compare four array geometries in the following steps: First, we present the *power pass through factors* and the user capacity expression, which are then applied to each of the arrays for the case of known direction-of-arrival (DOA). Second, the same procedure is applied to the case where the DOA is estimated. In this case we assume that the estimated DOA is represented by an unbiased Gaussian random variable with variance given by the Cramer-Rao lower Bound. We calculate the capacity values for

the arrays using the Monte-Carlo method, which is quite time and resource intensive and limits the scope of the array comparisons. The results thus obtained show that the effect of DOA estimation on the system capacities based on the CRB is small.

Third, we modify existing perturbed output SINR expression to take correlations between the array response vector elements into account, and apply the results to system capacity calculations. This approach is orders of magnitude faster than the Monte-Carlo approach and the capacity results yielded by these two methods are found to be in close agreement. Using this approach, we consider the effects of high power interfering signals on user capacities, and we find that high DOA resolution does not imply high user capacity or superior ability to suppress interfering signals when the DOAs need to be estimated .

Acknowledgements

I would like to thank my supervisor Dr. Steven D. Blostein for his patience, guidance and support throughout the course of this research. I would also like to thank CITR and Dr. Blostein for their financial support.

I would like to thank my parents and my sister for their love, support and encouragement during my years of study here at Queen's University.

Finally, I would like to thank all my friends at IPCL, past and present, whose friendship made my day, everyday.

Contents

Abstract **ii**

Acknowledgements **iv**

1 Introduction **1**

1.1 Motivation 1

1.2 Previous Works 2

1.2.1 DOA Resolution Ability 3

1.2.2 Optimized Array Geometry 4

1.2.3 System Capacity 5

1.3 Summary of Contributions 7

1.4 Thesis Outline 8

2 Background Information **10**

2.1 Introduction 10

2.1.1 Chapter Outline 11

2.2 Wireless Communication System Overview 11

2.3 DOA Estimation Fundamentals 13

2.3.1 The Array Response Vector (ARV) 14

2.3.2 Signal Autocorrelation Matrices 15

2.3.3 Received Signal Model 16

2.3.4 Conventional DOA Estimation Methods 16

2.3.4.1 Conventional Beamforming Method 16

2.3.4.2 Capon's Minimum Variance Method 17

2.3.5 Subspace Approach to DOA Estimation 18

2.3.5.1 The MUSIC Algorithm 18

2.4 Beamforming Fundamentals 20

2.4.1 Beamforming Weight Vector and Beampattern 20

2.4.2 The Classical and the Maximum SNR Beamformer 21

2.4.3 The Multiple Sidelobe Canceller and the Maximum SINR Beamformer 22

2.5 Antenna Array Geometries 24

2.5.1 Array Aperture 24

2.5.2 Uniformly Spaced Arrays 25

2.5.3 The Golomb Array 26

2.6 Cramer Rao Lower Bound (CRB) 28

2.6.1 Vector Parameter and General Gaussian Cramer Rao Lower Bound 29

2.6.2 CRB for the Azimuth and Elevation DOA Estimates 30

2.7 Chapter Summary 31

3 Antenna Array Geometry Comparison with Known DOAs 32

3.1 Introduction 32

3.1.1 Assumptions 33

3.1.2 Chapter Outline 35

3.2 Identical Users Scenario 36

3.2.1 Radiation Patterns 37

3.2.2 Power Pass-Through Factor (PPTF) 38

3.2.3 Expected Power Pass-Through Factor Calculations 39

3.2.4 System Capacity Calculations 43

3.3 Multi-Rate Users Scenario 45

3.3.1 Radiation Patterns 46

3.3.2 Expected Power Pass-Through Factor Calculations 47

3.3.3 System Capacity Calculations 49

3.4 Chapter Summary and Discussion 53

4 Antenna Array Geometry Comparison with Estimated DOAs 56

4.1 Introduction 56

4.1.1 Chapter Outline 57

4.2 Preparatory Considerations 58

4.2.1 Variance Bounds of Directions of Arrival 59

4.2.2 Distribution of the Desired Signal Array Response Vector . . . 61

4.2.3 Effective Beampattern and User Capacity Reduction 64

4.2.4 Implications for the Beamforming Weight Vectors 67

4.3 Identical Users Scenario 69

4.3.1 Distribution of the Expected Power Pass-Through Factors and System Capacities 69

4.3.2 System Capacity Calculations 71

4.3.3 Relationship between System Capacities and the DOA Estimation Variance 75

4.4 Multi-Rate Users Scenario 76

4.4.1 Distribution of the Expected Power Pass-Through Factors and System Capacities 78

4.4.2 System Capacity Calculations 81

4.4.3 Relationship between System Capacities and the DOA Estimation Variance 83

4.5 Chapter Summary and Discussion 87

5 The Perturbed Output SINR Approach and Further Array Comparisons 89

5.1 Introduction 89

5.1.1 Chapter Outline 90

5.2 Perturbed Output SINR Due to Desired Signal ARV Perturbations . 91

5.2.1 The Uncorrelated ARV Perturbation Model 91

5.2.2 The Correlated ARV Perturbation Model 92

5.2.3 Perturbed User Capacities 96

5.2.4 Relationship between System Capacities and the DOA Estimation Variance 97

5.3 Effects of Increasing Number of High Power Interfering Signals 101

5.3.1 Capacities as Functions of the DOA 104

5.3.2 Capacities as Functions of the Number of High Power Interfering Signals 108

5.4 Chapter Summary and Discussion 111

6 Conclusions and Future Directions **115**

6.1 Summary of Thesis 115

6.2 Future Directions 118

6.3 Conclusions 121

A CRB for the Azimuth and Elevation DOA Estimates **123**

B Desired Signal ARV Error Correlation Matrix **128**

Bibliography **139**

Vita **140**

List of Tables

3.1 The mean capacities for the identical users scenario 44

3.2 The mean capacities for the Multi-Rate users scenario based on Identical-User scenario capacities 51

3.3 The iterated mean capacities for the Multi-Rate users scenario based on previous Multi-Rate user scenario capacities 51

3.4 The mean capacities for the Multi-Rate users scenario when one high power interfering signal is present, calculated at 10 degree intervals, and the capacity variations compare to the one degree interval case. . 52

3.5 The mean capacities for the Multi-Rate users scenario when two high power interfering signals are present, calculated at 10 degree intervals, and the capacity reductions compare to the one high power interfering signal case. 53

4.1 The capacities for the Identical Users scenario based on known DOA Identical Users scenario capacities 74

4.2 The iterated capacities for the Identical Users scenario based on previous Identical Users scenario capacities 74

4.3 The ratio of capacities using estimated DOAs to the capacities using known DOAs 75

4.4 The capacities for the Multi-Rate users scenario based on known DOA Multi-Rate users scenario capacities 82

4.5 The iterated capacities for the Multi-Rate users scenario based on previous Multi-Rate user scenario capacities 82

4.6 The ratio of capacities using estimated DOAs to the capacities with known DOAs, when a single high power interfering signal is present . 82

4.7 The capacities for the Multi-Rate users scenario when one high power interfering signals is present, calculated at 10 degree intervals, and the capacity variations compare to the one degree interval case 84

4.8 The capacities for the Multi-Rate users scenario when two high power interfering signals are present, calculated at 10 degree intervals, and the capacity reductions compare to the one high power interfering signal case 84

5.1 Identical-Users scenario system capacities for the four different array geometries base on perturbed output SINR expression, first for uncorrelated Equation (5.3) then for correlated ARV perturbations Equation (5.18), and compare with results from Chapter Four 98

5.2 Multi-Rate Users scenario system capacities for the four different array geometries base on perturbed output SINR expression, first for uncorrelated Equation (5.2) then for correlated ARV perturbations Equation (5.16), and compare with results from Chapter Four 99

List of Figures

2.1 Elements of a communication system 12

2.2 Array Response Vector for a Uniform Linear Array 14

2.3 Three Uniform Arrays (ULA, UCA and UTA) 27

2.4 The Golomb Array 27

3.1 Maximum SNR beam patterns for four antenna array geometries for a desired signal at 30 degrees off the reference axis 38

3.2 Expected Interference Power Pass-Through Factor vs the Desired Signal DOA for the 120/120 scenario 41

3.3 Expected Interference Power Pass-Through Factor vs the Desired Signal DOA for the 120/360 scenario 42

3.4 Expected Interference Power Pass-Through Factor vs the Desired Signal DOA for the 360/360 scenario 42

3.5 Maximum SINR beam patterns when the desired signal is at 70 degrees and the five interfering signals are at 60, 80, 100, 120 and 140 degrees off the reference x-axis 47

4.1 CRB of DOA estimation variance vs the Desired DOA 61

4.2 Real and imaginary part of the array response vector element as functions of DOA for the array element located at position (1,1) 62

4.3 Distribution of the real part of the ARV element 65

4.4 Distribution of the imaginary part of the ARV element 65

4.5 Effective beampatterns when the DOA is estimated. 66

4.6 $E[\phi^{desired}]$ histogram with true desired DOA at 60 degrees 71

4.7 $E[\phi_k^{int}]$ histogram with true desired DOA at 60 degrees 72

4.8 User Capacity histogram with true desired DOA at 60 degrees 72

4.9 Average Capacity versus DOA variance for the Identical Users scenario 120/120 case 76

4.10 Average Capacity versus DOA variance for the Identical Users scenario 120/360 case 77

4.11 Average Capacity versus DOA variance for the Identical Users scenario 360/360 case 77

4.12 $E[\phi^{desired}]$ histogram with true desired DOA at 60 degrees 79

4.13 $E[\phi_k^{int}]$ histogram with true desired DOA at 60 degrees 79

4.14 $E[\phi_{hp}^{int}]$ histogram with true desired DOA at 60 degrees 80

4.15 Capacity histogram with true desired DOA at 60 degrees 80

4.16 Average Capacity versus DOA variance for the Multi-Rate users scenario 120/120 case 85

4.17 Average Capacity versus DOA variance for the Multi-Rate users scenario 120/360 case 86

4.18 Average Capacity versus DOA variance for the Multi-Rate users scenario 360/360 case 86

5.1 Average Capacity versus DOA variance for the Identical Users scenario 120/120 case 100

5.2 Average Capacity versus DOA variance for the Identical Users scenario 120/360 case 100

5.3 Average Capacity versus DOA variance for the Identical Users scenario 360/360 case 102

5.4 Average Capacity versus DOA variance for the Multi-Rate Users scenario 120/120 case 102

5.5 Average Capacity versus DOA variance for the Multi-Rate Users scenario 120/360 case 103

5.6 Average Capacity versus DOA variance for the Multi-Rate Users scenario 360/360 case 103

5.7 Mean Capacity versus DOA for the ULA when 2, 4, 6, 8, or 10 high power interfering signals are present 105

5.8 Mean Capacity versus DOA for the Golomb Array when 2, 4, 6, 8, or 10 high power interfering signals are present 105

5.9 Mean Capacity versus DOA for the UCA when 2, 4, 6, 8, or 10 high power interfering signals are present 106

5.10 Mean Capacity versus DOA for the UTA when 2, 4, 6, 8, or 10 high power interfering signals are present 106

5.11 Capacity Variance versus DOA for the ULA when 2, 4, 6, 8, or 10 high power interfering signals are present 109

5.12 Capacity Variance versus DOA for the Golomb Array when 2, 4, 6, 8, or 10 high power interfering signals are present 109

5.13 Capacity Variance versus DOA for the UCA when 2, 4, 6, 8, or 10 high power interfering signals are present 110

5.14 Capacity Variance versus DOA for the UTA when 2, 4, 6, 8, or 10 high power interfering signals are present 110

5.15 Average Capacity versus the number of high power interfering signals, 120/120 scenario 111

5.16 Average Capacity versus the number of high power interfering signals, 120/360 scenario 112

5.17 Average Capacity versus the number of high power interfering signals, 360/360 scenario 112

Chapter 1

Introduction

1.1 Motivation

In our ever-evolving society, two general trends are evident: enabled by modern technologies, people are enjoying greater freedom of movement than ever before; and in the information age, people are more reliant on timely information than ever before. As a result, more and more people demand ready information access on the move, requiring mobile communication systems of ever greater data rates and user capacities.

Based on the open literature, there are four schemes for which the base station can use to improve user capacity: time division multiple access (TDMA), frequency division multiple access (FDMA), code division multiple access (CDMA) and space division multiple access (SDMA). Modern systems often employ a combination of these schemes to optimize performance. The first three techniques of improving communication system capacity have been extensively studied in recent years [27] [58]

[42] [43] [3] [5]; in this thesis, our focus is on the spatial processing aspect of modern mobile communication systems.

Spatial signal processing techniques can be applied at both the mobile user and the base station, allowing the mobile transceiver to distinguish various base stations or allowing the base stations to distinguish various mobile users. Due to limitations on physical dimensions, current mobile user transceivers usually do not employ multi-element antenna arrays, thus their spatial processing potential is limited. The base stations, on the other hand, are able to employ large multi-element antenna arrays and have much greater system improvement potential using spatial processing.

One important aspect of designing a mobile communication system which utilizes an antenna array at the base station is finding the array geometry that provide the largest system capacity while satisfying the system requirements. While there have been some investigations into the area of antenna array geometry comparisons [8] [14] [4] [1] [9] [18] [59], all of them have focused on the resolution ability of the arrays and none have considered the impacts on user capacities. Thus in this thesis, we focus our efforts on the system user capacity comparisons between different array geometries in modern mobile communication scenarios.

1.2 Previous Works

In this thesis we compare the system user capacities for four different base station antenna array geometries. In this section, we outline the results obtained by other

researchers in the following related areas of our research: *DOA Resolution Ability*, *Optimized Array Geometry* and *System Capacity*.

1.2.1 DOA Resolution Ability

The resolution properties of antenna arrays have been extensively investigated by many researchers. The area of research that we are interested in is the derivation of Direction-of-Arrival (DOA) estimation performance bounds for any given array geometry.

The theoretical performance bound studies are concerned mostly with the derivation of the Cramer Rao Lower Bound (CRB) for DOA estimation variance given an arbitrary antenna array geometry. In the studies by Messer et al [37] as well as Mirkin and Sibul [38], CRB expressions for azimuth and elevation angle estimates of a single source using arbitrary two-dimensional array geometries are derived.

In Nielsen [39] as well as Goldberg and Messer [20], single source DOA estimation CRB expressions are derived for antenna arrays of arbitrary three-dimensional geometries. In Dogandzic and Nehorai [14], CRB expressions are derived for the range, velocity and DOA estimates of a single signal source when arbitrary 3-D antenna array geometries are used, and it was shown that the CRBs only depend on the "moment of inertia" of the array geometry.

Further more, in Ballance and Jaffer [6], and Bhuyan and Schultheiss [7], CRB expressions are derived for the case where there are two signal sources in the system.

No result for systems with three or more signal sources can be found in the published literature so far.

1.2.2 Optimized Array Geometry

The next logical step in the studies of different array geometries is the optimization of antenna array element locations for given performance requirements. There have been several studies in this area, and they are all concerned with the optimization of array geometry for signal DOA resolution, often obtained through the minimization of the Cramer-Rao Lower Bound on the DOA estimate.

Earlier studies concentrated on linear arrays, comparing the uniform linear array to non-uniform linear arrays. A representative study is the paper by Vertatschitsch and Haykin [59], in which linear arrays of several types are compared based on their CRB, and it was found that while the sparse arrays achieve higher resolution than linear arrays, they require higher SNR values for the same outlier probability. The outlier probability is defined as the probability of an estimation error greater than the beamwidth of the array, which is the probability that the desired signal will fall outside the main beam of the beampattern due to DOA estimation error.

Later studies also investigated optimization of non-linear array element locations. In Preetham and Branner [44], an optimizing method for circular arrays based on minimum redundancy array results is shown. In Abramovich and Spencer [1], a geometry optimizing technique that yields accurate DOA estimations of arbitrarily

correlated signal sources without compromising identifiability is presented.

In Chambers et al [8], the general expression relating the array element positions and the CRB of the DOA estimates is derived, and it is found that the resolving ability of an array has an expression dominated by the fourth central moment of the array element locations, irrespective to the array aperture or the number of sensor elements. In Dogandzic and Nehorai [14], the parameter estimation abilities of several array geometries are compared based on their "moment of inertia" expressions.

An interesting and different approach to the optimization of array geometries for any given parameter is through the use of genetic algorithms. The main advantage of this approach is the parallel search capability of the genetic algorithm. In Ang, See and Kot [4], genetic algorithms are employed to find the array geometry with the lowest CRB.

1.2.3 System Capacity

In practical wireless communication systems, the main challenge of designing a base station system is to increase the capacity of the system rather than pin-pointing the locations of individual users. Existing system capacity studies can be separated into three groups, each dealing with a different concept of *capacity* for a wireless communication system.

The first concept of capacity is the information theoretic *Channel Capacity* defined by Shannon [51], [52]. This capacity is the maximum information transfer possible

in the system and it has the units of *bits/sec*. For practical systems, especially packet based communication systems, the attained system capacity or *information throughput* is usually presented in units of *bits/sec/Hz*.

The second concept of capacity is the *Static User Capacity*. It is the number of users that can be supported by the wireless system simultaneously in the steady-state, given specific performance requirements for each of the users. In the paper by Gilhousen et al [19] and later on in the book by Viterbi [58], the static user capacity for a CDMA system is derived and discussed.

The third concept of capacity is the *Dynamic User Capacity*. This capacity is the maximum number of users that can expect to be supported by a wireless communication system given the usage patterns of users. The usage pattern parameters include the service request rate, service re-request model, user exiting rate, as well as user uplink/downlink data transfer patterns. This capacity is usually referred to as the *Erlang Capacity* [58].

In this thesis, we make the assumption that we are considering circuit-switched traffic as opposed to packet-switched traffic. We also assume that we are not considering dynamic behaviors of users in wireless communication systems. Thus in this thesis, references to *Capacity* mean the *Static User Capacity*

1.3 Summary of Contributions

The main contributions of our investigation as presented in this thesis to the study of optimizing base station antenna array geometry for a wireless beamforming system are:

- We identify and bridge the gap between published investigations on optimizing antenna array geometry for DOA resolution and the requirement for greater capacity for practical systems.
- We incorporate the effects of intrinsic limitations on DOA estimation in the calculations and comparisons of capacities, enabling algorithm-independent comparisons between four common antenna array geometries.
- We take emerging usage patterns into account by considering the effects of different data rates and interfering signal source distributions on the capacities through the calculations of the *Expected Power Pass-Through Factors*.
- We derive the perturbed output SINR expression given correlated ARV perturbations and apply the results to system capacity calculations.
- We consider the effects of increasing DOA estimation error and increasing number of high power interfering signals on the user capacities for different arrays.

1.4 Thesis Outline

This thesis has six chapters. In the first chapter we state the motivations of this investigation, present the previous works by other researchers in related areas, summarize the contributions of this investigation and outline the structure of this thesis.

In the second chapter we present the background information necessary for our investigation, including an overview of the wireless communication system structure, DOA estimation techniques, fundamentals of antenna signal processing, as well as the DOA estimation Cramer-Rao Lower Bound expression for arbitrary array geometries.

In the third chapter we compare the system user capacities for four antenna array geometries, with the assumption that the desired and interfering signal directions-of-arrival are known. User capacities for the arrays in different scenarios are calculated and compared.

In the fourth chapter we again compare the user capacities for the four arrays, but this time we take DOA estimation into account, and make the assumption that the estimated DOA is an unbiased Gaussian random variable with variance given by the DOA estimation Cramer-Rao Lower Bound.

In the fifth chapter, we derive the perturbed output SINR expression, taking into account the correlations between the perturbed array response vector elements. We compare this result to the uncorrelated case as well as the values obtained in Chapter

Four. We also consider the effect of increasing number of high power interfering signals on the system capacities for the arrays.

Finally in the sixth chapter, we summarize the results obtained in this investigation, indicate possible future research directions in this area, and outline the major conclusions drawn from the results.

Chapter 2

Background Information

2.1 Introduction

The rapidly expanding mobile communications market puts great demands on the current wireless communications infrastructure. Each base station is required to service a large number of users, facilitated by various signal processing techniques. As mentioned in the last chapter, we will concentrate our effort on the spatial aspect of signal processing for a mobile communication system. Before we present our investigations, we first provide the background information on several key areas of antenna signal processing.

2.1.1 Chapter Outline

In this chapter, background information on several aspects of antenna signal processing is provided. First we present an overview of the wireless communication system structure. Second we discuss direction-of-arrival estimation techniques. Third we introduce the fundamentals of antenna signal processing. Then we describe the different antenna geometries under investigation in this thesis. Finally, we outline the DOA estimation Cramer-Rao Lower Bound expression for arbitrary array geometries. In this thesis, we do not consider mobile communication channel impairments such as multi-path fading or scattering, nor do we consider mutual coupling effects, as they have been considered elsewhere [45] [60].

2.2 Wireless Communication System Overview

Virtually all communication systems have the same fundamental goal: to pass along the most information with the least errors; modern digital wireless communication systems are no exception. In order to accomplish these objectives, digital wireless communication systems can usually be separated into several elements as indicated by Figure (2.1).

Given any digital input, the source encoder gets rid of redundancy in the information bits, thus maximizing the amount of useful information transferred in the communication system. The output of the source encoder is then processed by the

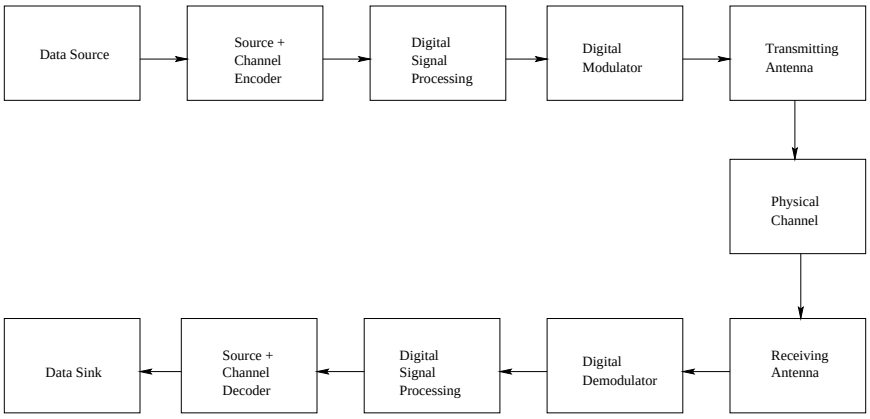

Figure 2.1: Elements of a communication system

channel encoder, which incorporate error control information in the data to minimize the probability of error.

The output of the channel encoder is then processed by further digital signal processing, in order to allow simultaneous communication of many users. An example of this would be digital beamforming, which by using the geometric properties of the antenna array, is able to concentrate the signal powers for different users in different desired directions, allowing more users to be served by the system.

The output is then processed by the modulator, which shifts the baseband signal at the input of the modulator into the band-pass version at the output, due to the bandwidth constraint of the communication system. The output of the modulator is then fed to the transmitter antenna or antenna array, which transmits the signals into the physical wireless channel.

On the other end of the physical channel is the receiver antenna or antenna array,

and the whole process is the reverse of that on the transmitting end. First the demodulator down-shifts the received band-pass signal into its baseband equivalent, then digital signal processing separates the different signals that are coming from different users. Channel decoder detects and corrects, if possible, errors that are caused by the effects of the physical channel; source decoder then restores the information bits from the compressed version, resulting in information bits that are identical to the ones that went into the transmitting end of the communication system.

As mentioned in the last chapter, we will focus on the spatial processing aspect of the wireless communication system in this thesis. Specifically, we will focus on the uplink base-station spatial processing of a mobile communication system, which is part of the receiver digital signal processing block in the Figure (2.1). In the next few sections, we will review relevant background information.

2.3 DOA Estimation Fundamentals

In this section we will discuss the received signal model and the DOA estimation algorithms, which can be separated into two groups, the *conventional* algorithms and the *subspace* algorithms. But before that, we introduce the concepts of *array response vectors* and *signal auto-correlation matrix*.

2.3.1 The Array Response Vector (ARV)

Assuming that the antenna array is composed of identical omni-directional elements, we can see that each element receives a time-delayed version of the same plane wave. In other words, each element receives a phase-shifted version of the signal. For instance with a uniform linear array, the relative phases are also uniformly spaced.

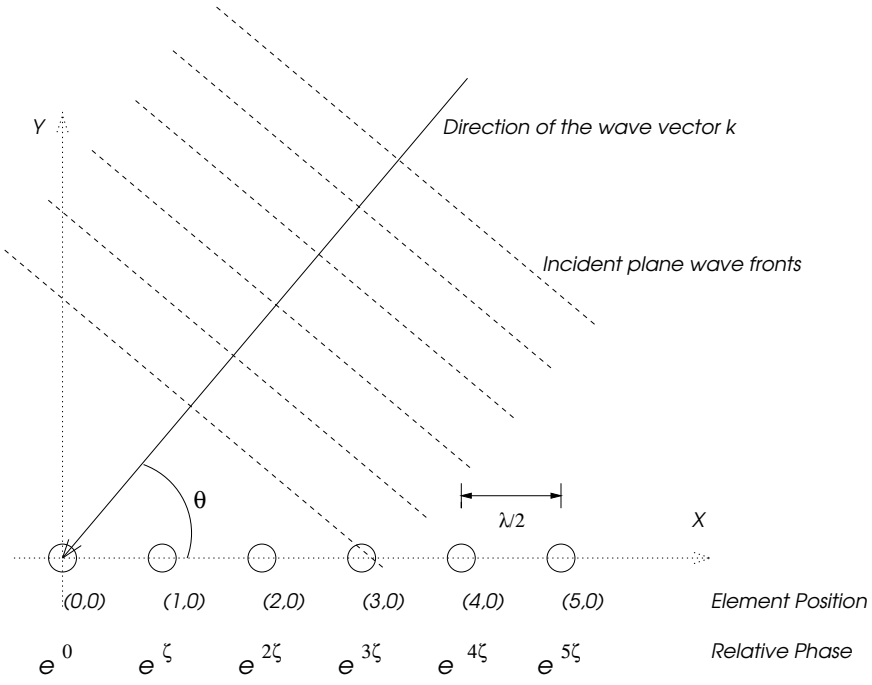

Figure 2.2: Array Response Vector for a Uniform Linear Array

The vector of relative phases is referred to as the *Steering Vector*. For arrays of identical omni-directional elements, the steering vector is also referred to as the *Array Response Vector*. In general, the array response vector is the response of the array to the incident plane wave, it is a combination of the steering vector and the responses of each individual element to the incident wave. The set of array response

vectors corresponding to all possible directions of arrival are referred to as the *Array Manifold*, which exists in N-dimensional space, N being the number of elements in the array. The generalized steering vector expression for a three dimensional array is:

$$\mathbf{a}(\theta, \phi) = [e^{-j\mathbf{k}^T\mathbf{x}_1} e^{-j\mathbf{k}^T\mathbf{x}_2} ... e^{-j\mathbf{k}^T\mathbf{x}_N}]^T \tag{2.1}$$

where N is the number of antenna elements, $\mathbf{k}$ is the vector wave number of the incident plane wave, $\mathbf{x}_i = [x_i, y_i, z_i]^T$ is the three dimensional coordinates of the i-th element in the array and θ, ϕ are the azimuth and elevation angles respectively.

2.3.2 Signal Autocorrelation Matrices

There has been extensive research in the area of DOA estimation, and in the following subsections we outline two important approaches to this problem: the conventional methods and the subspace methods. But before we discuss the algorithms, we first need to define two commonly used terms: the received signal autocorrelation matrix $\mathbf{R}_{xx}$ and the desired signal autocorrelation matrix $\mathbf{R}_{ss}$.

$$\begin{aligned} \mathbf{R}_{xx} &= E[\mathbf{x}(t)\mathbf{x}^H(t)] \\ \mathbf{R}_{ss} &= E[\mathbf{s}(t)\mathbf{s}^H(t)] \end{aligned} \tag{2.2}$$

where $\mathbf{x}$(t) is the complex baseband equivalent received signal vector at the antenna array, $\mathbf{s}$(t) is the desired signal portion of $\mathbf{x}$(t), H denotes the Hermitian transpose and E[z] is the expectation operator of argument z. In reality, the expected value cannot be obtained exactly; and estimates, such as the time average over a finite time interval, must be used.

2.3.3 Received Signal Model

The well-established narrow-band superposition model for the received signal, where the signals from all signal sources and noise are added linearly to form the received signal, can be represented as:

$$\mathbf{x}(t) = \mathbf{A}(\underline{\theta})\mathbf{s}(t) + \mathbf{n}(t) \tag{2.3}$$

where $\mathbf{x}(t)$ is the received signal vector at time t, $\mathbf{A}(\underline{\theta})$ is the array response vector matrix where each column represent the array response vector of a signal source, $\underline{\theta}$ is the vector of all DOAs, $\mathbf{s}(t)$ is the vector of the incoming plane waves from each signal source at time t and $\mathbf{n}(t)$ is the additive white Gaussian noise.

2.3.4 Conventional DOA Estimation Methods

Two methods are usually classified as conventional methods: *Conventional Beamforming Method* and *Capon's Minimum Variance Method* [31].

2.3.4.1 Conventional Beamforming Method

The conventional beamforming method is also referred to as the Delay-and-Sum method. The idea is to scan across the field of interest, and whichever direction produces the largest output power is the estimate of the desired signal's direction. More specifically, as the angle α is varied incrementally across the field of interest,

the array response vector $\mathbf{a}(\alpha)$ is computed and the output power of the beamformer is:

$$\mathbf{P}_{CBF}(\alpha) = \mathbf{a}^H(\alpha)\mathbf{R}_{xx}\mathbf{a}(\alpha) \tag{2.4}$$

this quantity is also referred to as the *Spatial Spectrum* and the estimate of the true direction of arrival is the angle α that corresponds to the peak value in the spatial spectrum.

This method has some obvious weaknesses, one of which is resolution. An array with only a few elements will not be able to form narrow beams and hence would not be able to resolve sources that are close to one another.

2.3.4.2 Capon's Minimum Variance Method

The Capon's minimum variance method is an attempt to solve the resolution problem of the conventional beamformer. In this method, the output power is minimized with the constraint that the gain in the desired direction remains unity. Solving this constrained optimization problem for the weight vector [31] [49]:

$$\mathbf{w} = \frac{\mathbf{R}_{xx}^{-1}\mathbf{a}(\alpha)}{\mathbf{a}^H(\alpha)\mathbf{R}_{xx}^{-1}\mathbf{a}(\alpha)} \tag{2.5}$$

and this gives the *Capon's Spatial Spectrum*:

$$\mathbf{P}_{Capon}(\alpha) = \mathbf{w}^H\mathbf{R}_{xx}\mathbf{w} = \frac{1}{\mathbf{a}^H(\alpha)\mathbf{R}_{xx}^{-1}\mathbf{a}(\alpha)} \tag{2.6}$$

again, the estimate of the true direction of arrival is the angle α that corresponds to the peak value in this spectrum.

2.3.5 Subspace Approach to DOA Estimation

The other main group of DOA estimation algorithms are called the subspace methods. Geometrically, the received signal vectors form the received signal vector space whose number of dimensions equal to the number of array elements N . The received signal vector space can be separated into two parts: the signal subspace and the noise subspace. The signal subspace is the subspace spanned by the columns of $\mathbf{A}(\underline{\theta})$ [41], and the subspace orthogonal to the signal subspace is known as the noise subspace. The subspace algorithms, including the MUSIC algorithm [50], exploit this orthogonality to estimate signal DOAs.

2.3.5.1 The MUSIC Algorithm

The MUtiple SIgnal Classification (MUSIC) algorithm [50] [49] is developed by Schmidt by noting that the desired signal array response vector is orthogonal to the noise subspace. The signal and noise subspaces are first identified using eigen-decomposition of the received signal covariance matrix, then the *MUSIC spatial spectrum* is computed, from which the DOAs are estimated.

The signal and noise subspaces are formed by the span of the eigenvectors of the received signal covariance matrix, and they can by separated by the values of their corresponding eigenvalues. The received signal covariance matrix is expressed as:

$$\mathbf{R}_{xx} = E[\mathbf{x}(t)\mathbf{x}^H(t)] = \mathbf{A}(\underline{\theta})E[\mathbf{s}(t)\mathbf{s}^H(t)]\mathbf{A}^H(\underline{\theta}) + E[\mathbf{n}(t)\mathbf{n}^H(t)] = \mathbf{A}\mathbf{R}_{ss}\mathbf{A}^H + \sigma_n^2\mathbf{I} \tag{2.7}$$

where $\mathbf{R}_{ss} = E[\mathbf{s}(t)\mathbf{s}^H(t)]$ is the desired signal covariance matrix.

Eigen-decomposition of $\mathbf{R}_{xx}$ will give the eigenvalues λ_i such that $\lambda_1 > \lambda_2 > ... > \lambda_k > \lambda_{k+1} = ... = \lambda_N = \sigma_n^2$, where k is the number of signal sources and N is the number of array elements. The corresponding eigenvectors can be grouped as $E_s = [e_1 e_2 ... e_k]$ and $E_n = [e_{k+1} ... e_N]$, which spans the signal subspace and noise subspace, respectively. The procedure of the MUSIC algorithm assumes that the number of signal sources is less than the number of antenna elements.

Once the subspaces are determined, the DOAs of desired signals can be estimated by calculating the MUSIC spatial spectrum over the region of interest [41]:

$$\mathbf{R}_{music}(\alpha) = \frac{\mathbf{a}^H(\alpha)\mathbf{a}(\alpha)}{\mathbf{a}^H(\alpha)\mathbf{E}_n\mathbf{E}_n^H\mathbf{a}(\alpha)} \tag{2.8}$$

Note the $\mathbf{a}(\alpha)s$ are the array response vectors calculated for all angles α within the range of interest, whereas the $\mathbf{a}(\theta)s$ are the array response vectors for the signal sources. Because the desired array response vectors $\mathbf{a}(\underline{\theta})$ are orthogonal to the noise subspace, the peaks in the MUSIC spatial spectrum represent the DOA estimates for the desired signals.

Due to the imperfections in the estimation of $\mathbf{R}_{xx}$, the noise subspace eigenvalues will not be exactly equal to σ_n^2. They do, however, form a group around the value σ_n^2, and can be distinguished from the signal subspace eigenvalues. Note that the separation will become more pronounced as the number of samples used in the estimation of $\mathbf{R}_{xx}$ increases.

There are other techniques similar to the ones we have introduced here, for instance the cyclic-MUSIC, ESPRIT, and extensions of MUSIC such as the Spatial Smoothing technique as discussed by Schell and Gardner [49] and Paulraj et al [41], but they are beyond the scope of this introduction.

2.4 Beamforming Fundamentals

With the direction of the desired signal known or estimated, the next step is to use a spatial signal processing technique to improve the reception performance of the receiving antenna array base on this information. Some of these spatial processing techniques are referred to as *Beamforming* because they can be seen as techniques to form beams in the beampattern in the direction of the desired signal. In this section we will look at four beamformers: the classical beamformer, the maximum SNR beamformer, the multiple sidelobe canceller (MSC) and the maximum SINR beamformer. But first, we define the terms *beamforming weight vector* and *beampattern*.

2.4.1 Beamforming Weight Vector and Beampattern

As mentioned before, a beamformer is a spatial signal processor that produces an output with an emphasized desired signal compare to the input, which is the received signal at the array elements. It accomplishes this by applying a complex *beamforming*

weight vector $\mathbf{w} = [w_1 w_2 ... w_N]^T$ to the input signal vector:

$$y(k) = \sum_{i=1}^{N} w_i x_i(k) \tag{2.9}$$

where i is the array element index and k is the time index of the received signal sample being considered. Different beamformers are devised to satisfy different constraints and thus use different beamforming weights.

With the beamforming weight vector $\mathbf{w}$ calculated, the magnitude square of the beamformer response $r(\alpha) = \mathbf{w}^H \mathbf{a}(\alpha)$ for all directions can be computed and plotted; this plot is referred to as the *beampattern* or the *radiation pattern*. Normally this pattern will show a main beam in the direction of the desired signal; and if the interference signals are considered, the beamformer may form nulls in those directions.

2.4.2 The Classical and the Maximum SNR Beamformer

In classical beamforming, the beamforming weight is set to be equal to the array response vector of the desired signal. Because all elements of the beamforming weight vector are pure phase shifts with magnitude one, it is also referred to as the *phased array*. This beamforming weight vector produces a beampattern with the main beam in the desired signal direction and some sidelobes in others.

An extension of the classical beamformer is the Maximum SNR beamformer. The Maximum *Signal power to Noise power Ratio* (SNR) beamformer uses the weight vector with the expression $\mathbf{w}_{maxSNR} = \mathbf{R}_n^{-1} \mathbf{a}(\underline{\theta})$, where $\mathbf{R}_n$ is the noise covariance matrix.

This beamforming weight vector gives the output with the maximum SNR when the noise covariance matrix is known, and is equivalent to the classical beamformer when the noise covariance matrix is a multiple of $\mathbf{I}$, the identity matrix.

Although these beamformers work reasonably well in a single-source scenario, they clearly cannot deal with interference sources in a satisfactory fashion, since only the desired signal direction is taken into account when calculating the beamformer weight vector.

2.4.3 The Multiple Sidelobe Canceller and the Maximum SINR Beamformer

When there is more than one user in the communication system, we often would like to suppress the interfering signals in addition to noise using signal processing. There are some intuitive methods to accomplish this, for example, the *Multiple Sidelobe Canceller* (MSC) [57]. The basic idea of the MSC is as follows: calculate the conventional beamforming weight vectors for each of the signal sources, then the final beamforming weight vector is the linear combination of the conventional beamforming weight vectors such that the interference components are eliminated.

This method has some limitations. For instance, when the number of interfering signals is large, this beamformer cannot cancel all of them adequately, and can result in significant gain for the noise component [57]. The solution to these limitations is a statistically optimal maximum SINR beamformer which maximizes the output signal

to interference and noise power ratio.

Recall that the output vector of the beamformer is $\mathbf{y} = \mathbf{w}^H\mathbf{x} = \mathbf{w}^H(\mathbf{s} + \mathbf{i} + \mathbf{n})$, where $\mathbf{s}$ is the desired component, $\mathbf{i}$ is the interference component and $\mathbf{n}$ is the noise component of the baseband received signal vector. Based on that, the output SINR expression is:

$$SINR = \frac{\mathbf{w}^H E[\mathbf{s}\mathbf{s}^H]\mathbf{w}}{\mathbf{w}^H E[|\mathbf{i} + \mathbf{n}|^2]\mathbf{w}} = \frac{\mathbf{w}^H \mathbf{R}_{ss}\mathbf{w}}{\mathbf{w}^H \mathbf{Q}_{in}\mathbf{w}} \tag{2.10}$$

where $\mathbf{Q}_{in} = E[|\mathbf{i} + \mathbf{n}|^2]$ is the interference-plus-noise covariance matrix.

With appropriate factorisation of $\mathbf{Q}_{in}$ and manipulation of the SINR expression, the maximization problem can be recognized as an eigen-decomposition problem. The expression for $\mathbf{w}$ that would maximize the SINR is found to be [53]:

$$\mathbf{w}_{maxSINR} = \mathbf{Q}_{in}^{-1}\mathbf{a}(\underline{\theta}) \tag{2.11}$$

This is the statistical optimal solution in maximizing the output SINR in an interference plus noise environment, but it requires the computationally-intensive inversion of $\mathbf{Q}_{in}$, which may be problematic when the number of elements in the antenna array is large.

There are other beamforming approaches, for instance the *Linearly Constrained Minimum Variance* beamforming and adaptive beamforming methods [57], but they are beyond the scope of our discussion here.

2.5 Antenna Array Geometries

In this section we describe the different array geometries that will be investigated in this thesis. But before we present them, we need to be familiar with the concept of *array aperture*.

2.5.1 Array Aperture

Array aperture is the size of the array, it determines the maximum array gain achievable - the theoretical maximum array gain is proportional to the array aperture [31]. A competing concern is that when the array elements are too far apart, undesirable grating lobes and nulls can form in the beampattern and the performance of the array will be degraded. Ambiguity problems with directions of arrival estimation can also arise. Balancing these two constraints results in the commonly used half-wavelength spacing, which does not have ambiguity or grating problems. In our discussions we denote the dimensions in units of half-wavelength. For instance, the distance between elements located at (0,0) and (1,0) is half-wavelength.

An approach to increase the aperture of the array without creating ambiguity or grating problems is to use a non-uniform array geometry. One of these arrays is called the Golomb array, whose performance will be compared to several other uniformly spaced arrays, all of which have six elements.

2.5.2 Uniformly Spaced Arrays

In this section we introduce three popular configurations of antenna arrays: the Uniform Linear Array (ULA), the Uniform Circular Array (UCA) and the Uniform Triangular Array (UTA), they are depicted in Figure (2.3). Note that we refer to the x-axis in Figure (2.3) as the *reference axis*.

The uniform linear array is the simplest array for analysis, and is extensively used in many antenna array applications. We include the ULA in our comparison because it may find future application in antenna arrays located at the mobile receiver, as well as for reference purposes. The ULA is represented by the coordinates (0,0) to (5,0).

Another array geometry popular in the open literature is the uniform circular array. This configuration has the advantage that the performance is asymptotically uniform across all azimuth angles as the number of elements increases. The distance between each consecutive pair of elements along the circumference is half-wavelength.

The last uniform array that we consider is the uniform triangular array. Triangular arrays are of interest because often in real-life mobile communication system implementations, a base station's coverage area is sectored into three zones covering 120 degrees each. Each of these sectors would be faced by a uniform linear array. In order to distinguish from the ULA, we consider the case where elements on all three sides are taken into account; thus the array has three elements on each side for a total of six elements.

2.5.3 The Golomb Array

A Golomb array is an array defined by the Golomb sequence [8]: the integer sequence $[0 = a_1 < a_2 < ... < a_m]$ such that $(a_i - a_j) \neq (a_k - a_l)$ unless $i = k$ and $j = l$. The motivation for this array geometry is to enlarge the aperture of the array by increasing the spacings between most of the elements, while at the same time retain some small spacings to eliminate ambiguity in DOA estimation. A Golomb array has non-repeating inter-elemental distances amongst its elements, resulting in a large array aperture. The Golomb sequences for three to fifteen elements are listed in the paper by Chambers et al [8], and the six-element sequence we consider is the [0,1,4,10,12,17] sequence, which is depicted in Figure (2.4).

An related type of arrays is the *Minimum Redundancy Arrays* [8], which have consecutive but possibly repeated inter-elemental distances, compared to the Golomb arrays which have non-repeating inter-elemental distances. A *restricted minimum redundancy array* is an array defined by the integer sequence $[0 = a_1 < a_2 < ... < a_m]$ such that all positive integers $[1, 2, ..., L = a_m]$ can be formed by $(a_i - a_j)$ where $\{1 \leq i \leq M; 1 \leq j \leq M, j \neq i\}$. A *general minimum redundancy array* is the same as an *restricted minimum redundancy array* except that $L < a_m$. Due to time and space constraints, considerations for the minimum redundancy arrays are beyond the scope of this thesis.

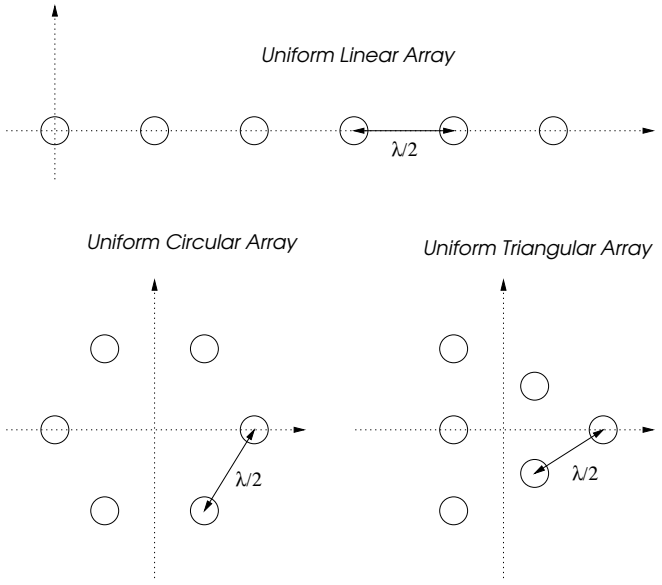

Figure 2.3: Three Uniform Arrays (ULA, UCA and UTA)

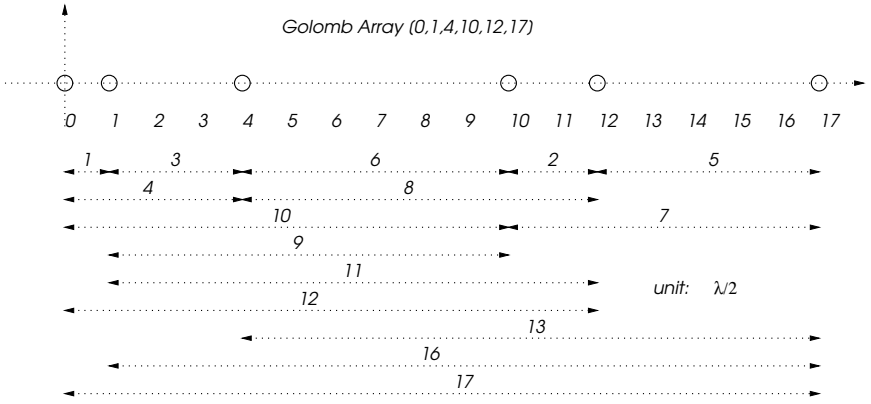

Figure 2.4: The Golomb Array

2.6 Cramer Rao Lower Bound (CRB)

In the previous sections, we described DOA estimation and beamforming methods, as well as several basic array geometries. Now we wish to compare the performances of the various arrays. We want to compare the arrays in an algorithm-independent way, because specific algorithms may exploit special properties of certain geometries and thus performance comparisons using any given algorithm cannot be considered conclusive.

One way to compare the different arrays more objectively is to compare the theoretical performance bounds, the most popular of which is the *Cramer Rao Lower Bound*. In the book "Fundamentals of Statistical Signal Processing - Estimation Theory" by Kay [25], there are detailed discussions as well as derivations of the CRB for various scenarios. The two scenarios that are useful here are the *vector parameter CRB* and the *general Gaussian CRB*, which are briefly described in the following subsection. We then present the CRB expression for DOA estimation variance for an arbitrary three-dimensional array, the derivation of the expression is presented in Appendix A.

2.6.1 Vector Parameter and General Gaussian Cramer Rao Lower Bound

The Cramer Rao Lower Bound is the variance lower bound of the unbiased estimator of a parameter or parameter vector. For the case where a vector of parameters $\underline{\theta} = [\theta_1, \theta_2, ..., \theta_q]$ is to be estimated from the data vector $\mathbf{x}[n] = \mathbf{s}[n; \underline{\theta}] + \mathbf{w}[n]$, where $\mathbf{w}[n]$ represents additive white Gaussian noise, the CRB for the $\underline{\theta}$ estimates are described as:

$$var(\hat{\underline{\theta}}_i) \geq [\mathbf{I}^{-1}(\underline{\theta})]_{ii} = CRB(\hat{\underline{\theta}}_i) \tag{2.12}$$

where $\hat{\theta}_i$ is the estimate of the i-th element of the parameter vector $\underline{\theta}$, and $\mathbf{I}^{-1}$ is the inverse of the q-by-q *Fisher Information Matrix*, defined by the following expression:

$$[\mathbf{I}(\underline{\theta})]_{ij} = -E[\frac{\partial^2 lnp(\mathbf{x}; \underline{\theta})}{\partial \underline{\theta}_i \partial \underline{\theta}_j}] \tag{2.13}$$

for $i, j = 1...q$. The derivative is evaluated at the true values of $\underline{\theta}$, and the expectation is taken with respect to $p(\mathbf{x}; \underline{\theta})$, the probability distribution function of $\mathbf{x}$ given $\underline{\theta}$. Note that we assume the PDF satisfies regularity conditions, as described in [25].

If the observed data vector is Gaussian distributed with mean vector $\mu(\underline{\theta})$ and covariance matrix $\mathbf{C}(\underline{\theta})$, as represented by $\mathbf{x} \sim \mathcal{N}(\mu(\underline{\theta}), \mathbf{C}(\underline{\theta}))$, then it can be shown that the (i,j)th element of the Fisher information matrix is given by the following expression [25]:

$$[\mathbf{I}(\underline{\theta})]_{ij} = [\frac{\partial \mu(\underline{\theta})}{\partial \underline{\theta}_i}]^T \mathbf{C}^{-1}(\underline{\theta}) [\frac{\partial \mu(\underline{\theta})}{\partial \underline{\theta}_j}] + \frac{1}{2} tr[\mathbf{C}^{-1}(\underline{\theta}) \frac{\partial \mathbf{C}(\underline{\theta})}{\partial \underline{\theta}_i} \mathbf{C}^{-1}(\underline{\theta}) \frac{\partial \mathbf{C}(\underline{\theta})}{\partial \underline{\theta}_j}] \tag{2.14}$$

where

$$\frac{\partial \mu(\underline{\theta})}{\partial \underline{\theta}_i} = \begin{bmatrix} \frac{\partial [\mu(\underline{\theta})]_1}{\partial \underline{\theta}_i} \\ \frac{\partial [\mu(\underline{\theta})]_2}{\partial \underline{\theta}_i} \\ \vdots \\ \frac{\partial [\mu(\underline{\theta})]_N}{\partial \underline{\theta}_i} \end{bmatrix} \tag{2.15}$$

and

$$[\frac{\partial \mathbf{C}(\underline{\theta})}{\partial \underline{\theta}_j}]_{ij} = \frac{\partial [\mathbf{C}(\underline{\theta})]_{ij}}{\partial \underline{\theta}_j} \tag{2.16}$$

The inverse of the Fisher information matrix gives the Cramer Rao bound.

2.6.2 CRB for the Azimuth and Elevation DOA Estimates

In the paper by Chambers et al [8], the CRB for the Azimuth and Elevation DOA estimation variances for arbitrary three-dimensional array geometries are given by the following expressions:

$$\begin{aligned} \mathbf{CRB}(\theta) &= \frac{1 + ASNR}{2M(ASNR)^2} \frac{AV_{zz}}{AV_{xx}AV_{zz} - AV_{xz}^2} \\ \mathbf{CRB}(\phi) &= \frac{1 + ASNR}{2M(ASNR)^2} \frac{AV_{xx}}{AV_{xx}AV_{zz} - AV_{xz}^2} \end{aligned} \tag{2.17}$$

where ASNR is the Antenna Signal to Noise Ratio, M is the number of array elements and $\mathbf{AV}_{xz} = \mathbf{AV}_{zx} = \frac{\partial \mathbf{a}^H}{\partial \theta} \frac{\partial \mathbf{a}}{\partial \phi}$, $\mathbf{AV}_{xx} = \frac{\partial \mathbf{a}^H}{\partial \theta} \frac{\partial \mathbf{a}}{\partial \theta}$ and $\mathbf{AV}_{zz} = \frac{\partial \mathbf{a}^H}{\partial \phi} \frac{\partial \mathbf{a}}{\partial \phi}$, where $\mathbf{a}$ is the normalized ARV of the desired signal. The proof of Equation (2.17) is shown in Appendix A.

2.7 Chapter Summary

We introduced some background information on several aspects of antenna signal processing in this chapter. First we discussed the Direction-of-Arrival estimation techniques; secondly we introduced the fundamentals of antenna signal processing; thirdly we showed the different antenna geometries under investigation in this thesis; finally, we presented the DOA estimation Cramer-Rao Lower Bound expressions for general three-dimensional arrays as found in [8]. In the next chapter, we will discuss the comparisons in more detail.

Chapter 3

Antenna Array Geometry Comparison with Known DOAs

3.1 Introduction

Of the various approaches that are available to increase the performance of a wireless communication system, the effects of different antenna array geometries have been largely neglected by the research community. Most of the results available in this area are piece meal and lack systematic analysis. In addition, the investigations have been mostly in the area of direction of arrival estimation comparisons rather than system performance comparisons in practical scenarios.

In this chapter we compare the uplink performances of the four six-element antenna arrays introduced in the last chapter: the uniform linear array (ULA), the Golomb array, the uniform circular array (UCA) and the uniform triangular array

(UTA). We will compare the capacities of the arrays in two different scenarios, employing the maximum SNR and the maximum SINR beamformers which were described in the last chapter.

The two scenarios being considered are the *Identical Users* scenario and the *Multi-Rate Users* scenario. In the first scenario, all users have the same received power level at the antenna array due to power control schemes to combat near-far effects. The near-far effect occurs when a user close to the base station over-powers the other users due to the lower path-loss experienced. An example case of the *Identical Users* scenario would be 2G wireless communication systems consisting of cellular phone users only. In the *Multi-Rate Users* scenario, although the power control scheme is still in place, some users have higher power levels to facilitate higher data rates. An example of this would be in 2.5G or 3G multi-media wireless services, where the power levels adapt to different data rate requirements.

3.1.1 Assumptions

We make several assumptions in this thesis in order to reduce the problem of array performance comparison to a more manageable complexity.

First of all we assume that the dimensions of the antenna arrays are small compared to the distances from the mobile signal sources, which means that we do not deal with near-field effects and assume the incoming waveforms are plane waves. We also assume that the signal are narrowband signals, whose signal bandwidth is small

compared to the carrier frequency. In other words, the signal envelope is essentially constant as the incident wavefronts pass through the array.

Secondly we assume that perfect power control is in place to combat the near-far problem and there is out-of-sector but no out-of-cell interference present. This is desirable since considering out-of-cell interference power distribution in a power control situation greatly complicates the problem. By making this assumption, the uplink system capacities obtained will be slightly increased from the case where there are out-of-cell interferences present, but the relative performances of the arrays should be relatively stable, because all array are subject to similar change in interference power level.

Thirdly we assume that the idealized wireless system coverage area can be considered as a large flat plane, with users uniformly distributed on the surface. The communication coverage of such a scenario is most often provided by a system of base stations each with a hexagonal coverage area. Based on these assumptions, we can further assume that the angular distribution of users are uniform. This means that we can consider the system as having users uniformly distributed along the circumference of a circle with the base station at its center. This assumption is reasonable since the hexagonal cell shape is roughly equivalent to a circular cell shape, where each arc-section of equal arc length has the same area. Thus uniform distribution of users under perfect power control in a hexagonal cell can be roughly represented by uniform distribution of users along the circumference of a circle around the base station.

Fourthly, we assume that line-of-sight paths exist between the antenna array and all users, and exclude effects such as mutual coupling, scattering and multi-path fading from consideration because we want to concentrate on the comparison between different array geometries. The effects aforementioned have been studied [12] [60], and can be integrated with the results of this research, but that is beyond the scope of this thesis.

Finally, in this chapter we additionally assume that the signal and interference DOAs are known exactly. Although for mobile communication systems the DOAs must be estimated from the received signals, for certain types of wireless systems the locations of the users may be known. For instance, some wireless systems are designed to provide fixed-location broadband services to homes in remote or developing areas. For these systems the user receiver locations would be known in advance. This assumption is valid in this chapter only, whereas the previous assumptions are valid throughout this thesis.

3.1.2 Chapter Outline

In this chapter we investigate the effects of several base station antenna array geometries on the performance of a wireless communication system, with the assumption that the signal and interference directions of arrival are known.

In the second section we consider the *Identical Users* scenario, where all users under consideration occupy the same time-frequency channel, but different spatial

locations. We calculate the beamforming user capacities for the different arrays using IS-95 CDMA system parameters. In the third section we consider the *Multi-Rate Users* scenario, where high-power users exist in the system. Interference suppression prevents the severe degradation in the communication channel for the other users in this scenario, and we again calculate the capacities of the different arrays.

In each of the scenarios, we consider three user distribution cases. In the 120/120 case, the desired user as well as the interfering users are uniformly distributed in a 120-degree sector. This can be used to model a suburban base station deployment where most users are located within a range of angles to the antenna array. In the 360/360 case, all users are uniformly distributed throughout 360 degrees. This is typical of an urban base station deployment. In between these two types is the 120/360 case, where the desired user is located within a 120-degree sector but the interfering signals come from all directions. This models the urban deployment with sectored coverage areas while taking out-of-sector interference into account.

3.2 Identical Users Scenario

In this section we consider the system capacities where all users generate the same incident power on the base station antenna array. We first plot the radiation beam-patterns of the arrays, then we outline the *Power Pass-Through Factor* expressions and calculate their values, and finally we compare the system capacities of the four antenna arrays.

3.2.1 Radiation Patterns

We first plot and compare the radiation patterns of the arrays, since the main beam width and side lobe levels can often give us intuitive ideas on certain aspects of array performances, such as the ability to resolve two closely located users.

In the identical users scenario, the number of interfering users is much larger than the number of antenna array elements, and they cannot be individually suppressed by the maximum SINR beamformer. Thus in this case we use the maximum SNR beamformer and treat the interfering signals as part of the noise. As an example, the beampatterns generated by the arrays using the maximum SNR beamforming weight vector when the desired signal is located at 30 degrees off the reference x-axis are shown in Figure (3.1).

From Figure (3.1), we can observe that the Golomb array produces a pattern with the narrowest beams. This is expected since the Golomb array has the largest aperture of all the arrays considered. This allows for pinpoint interference suppression, but the nulls are not very deep. For some of the other arrays the nulls are deeper, but the side lobes are quite wide. Thus we cannot draw definite conclusions on the relative performances between the arrays from the radiation patterns. Instead we need to compare the user capacities allowed by each array geometry. But before we calculate and compare the capacities of the four array geometries, we need to introduce the term *power pass-through factor*.

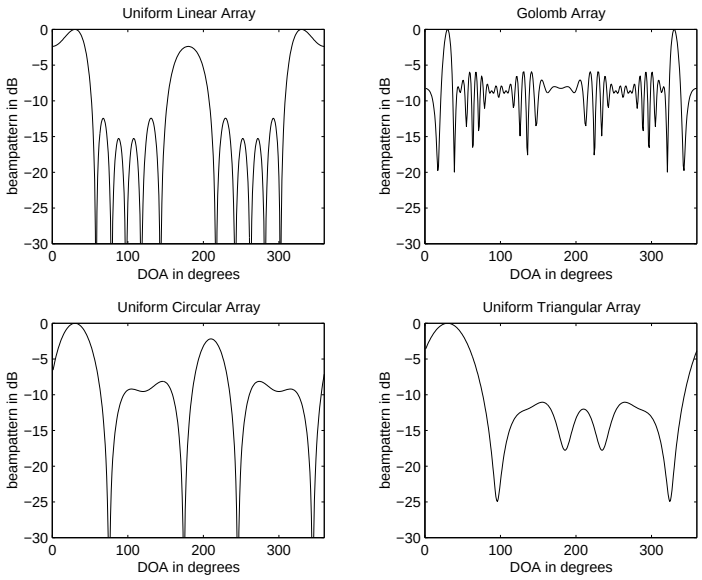

Figure 3.1: Maximum SNR beam patterns for four antenna array geometries for a desired signal at 30 degrees off the reference axis

3.2.2 Power Pass-Through Factor (PPTF)

In order for a user to communicate reliably in a digital wireless system, a certain *energy per bit to noise ratio* level must be obtained. The relationship between the incident signal power, the data transmission rate, the noise power and the energy per bit to noise ratio in the interference-free, single antenna element case is given by the following expression [13]:

$$\frac{E_b}{N_o} = \frac{P_{signal}/R_{data}}{\sigma_n^2} \tag{3.1}$$

where P_{signal} is the incident signal power, R_{data} is the data transmission rate, σ_n^2 is the noise power spectral density equal to kT_{system}, the product of the Boltzmann's constant k and the system noise temperature T_{system}, and $\frac{E_b}{N_o}$ is the energy per bit to

noise ratio.

Now we consider the antenna array case. Due to our assumed perfect power control, the received signal strength from each user is the same. Thus the total received interference power is $P_{interference} = \sum_{k=1}^{M-1} \phi_k^{int} P_{signal}$, where P_{signal} is the incident power from each user, M is the total number of users and the *Power Pass-Through Factor* ϕ_k^{int} is the ratio of interference power from the k-th interference source that is passed through by the beamforming weight vector to the incident interference power from the k-th interference source. Taking the expected value of the above equation gives the expected received interference power $P_{int-expected} = E[\phi_k^{int}](M-1)P_{signal}$. By the same token, the expected received desired signal power is $P_{desired} = E[\phi^{desired}]P_{signal}$, where $E[\phi^{desired}]$ is the expected power pass-through factor for the desired signal.

The interference power spectral density $P_{int-expected}/BW$ is treated like noise and substituted into the $\frac{E_b}{N_o}$ expression:

$$\frac{E_b}{N_o} = \frac{E[\phi^{desired}]P_{signal}/R_{data}}{E[\phi_k^{int}](M-1)P_{signal}/BW + N_A\sigma_n^2} \tag{3.2}$$

where BW is the communication bandwidth and N_A is the number of antenna elements.

3.2.3 Expected Power Pass-Through Factor Calculations

In this subsection we calculate the expected interference power pass-through factor

$E[\phi_k^{int}]$ and the expected desired power pass-through factor $E[\phi^{desired}]$ for the different arrays.

Recall that the beamforming weight vector for the maximum SNR beamformer when the desired signal is located at angle θ is $\mathbf{w} = \mathbf{R}_n^{-1}\mathbf{a}(\theta)$, where $\mathbf{R}_n$ is the noise covariance matrix and $\mathbf{a}(\theta)$ is the array response vector of the desired signal. When the noise is uncorrelated and white, $\mathbf{R}_n = \sigma^2\mathbf{I}$. Since a constant scalar factor does not effect the output SNR of the beamformer, we ignore the constant factor and let $\mathbf{w} = \mathbf{a}(\theta)$.

The ratio of signal power from direction θ_k at the output of the maximum SNR beamformer to the incident signal power from θ_k, when the desired signal is at $\theta_{desired}$, is $\phi_k^{int}(\theta_k, \theta_{desired}) = \left|\mathbf{w}^H(\theta_{desired})\mathbf{a}(\theta_k)\right|^2$. The expected power pass-through factor for users with interfering signal DOA distribution $f(\theta)$, when the beamforming weight vector is $\mathbf{w}(\theta_{desired})$ can be written as:

$$E[\phi_k^{int}(\theta_k, \theta_{desired})] = \int_{range-of-\theta_k} f(\theta_k) \left|\mathbf{w}^H(\theta_{desired})\mathbf{a}(\theta_k)\right|^2 d\theta_k \tag{3.3}$$

where θ_k is the DOA of interfering user k and $\theta_{desired}$ is the DOA of the desired user.

Due to the assumption of coverage area in the array plane and uniform angular distribution of interfering users, the value of $E[\phi_k^{int}]$ for each array can be calculated by integrating the radiation pattern over the DOA range under consideration for a given desired user DOA $\theta_{desired}$.

$$E_{\theta_k}[\phi_k^{int}(\theta_k, \theta_{desired})] = \frac{1}{(\theta_2 - \theta_1)} \int_{\theta_1}^{\theta_2} \left|\mathbf{w}^H(\theta_{desired})\mathbf{a}(\theta_k)\right|^2 d\theta_k \tag{3.4}$$

for any given $\theta_{desired}$. The discrete DOA version of Equation (3.4) is:

$$E_{\theta_k}[\phi_k^{int}(\theta_k, \theta_{desired})] = \frac{1}{(\theta_2 - \theta_1)} \sum_{\theta_k=\theta_1}^{\theta_2} \left| \mathbf{w}^H(\theta_{desired}) \mathbf{a}(\theta_k) \right|^2 \tag{3.5}$$

for any given $\theta_{desired}$.

As reference, we plot the expected interference power pass-through factor value versus the desired signal DOA in Figures (3.2), (3.3) and (3.4), which show the angular variations in performance for each of the arrays.

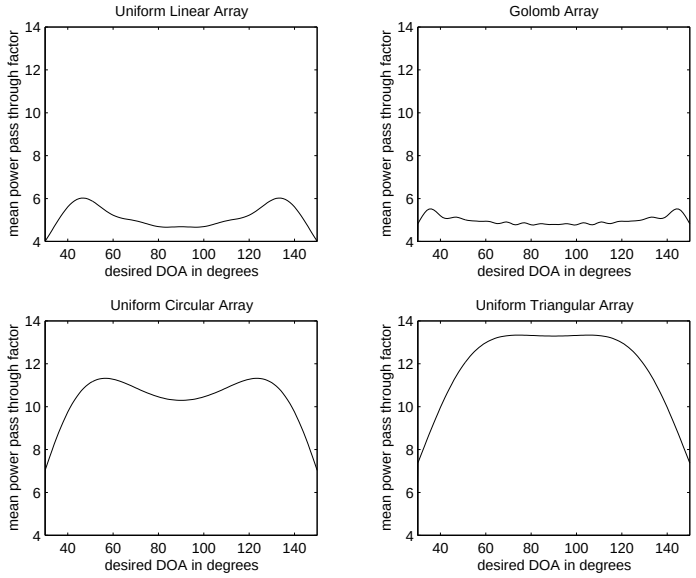

Figure 3.2: Expected Interference Power Pass-Through Factor vs the Desired Signal DOA for the 120/120 scenario

For 360/360 coverage, θ_1 is 0 and θ_2 is 360 degrees, and all signal sources are assumed to have uniform position distribution inside this range. For 120/120 coverage, θ_1 is 30 and θ_2 is 150 degrees for both θ_k and $\theta_{desired}$. For 120/360 coverage, range of $\theta_{desired}$ is [30, 150] degrees and range of θ_k is [0, 360] degrees.

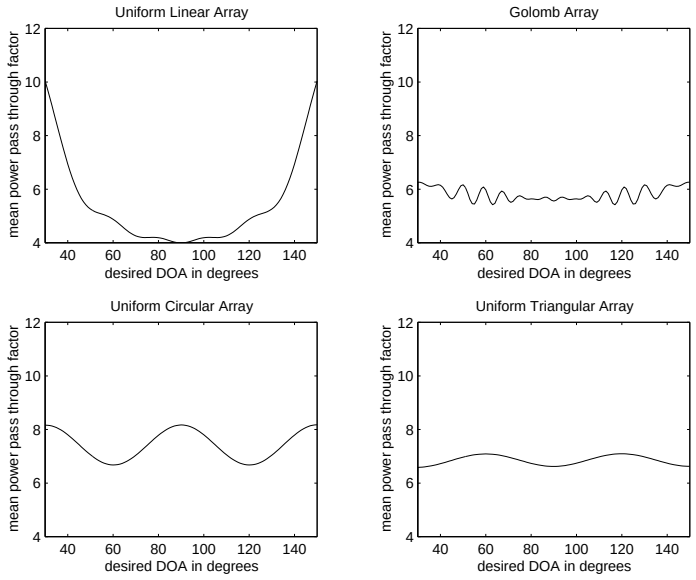

Figure 3.3: Expected Interference Power Pass-Through Factor vs the Desired Signal DOA for the 120/360 scenario

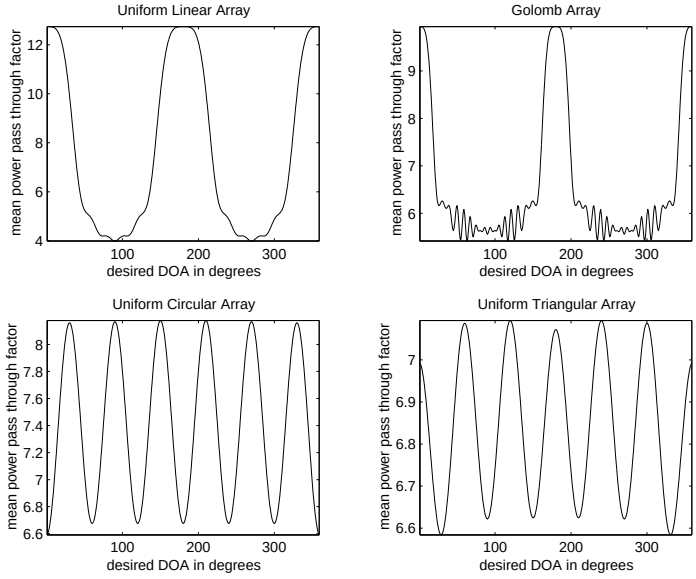

Figure 3.4: Expected Interference Power Pass-Through Factor vs the Desired Signal DOA for the 360/360 scenario

The other important factor required is the expected desired signal power pass-through factor, which is given by the following expression due to the assumption of known directions of arrival:

$$E_{\theta_k}[\phi^{desired}(\theta_{desired})] = \left|\mathbf{w}^H(\theta_{desired})\mathbf{a}(\theta_{desired})\right|^2 = \left|\mathbf{a}^H(\theta_{desired})\mathbf{a}(\theta_{desired})\right|^2 = N_A^2 \tag{3.6}$$

for any given $\theta_{desired}$, where the maximum SNR beamforming weight vector $\mathbf{w}$, as we recall, is equal to the array response vector $\mathbf{a}(\theta_{desired})$ due to assumption of uncorrelated AWGN at the array elements.

3.2.4 System Capacity Calculations

Recall that the relationship between the required energy-per-bit-to-noise ratio, the incident signal power, the noise power level, the data rate, the communication bandwidth and the mean expected power pass-through factors for both the desired and interfering signal sources is given by the following equation:

$$\frac{E_b}{N_o} = \frac{E[\phi^{desired}]P_{signal}/R_{data}}{E_{\theta_k}[\phi_k^{int}](M-1)P_{signal}/BW + N_A\sigma_n^2} \tag{3.7}$$

Given the system parameters $\frac{E_b}{N_o}$, R_{data}, BW, σ_n and P_{signal}, the capacity of an antenna array is given by the largest M that yields satisfactory $\frac{E_b}{N_o}$.

For instance, the IS-95 system has the following parameter values [47]: R_{data} is 9600bps, BW is 1.2288MHz, σ_n^2 is 2.025E-21, and the average uplink carrier frequency is 836.5 MHz. In addition we assume that the power control is such that all incident

power at the array is the same as the incident power due to a 1mW transmitter at a distance of 5km.

For the bit error rate of 0.001, the required $\frac{E_b}{N_o}$ is 7dB, or a factor of approximately 5.012. Also recall that the number of antenna elements N_A is 6 for all of the arrays under consideration. Substituting these values as well as the power pass-through factors for each $\theta_{desired}$ into Equation (3.7), we obtain the capacity value for each $\theta_{desired}$. Averaging over all $\theta_{desired}$ and the resulting mean capacity values are summarized in the Table (3.1). As reference, for the single element case the capacity is found to be 26.

Array	ULA	Golomb	UCA	UTA
Capacity(120/120)	145.1405	148.5785	71.7603	63.0992
ratio to ULA capacity	1.0000	1.0237	0.4944	0.4347
Capacity(120/360)	181.4380	157.9421	124.0496	133.9091
ratio to ULA capacity	1.0000	0.8705	0.6837	0.7380
Capacity(360/360)	146.4833	143.4444	124.1500	133.8667
ratio to ULA capacity	1.0000	0.9793	0.8475	0.9139

Table 3.1: The mean capacities for the identical users scenario

The results obtained here are used as the base line numbers to calculate the incident SNR in the multi-rate users scenario for the calculation of the maximum SINR beamforming weight vector.

Intuitively, because linear arrays have larger one-dimensional apertures, they are expected to perform better than the two-dimensional arrays for a range of angles along the broad side. This is apparent for the 120/120 and 120/360 scenarios, where the desired signal is confined to the 120-degree arc on the broad side. When the range of coverage is expanded, the advantage of the linear arrays is reduced because the end-fire directions are now taken into account, whereas the two-dimensional arrays UCA and UTA have relatively consistent performances in all directions.

From Table (3.1), we can see that this is indeed the case. For the 120/120 scenarios, the linear arrays have a large advantage over the circular and triangular arrays, where the Golomb array performs marginally better than the ULA. As the coverage angle range extends to the 360/360 scenario, the arrays have more comparable performances.

3.3 Multi-Rate Users Scenario

Next-generation wireless communication systems require multi-rate services to provide multi-media contents or video phones. In this type of system, some users in the coverage area require higher data rates than others, and one way to accomplish this is for them to operate at a higher power level, due to the requirement of constant energy-per-bit-to-noise-ratio. The relationship between the desired signal power level, the energy-per-bit-to-noise-ratio and the data rate is shown by the Equation (3.2). Therefore given the constant $\frac{E_b}{N_o}$ constraint, user signal powers need to be proportional

to the data rates. In this section, we consider the case where the system needs to support some users at 100 times the normal data rate.

Due to the presence of these few high power users, the performance of the system using the maximum SNR beamformer would be severely degraded, and it is necessary to suppress these high power interfering signals individually. The statistically optimum way to accomplish this is the maximum SINR beamformer, and in this section we examine the performances of each of the array geometries when utilizing the maximum SINR beamformer.

3.3.1 Radiation Patterns

We again plot the radiation patterns first to obtain a qualitative comparison between the interference suppression characteristics of each of the arrays using the maximum SINR beamformer. For this purpose, we look at an example case where a desired signal is at 70 degrees and five high power interfering signals are at 60, 80, 100, 120 and 140 degrees off the reference x-axis, respectively. All high power interfering signal sources have the same incident power at the array which is one hundred times the desired user incident power level, corresponding to a one-hundred-fold increase in data transfer rate.

From Figure (3.5), we can see that the Golomb array is the only array that can produce nulls at all interfering signal directions as well as a peak at the desired signal direction. The ULA is able to form nulls for the interferers that are away from the

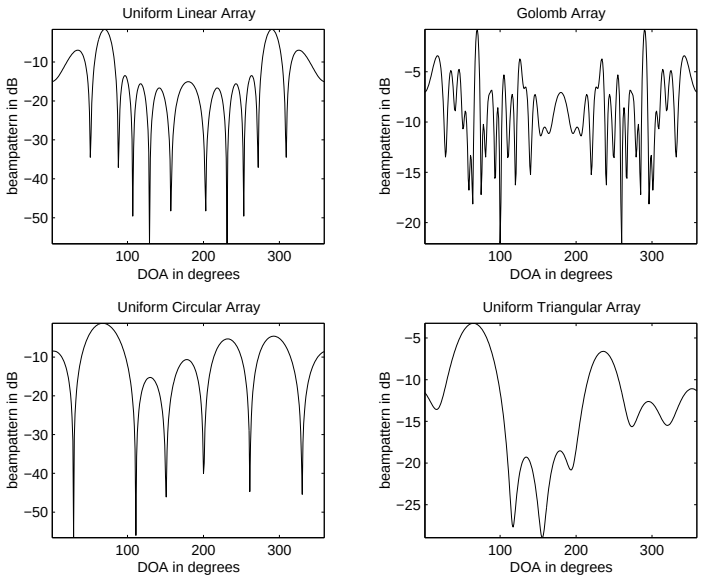

Figure 3.5: Maximum SINR beam patterns when the desired signal is at 70 degrees and the five interfering signals are at 60, 80, 100, 120 and 140 degrees off the reference x-axis

desired signal direction, but not for the ones that are close. This can be explained by the larger aperture of the the Golomb array, which has higher spatial resolution. The ULA does produce deeper nulls, however.

3.3.2 Expected Power Pass-Through Factor Calculations

The next step in the array performance comparison is the calculation of the *Expected Interference Power Pass-Through Factor*. In the multi-rate users scenario, the factors for the low power interfering signals and high power interfering signals are calculated separately. This is necessary since the power levels are different and must be taken

into account when calculating the expected interference power, and Equation (3.7) is extended to account for this consideration:

$$\frac{E_b}{N_o} = \frac{E[\phi^{desired}]P_{signal}/R_{data}}{\left(\underbrace{E[\phi_k^{int}](M-1-M_{hp})P_{signal}}_{low-power-interference} + \underbrace{\sum_{hp=1}^{M_{hp}} E[\phi_{hp}^{int}]P_{hp}}_{high-power-interference} \right)/BW + N_A\sigma_n^2} \tag{3.8}$$

The procedure to calculate the mean expected power pass-through factor (PPTF) values for the low power interfering signals is much the same as the identical users scenario, but the PPTF for the desired signal DOA is no longer 36 due to the need to suppress high power interfering signals. In other words, the desired signal PPTF is a function of the high power interfering signal DOAs, because the maximum SINR weight vector is a function of both the desired signal DOA and the high power interfering signal DOAs. The high power interfering signal PPTF must be calculated this way as well. Thus for each new set of DOAs $[\theta_{desired}, \Theta_{highpower}]$, new beamforming weight vector is calculated and the PPTF for desired and high power interfering signals are calculated individually. Note that $\Theta_{highpower}$ is the vector of θ_{hp}, the high power interfering signal DOAs.

The low power interfering signal PPTF expression for the case with only one high power interfering signal present is written as:

$$E[\phi_k^{int}(\theta_k, \theta_{desired}, \theta_{hp})] = \frac{1}{(\theta_2 - \theta_1)} \int_{\theta_1}^{\theta_2} \left| \mathbf{w}^H(\theta_{desired}, \theta_{hp})\mathbf{a}(\theta_k) \right|^2 d\theta_k \tag{3.9}$$

for given $\theta_{desired}$ and θ_{hp}, where $\mathbf{w} = \mathbf{Q}_{in}^{-1}(\theta_{hp})\mathbf{a}(\theta_{desired})$, $\mathbf{a}(\theta_{desired})$ is the array response vector of the desired signal and $\mathbf{Q}_{in}(\theta_{hp})$ is the interference plus noise covariance matrix when the DOA of the high-power interfering signal is θ_{hp}. The general expression for the interference plus noise covariance matrix is given by Equation (3.10).

$$\begin{aligned} \mathbf{Q}_{in} &= P_{signal} \sum_{j}^{M_{low-power}} \mathbf{a}_j \mathbf{a}_j^H + P_{hp} \sum_{i}^{M_{high-power}} \mathbf{a}_i \mathbf{a}_i^H + \sigma^2 \mathbf{I} \\ &\approx P_{hp} \sum_{i}^{M_{high-power}} \mathbf{a}_i \mathbf{a}_i^H + \sigma^2 \mathbf{I} \end{aligned} \tag{3.10}$$

The discrete version of Equation (3.9) is:

$$E[\phi_k^{int}(\theta_k, \theta_{desired}, \theta_{hp})] = \frac{1}{(\theta_2 - \theta_1)} \sum_{\theta_k=\theta_1}^{\theta_2} \left| \mathbf{w}^H(\theta_{desired}, \theta_{hp}) \mathbf{a}(\theta_k) \right|^2 \tag{3.11}$$

for any given $\theta_{desired}$, θ_{hp}. Similarly, the power pass-through factors for the high power interfering signals are given by the following equation:

$$E[\phi_{hp}^{int}(\theta_{desired}, \theta_{hp})] = \left| \mathbf{w}^H(\theta_{desired}, \theta_{hp}) \mathbf{a}(\theta_{hp}) \right|^2 \tag{3.12}$$

and the power pass-through factor for the desired signal is calculated in the same way.

$$E[\phi^{desired}(\theta_{desired}, \theta_{hp})] = \left| \mathbf{w}^H(\theta_{desired}, \theta_{hp}) \mathbf{a}(\theta_{desired}) \right|^2 \tag{3.13}$$

3.3.3 System Capacity Calculations

Based on the results from the previous subsection, we proceed to calculate the number of low-power users that can simultaneously communicate when high-power users are

present in the system. Recall that the capacity of an antenna array is given by the largest M that produces satisfactory $\frac{E_b}{N_o}$ in the following equation:

$$\frac{E_b}{N_o} = \frac{E[\phi^{desired}]P_{signal}/R_{data}}{\left(\underbrace{E[\phi_k^{int}](M-1-M_{hp})P_{signal}}_{low-power-interference} + \underbrace{\sum_{hp=1}^{M_{hp}} E[\phi_{hp}^{int}]P_{hp}}_{high-power-interference} \right) /BW + N_A\sigma_n^2} \quad (3.14)$$

For each new set of DOAs $[\theta_{desired}, \Theta_{highpower}]$, the new beamforming weight vector is calculated and then the PPTFs for desired and high power interfering signals as well as mean PPTF for low power users are calculated. The PPTF factors are then substituted into the Equation (3.14) in addition to the IS-95 system parameters to calculate the user capacity.

Note that in Equation (3.14), the quantities $E[\phi^{desired}]$, $E[\phi_k^{int}]$ and $E[\phi_{hp}^{int}]$ are functions of M through the matrix $\mathbf{Q}_{in}$. As a result, it is difficult to obtain a closed-form solution for M. Therefore, we use an iterative approach where we assume an initial capacity $M_{initial}$, calculate the factors $E[\phi^{desired}]$, $E[\phi_k^{int}]$ and $E[\phi_{hp}^{int}]$ as functions of $M_{initial}$, then solve Equation (3.14) for M, and the whole process may be repeated. We choose the solution to Equation (3.7) as $M_{initial}$, and we observe that a fixed point is approximated after two iterations.

First we consider the case where there is only one high power interfering user in the system, and the PPTF factors as well as the resulting capacities are calculated at one degree intervals. The results are tabulated in the Tables (3.2) and (3.3).

Based on the results tabulated in Tables (3.2) and (3.3), we conclude that the capacity values for the iterated calculation is very close to the capacity values for the

Array	ULA	Golomb	UCA	UTA
Capacity(120/120)	119.9286	114.2546	53.1921	41.5927
Capacity(120/360)	155.4585	124.0705	100.8374	105.1608
Capacity(360/360)	121.6111	111.1760	100.9693	105.1301

Table 3.2: The mean capacities for the Multi-Rate users scenario based on Identical-User scenario capacities

Array	ULA	Golomb	UCA	UTA
Capacity(120/120)	119.9174	114.2374	53.1811	41.5689
Capacity(120/360)	155.4465	124.0488	100.8191	105.1441
Capacity(360/360)	121.5989	111.1578	100.9511	105.1133

Table 3.3: The iterated mean capacities for the Multi-Rate users scenario based on previous Multi-Rate user scenario capacities

calculation using Identical-User capacity values. This imply that the maximum SINR beamforming weight vector is not very sensitive to variations in the user capacity of the low power interfering signals for the IS-95 system we are considering.

When more than one high-power interfering signals are present, the calculations for the PPTF factors and the system capacities are repeated for each DOA vector $[\theta_{desired}, \Theta_{highpower}]$. Due to time and memory constraint, we only consider the case where there are two high power interfering signals present in the system. And for this case the calculations for the PPTF factors and the capacities are repeated at ten

degree intervals instead of one degree intervals as was done previously. For comparison purposes, we repeat the single high power interfering signal case at ten degree intervals. The results are tabulated in Table (3.4). The two high power interfering signal results are tabulated in Table (3.5).

Array	ULA	Golomb	UCA	UTA
Capacity(120/120)	123.6686	107.6095	56.6746	46.1893
Δ from 1 degree intervals	3.128%	-5.802%	6.569%	11.115%
Capacity(120/360)	149.2906	116.8291	99.6902	105.3547
Δ from 1 degree intervals	-3.960%	-5.820%	-1.120%	0.200%
Capacity(360/360)	120.4074	105.7531	100.9900	105.2654
Δ from 1 degree intervals	-0.980%	-4.862%	0.039%	0.145%

Table 3.4: The mean capacities for the Multi-Rate users scenario when one high power interfering signal is present, calculated at 10 degree intervals, and the capacity variations compare to the one degree interval case.

From Table (3.4), we observe that the differences in the mean capacities when using 10 degree and 1 degree intervals for calculation can be up to about 11%. Thus the results in Table (3.5) can only be taken as rough estimates of the actual capacities of the respective arrays.

Data in Table (3.5) indicate that counter to the intuition that the Golomb array should have higher interference suppression capabilities, it actually has lower capacities than the ULA, and is only significantly better than the circular and the triangular

Array	ULA	Golomb	UCA	UTA
Capacity(120/120)	102.0400	82.5073	41.3386	37.6517
Δ from 1 HP case	-17.489%	-23.327%	-27.060%	-18.484%
Capacity(120/360)	123.8672	91.4374	79.6781	82.6305
Δ from 1 HP case	-17.029%	-21.734%	-20.074%	-21.569%
Capacity(360/360)	97.9310	81.5678	82.2810	83.4451
Δ from 1 HP case	-18.667%	-22.870%	-18.526%	-20.729%

Table 3.5: The mean capacities for the Multi-Rate users scenario when two high power interfering signals are present, calculated at 10 degree intervals, and the capacity reductions compare to the one high power interfering signal case.

arrays in the 120/120 scenario. More importantly, the percentage drop values of the capacities from the one high power user capacities indicate that the Golomb array has poor performance in dealing with additional high power interfering signals.

3.4 Chapter Summary and Discussion

In this chapter we investigated the effects of different antenna array geometries on the capacities of a wireless communication system. We considered two scenarios that are applicable to present and future system deployments: the identical-users scenario and multi-rate users scenario.

For the identical-users scenario, all users have the same incident power level at

the receiving antenna array. For this scenario, maximum SNR beamforming weight vectors are used, and the resulting capacities were calculated and summarized in the Table (3.1). The data show that even though the Golomb array has superior DOA resolution performance, the capacity on the whole is inferior to uniform linear arrays. This is likely due to the relatively high sidelobe levels of the Golomb array beampattern, as shown in Figure (3.1). Also worthy of notice is that there are significant differences between the capacities of the uniform circular and triangular arrays, even though their array geometries are quite similar. This indicates that relatively minor changes in the array geometry may cause significant changes in the capacity performance.

For the high-power user scenario, a number of high power users are present. The maximum SINR beamformer is utilized to suppress the high power interfering signals so the low power users can obtain satisfactory performances. We calculated the number of regular power users that can be served in the presence of one or two high-power users for each of the array geometries. The results for the one high power interfering signal case are summarized in Table (3.3). From the data we conclude that the maximum SINR beamforming weight vector is not very sensitive to the number of low power users in the system. We also notice that linear arrays have larger capacities than the circular and triangular arrays in all cases, although for the 360/360 case the differences in capacities are relatively small.

The capacity results for the two high power interfering signals case are summarized in Table (3.5). The data show the perhaps counter-intuitive result of low capacity

performance for the Golomb array. Two reasons may have contributed to this result, first, the high levels of sidelobes reduce the capacity even though the high power interfering signals are well suppressed; second, the data show the average values for all DOA cases, reducing the advantages of the Golomb array. Because for most of these cases, the high power interfering signal DOAs are away from the desired signal DOA and all four arrays were able to suppress them. The Golomb array has better performance when the desired and interfering signal DOAs are close together, but unfortunately these cases are relatively rare.

Chapter 4

Antenna Array Geometry Comparison with Estimated DOAs

4.1 Introduction

In the last chapter, we investigated the performances of four antenna array geometries in two important scenarios of wireless communication system deployment. An important assumption made was that the DOAs of all signal sources are known exactly. The considerations in the previous chapter are applicable to fixed wireless services, where the locations of users are fixed and known in advance. For mobile communication systems, the locations of mobiles are not known in advance and thus must be estimated from the received signal. In this chapter, we will take uncertainty in desired signal DOA estimation into account in the performance comparisons.

Several algorithms exist for the estimation of the DOAs of incident signals for

arbitrary receiving antenna array geometries, for instance, the MUSIC algorithm by Schmidt [50]. Since the algorithms often exploit the mathematical structures of the received signal vectors differently, their performances are also dependent on the array geometry. Since we want to compare the effects of the different array geometries independent of specific algorithms, we model the estimated DOA as an unbiased Gaissian distributed random variable with variance equal to the CRB. We then calculate and compare the user capacities of the four array geometries under consideration base on this assumption,

4.1.1 Chapter Outline

In this chapter we investigate the effects of different base-station antenna array geometries on the uplink performance of a wireless communication system, given the assumptions discussed in Chapter Three, except that the desired signal DOA is now assumed to be an unbiased Gaussian random variable. The variances of the DOA distributions are assumed to be the Cramer Rao Lower Bound (CRB) for the various array geometries.

In the second section we outline the preparatory considerations. First we review the CRB results for estimated DOA variance. Then we consider the implications of the estimated DOA distribution on the *Identical Users* and the *Multi-Rate Users* scenarios, both of which were described in detail in the previous chapter.

In the third section we consider the *Identical Users* scenario. Using the Gaussian

model for estimated DOAs, we calculate the approximate perturbed expected power pass-through factors for the different array geometries. Based on these results, we compare the system capacities provided by the different antenna geometries.

In the fourth section, we consider the *Multi-Rate Users* scenario. While we treat the desired signal DOA as a Gaussian distributed random variable, the interfering signal DOAs are assumed to be perfectly known. We again calculate the expected power pass-through factors and the corresponding system capacities for the different array geometries.

We also consider the relationship between the system capacity and the variance of the estimated DOA distribution. We do so by calculating and plotting the average capacities for the four arrays in various scenarios for a range of estimated DOA distribution variances.

4.2 Preparatory Considerations

Before we proceed to calculate and compare the system capacities of the four antenna arrays for the scenario where the signal DOAs are estimated, we need to review and consider some necessary background information. In the first subsection we will review the CRB results for DOA estimation variance. In the second subsection we will present the distribution of the desired signal ARV due to DOA estimation. In the third section we will discuss the intuitive reason for user capacity reduction due to DOA estimation. And in the fourth subsection we will consider the implication of

the DOA distribution on the beamforming weight vectors for the *Identical Users* and the *Multi-Rate Users* scenarios.

4.2.1 Variance Bounds of Directions of Arrival

In this section we review the CRB of DOA estimation results for a two-dimensional array. Based on the work of Chambers et al [8], the Cramer-Rao Lower Bound for the DOA estimation variance for an array with arbitrary three dimensional geometry is given as:

$$\mathbf{CRB}(\theta) = \frac{1 + ASNR}{2N_s(ASNR)^2} \frac{\mathbf{AV}_{zz}}{\mathbf{AV}_{xx}\mathbf{AV}_{zz} - \mathbf{AV}_{xz}^2} \tag{4.1}$$

where $\mathbf{AV}_{xz} = \mathbf{AV}_{zx} = \frac{\partial \mathbf{a}^H}{\partial \theta}\frac{\partial \mathbf{a}}{\partial \phi}$, $\mathbf{AV}_{xx} = \frac{\partial \mathbf{a}^H}{\partial \theta}\frac{\partial \mathbf{a}}{\partial \theta}$ and $\mathbf{AV}_{zz} = \frac{\partial \mathbf{a}^H}{\partial \phi}\frac{\partial \mathbf{a}}{\partial \phi}$ as shown in Chapter Two, Section 6.2. For the two-dimensional scenario where the signal sources are located on the array plane, the factors involving ϕ are not considered. Thus the Fisher Information Matrix in Equation (A.9) has only one element $\mathbf{I}_{\theta\theta}$, and the inverse of the Fisher Information Matrix has the following expression:

$$\mathbf{CRB}(\theta) = \frac{1 + ASNR}{2N_s(ASNR)^2\mathbf{AV}_{xx}} \tag{4.2}$$

where N_s is the number of snapshots considered, ASNR is the Array Signal to Noise Ratio, and $\mathbf{AV}_{xx}$ is given by the following expression:

$$\begin{aligned}
\mathbf{AV}_{xx} &= \frac{\partial \mathbf{a}^H}{\partial \theta}\frac{\partial \mathbf{a}}{\partial \theta} \\
&= \sum_{l=1}^{N_A} \left([-j\frac{2\pi}{\lambda}(\cos\theta_i \cos\phi_i x_l - \sin\theta_i \cos\phi_i y_l)][\mathbf{a}_i]_l \right)^H \\
&\quad \left([-j\frac{2\pi}{\lambda}(\cos\theta_i \cos\phi_i x_l - \sin\theta_i \cos\phi_i y_l)][\mathbf{a}_i]_l \right)
\end{aligned}$$

$$= \sum_{l=1}^{N_A} \left(\frac{2\pi}{\lambda} (\cos\theta_i \cos\phi_i x_l - \sin\theta_i \cos\phi_i y_l) \right)^2 [\mathbf{a}_i]_l^H [\mathbf{a}_i]_l$$

$$= \sum_{l=1}^{N_A} \left(\frac{2\pi}{\lambda} (\cos\theta_i \cos\phi_i x_l - \sin\theta_i \cos\phi_i y_l) \right)^2 \tag{4.3}$$

Substituting the above expression into Equation (4.2) gives the Cramer-Rao Lower Bound on the DOA estimate in a two-dimensional system.

$$CRB(\theta) = \frac{1 + (ASNR)}{2N_s(ASNR)^2} \left\{ (\frac{2\pi}{\lambda})^2 \sum_{k=1}^{N_A} (x_k \sin\theta - y_k \cos\theta)^2 \right\}^{-1} \tag{4.4}$$

where (x_k, y_k) are the coordinates of the k-th out of N_A array elements, λ is the wavelength of the signal, and θ is the DOA.

Note that the CRB results of Chambers et al. only consider the case where there is no interfering signal present. Although this is not the most accurate model of a wireless communication system, it is a useful approximation in the identical-users case, where the uniformly-distributed interfering signals may be treated as noise. We also use this approximation in the multi-rate users case.

When only one data sample is considered, the relationship between the CRB value and the DOA θ as described by Equation (4.4) is shown in the Figure (4.1).

From Figure (4.1) we observe that the circular array has a slight advantage compare to the triangular array, and the circular and triangular arrays have uniform performances across the whole 360-degree range, as expected because of the symmetry of the array geometries. The linear arrays have very good performances on the broad side, but worsen quickly as the DOA approaches the endfire positions near 0 and 180 degrees. The Golomb array has a lower CRB than the ULA due to its larger

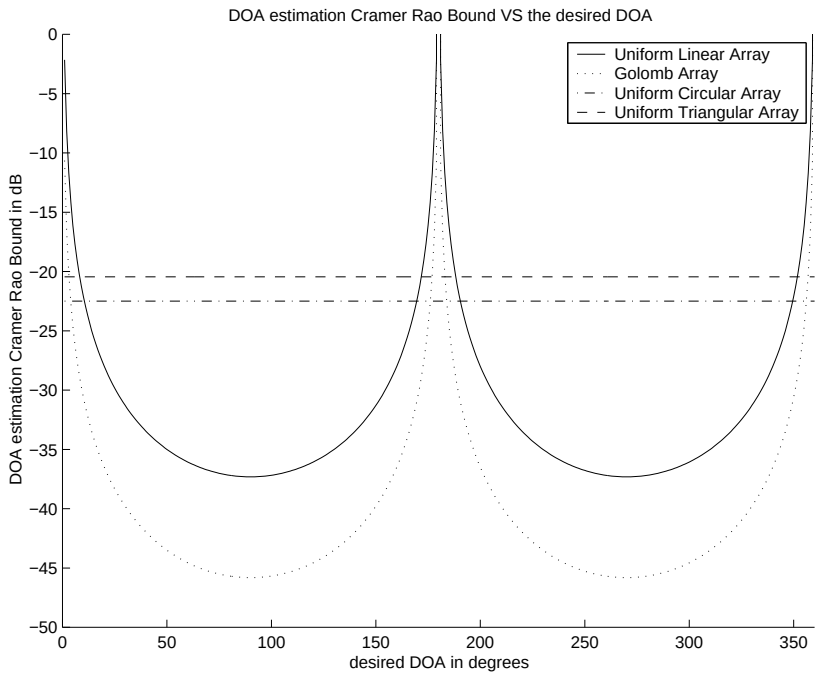

Figure 4.1: CRB of DOA estimation variance vs the Desired DOA

antenna aperture. Note that this is a comparison of theoretical performance bounds, and achievable performances using existing DOA estimation algorithms may vary.

4.2.2 Distribution of the Desired Signal Array Response Vector

The next step in our investigation is to extend the distribution of the estimated DOA into the distribution of the desired signal array response vector. Recall that the un-normalized array response vector $\mathbf{a}$ is defined by the following expression:

$$\mathbf{a} = \left[e^{-j\pi(x_1 \cos\theta + y_1 \sin\theta)}, e^{-j\pi(x_2 \cos\theta + y_2 \sin\theta)}, \ldots, e^{-j\pi(x_{N_A} \cos\theta + y_{N_A} \sin\theta)}\right]^T$$

$$= \left[\mathbf{g}_1\left(x_1, y_1, \theta\right), \mathbf{g}_2\left(x_2, y_2, \theta\right), \ldots, \mathbf{g}_{N_A}\left(x_{N_A}, y_{N_A}, \theta\right)\right]^T \tag{4.5}$$

First we consider the first element of the array response vector $a_1 = \mathbf{g}_1\left(x_1, y_1, \theta\right) = e^{-j\pi(x_1\cos\theta + y_1\sin\theta)}$, which is a complex-valued function of θ. The distribution of a_1 is represented by a probability curve in three-dimensional space, whose domain is a two dimensional curve of possible a_1 values in the complex plane. Using Euler's formula, the real and imaginary parts are expressed by the functions $a_1^r = g_{1r}(\theta) = \cos(\pi(x_1\cos\theta + y_1\sin\theta))$ and $a_1^i = g_{1i}(\theta) = -\sin(\pi(x_1\cos\theta + y_1\sin\theta))$, respectively. For an array element located at position (1,1), the functions g_{1r} and g_{1i} are shown in Figure (4.2).

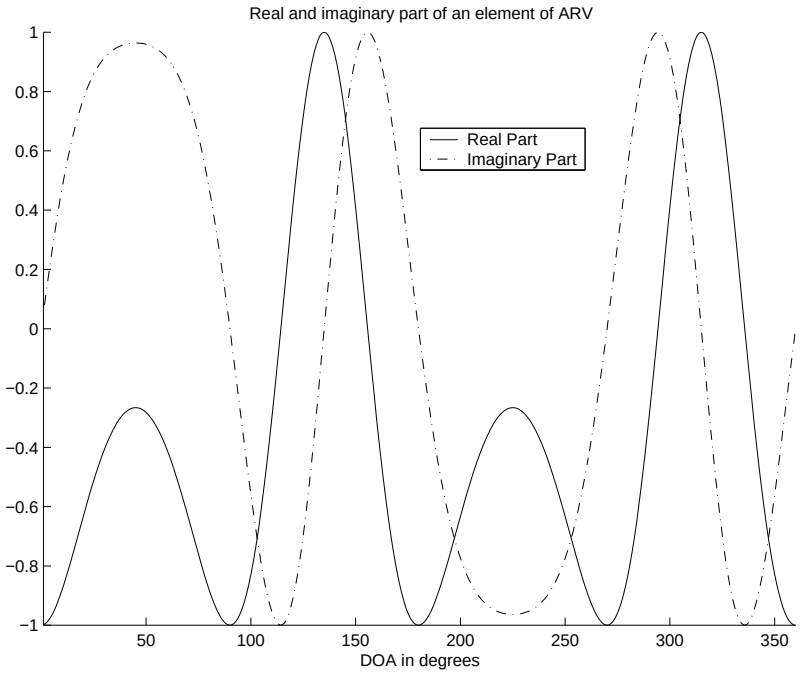

Figure 4.2: Real and imaginary part of the array response vector element as functions of DOA for the array element located at position (1,1)

Recall the fundamental theorem on transformation of a function of a single random

variable [40]: if random variable $\mathbf{y}$ is a function of the random variable $\mathbf{x}$: $\mathbf{y} = g(\mathbf{x})$, then the distribution $f_y(y)$ is given by the following formula:

$$f_y(y) = \frac{f_x(x_1)}{\|g'(x_1)\|} + \ldots + \frac{f_x(x_n)}{\|g'(x_n)\|} + \ldots \tag{4.6}$$

where $g'(x)$ is the derivative of $g(x)$, and $x_1 \ldots x_n \ldots$ are the roots of the equation $\mathbf{y} = g(\mathbf{x})$.

Thus in order to find the distributions of a_1^r and a_1^i, we first need to solve for the roots of $a_1^r = g_{1r}(\theta)$ and $a_1^i = g_{1i}(\theta)$. Since the variance of the θ distribution is small for each of the antenna arrays, we can make the assumption that the θ distribution is a truncated Gaussian distribution, and within this truncated range of θ values the functions $g_{1r}(\theta)$ and $g_{1i}(\theta)$ have unique roots. This means that their inverse functions $g_{1r}^{-1}(a_1^r)$ and $g_{1i}^{-1}(a_1^i)$ exist.

Based on the above results, the distributions of a_1^r and a_1^i can be written using the following expressions:

$$\begin{aligned} f_{a_1^r}(a_1^r) &= \frac{f_x(g_{1r}^{-1}(a_1^r))}{\|g'_{1r}(g_{1r}^{-1}(a_1^r))\|} \\ f_{a_1^i}(a_1^i) &= \frac{f_x(g_{1i}^{-1}(a_1^i))}{\|g'_{1i}(g_{1i}^{-1}(a_1^i))\|} \end{aligned} \tag{4.7}$$

Similarly, the distributions of the rest of the array response vector elements can be calculated.

Alternatively, the approximate distributions can be obtained by first generating the Gaussian distributed random DOA values and then calculating the corresponding ARV values. When the true desired DOA is 30 degrees off the reference axis and

the DOA estimation variance is 0.05 degrees squared, we generate the approximate distribution for the ARV element corresponding to an antenna element at location (1,1) using 10000 Monte Carlo trials. The real and imaginary parts of the resulting distribution of the ARV element are shown in the Figures (4.3) and (4.4).

From Figures (4.3) and (4.4) we observe that, for small DOA variance values typical of the CRB, the distributions for real and imaginary parts of the ARV elements are quite narrow. Also, the functions g_{1r} and g_{1i} are roughly linear since the range of DOA θ considered is small. Due to this linearity, the distributions of $g_{1r}(\theta)$ and $g_{1i}(\theta)$ should be roughly Gaussian because the variable θ is Gaussian distributed. This is confirmed by the Figures (4.3) and (4.4).

4.2.3 Effective Beampattern and User Capacity Reduction

Intuitively, uncertainty in the DOA reduces the beamforming capacity. This can be seen from the beampattern perspective. Each estimated desired signal DOA produces a beampattern that is slightly shifted from the ideal, resulting in reduced output signal-to-noise-ratio and system capacity. Averaging the perturbed beampatterns weighted by the estimated DOA distribution gives the *effective beampattern*. The expression for the effective beampattern given the true DOA θ_m is given by Equation (4.8).

$$ebp(\theta;\theta_m) = \int_{-\infty}^{\infty} f(\theta_m^{est};\theta_m) \left|\mathbf{w}^H(\theta_m^{est})\mathbf{a}(\theta_m)\right|^2 d\theta_m^{est} \tag{4.8}$$

where $f(\theta_m^{est};\theta_m)$ is the pdf of θ_m^{est} given θ_m, which we assume to be Gaussian.

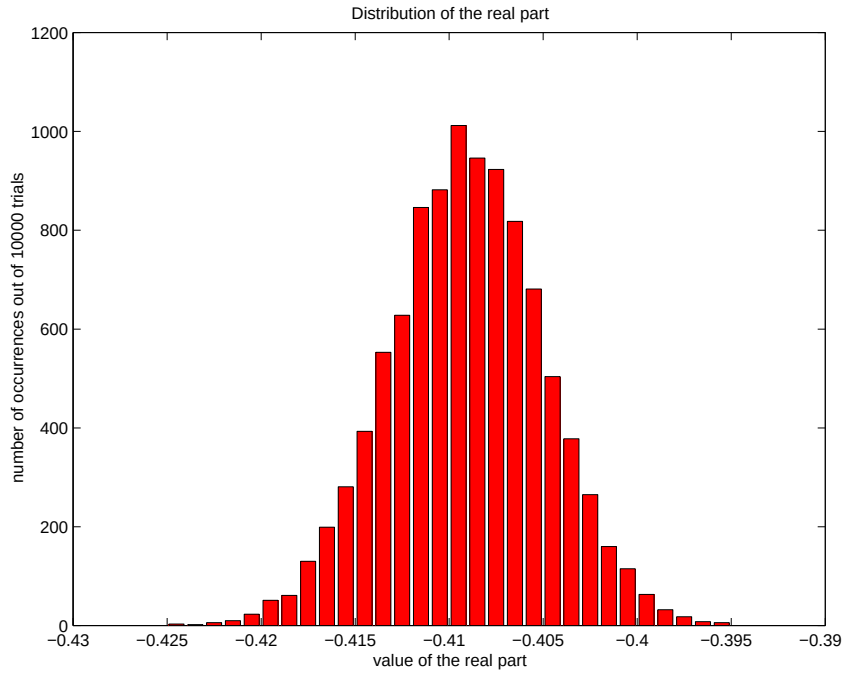

Figure 4.3: Distribution of the real part of the ARV element

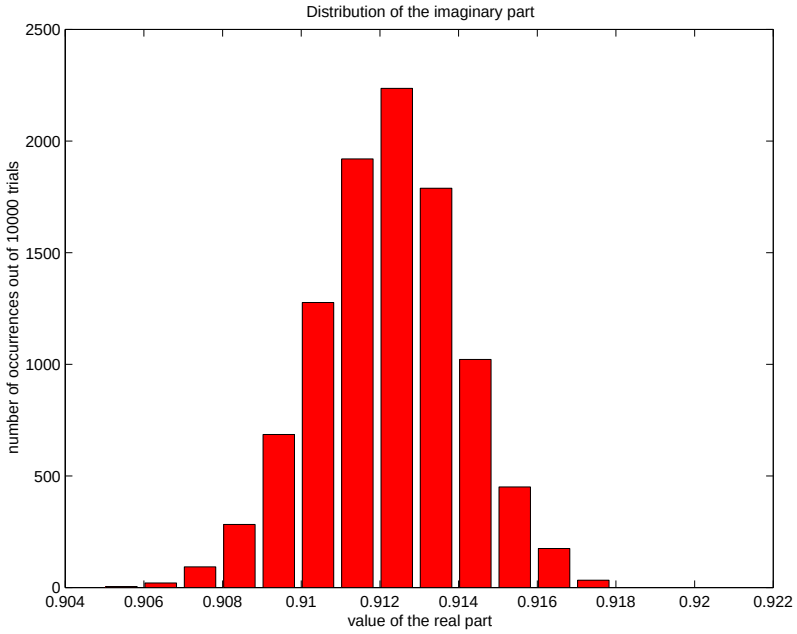

Figure 4.4: Distribution of the imaginary part of the ARV element

In Figure (4.5) we plot the effective beampatterns for the case where the desired signal is at 60 degrees from the reference axis, and the estimated DOA variance is calculated based on the SNR before de-spreading for an IS-95 system, which are 0.0319, 0.0392, 0.0438 and 0.0465 for ULA, Golomb, UCA and UTA respectively. These values are calculated based on the number of low-power interfering signals present as discussed in the Identical Users Scenario in Chapter Three. For all four arrays we observe that the effective beampatterns have wider mainlobes, and the resulting system capacities are expected to be reduced.

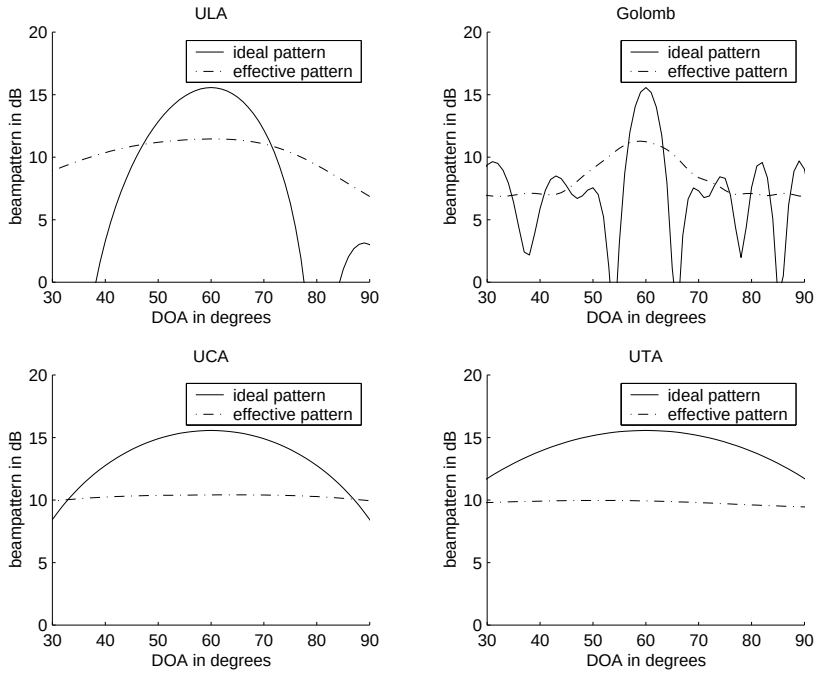

Figure 4.5: Effective beampatterns when the DOA is estimated.

From Figure (4.5), we observe the broadening of the main lobes and lowering of the main lobe magnitude levels. This effect is quite pronounced for all arrays because the SNR is low before de-spreading. After de-spreading the SNR is much higher and

the effective and ideal patterns are virtually indistinguishable for all arrays.

4.2.4 Implications for the Beamforming Weight Vectors

For the *Identical Users* scenario, maximum SNR beamforming is used. The beamforming weight vector $\mathbf{w} = \mathbf{a}(\theta)$ is dependent on the desired signal DOA only, and all interfering signals are treated as noise. The estimated desired signal DOA has a probability distribution due to estimation errors, and it results in a probability distribution of the desired array response vector, which then results in the same probability distribution of the beamforming weight vector.

For the *Multi-Rate Users* scenario, maximum SINR beamforming is used; which means that the high power interfering signals are considered in the calculation for the beamforming weights. Because the interfering signal DOAs are also estimated in the same manner as the desired signal DOA, the expression for the beamforming weights in this case is much more complicated than in the identical users scenario.

Recall that the beamforming weight vector for the maximum SINR beamformer is given by the expression $\mathbf{w} = \mathbf{Q}_{in}^{-1}\mathbf{a}(\theta)$; where $\mathbf{a}(\theta)$ is the array response vector of the desired signal, and $\mathbf{Q}_{in}$ is the interference-plus-noise covariance matrix, which has the following expression:

$$\mathbf{Q}_{in} = P_{signal} \sum_{j}^{M_{low}} \mathbf{a}_j(t)\mathbf{a}_j(t)^H + P_{high-power} \sum_{i}^{M_{high-power}} \mathbf{a}_i(t)\mathbf{a}_i(t)^H + \sigma_n^2\mathbf{I} \qquad (4.9)$$

where $\mathbf{a}_i, \mathbf{a}_j$ are the array response vectors for the interfering signals; P_{signal} and $P_{high-power}$ are the incident power levels for the low and high power interfering signals;

M_{low} and $M_{high-power}$ are the numbers of low and high power users, and σ_n^2 is the thermal noise variance.

For the case where the DOAs of the arriving signals are estimated, we model both the desired and interference DOAs as non-biased Gaussian random variables. The maximum SINR beamforming weight vector expression is rewritten as $\hat{\mathbf{w}} = \hat{\mathbf{Q}}_{in}^{-1}\hat{\mathbf{a}}(\theta)$, where $\hat{\mathbf{a}}(\theta)$ is the perturbed array response vector of the desired signal, and $\hat{\mathbf{Q}}_{in}$ is the perturbed interference-plus-noise covariance matrix, which has the following modified expression:

$$\hat{\mathbf{Q}}_{in} = P_{signal} \sum_{j}^{M_{low}} \hat{\mathbf{a}}_j(t)\hat{\mathbf{a}}_j(t)^H + P_{high-power} \sum_{i}^{M_{high-power}} \hat{\mathbf{a}}_i(t)\hat{\mathbf{a}}_i(t)^H + \sigma_n^2\mathbf{I} \qquad (4.10)$$

Since we have assumed that the DOA random variable $\hat{\theta}$ is Gaussian distributed, the perturbed array response vector $\hat{\mathbf{a}}$, which is given by the following expression:

$$\hat{\mathbf{a}} = \left[e^{-j\pi(x_1\cos\hat{\theta}+y_1\sin\hat{\theta})}, e^{-j\pi(x_2\cos\hat{\theta}+y_2\sin\hat{\theta})}, \ldots, e^{-j\pi(x_{N_A}\cos\hat{\theta}+y_{N_A}\sin\hat{\theta})}\right]^T \qquad (4.11)$$

has a rather complicated distribution. The perturbed interference-plus-noise covariance matrix $\hat{\mathbf{Q}}_{in}$, the weighted sum of the cross product of the perturbed interfering signal ARVs, has an even more complicated distribution because its elements are the sum of products of two correlated Gaussian random variables.

To obtain the distribution of the beamforming weight vector $\hat{\mathbf{w}} = \hat{\mathbf{Q}}_{in}^{-1}\hat{\mathbf{a}}(\theta)$, we need to invert the perturbed interference-plus-noise covariance matrix $\hat{\mathbf{Q}}_{in}$, then multiply it by the perturbed desired signal ARV. Since these operations are non-linear, it is very difficult to obtain analytical expressions for the distribution of the beamforming weight vector and compare the array performances analytically.

Due to this limitation, we use the Monte Carlo approach and make the assumption that the interfering signal DOAs are perfectly known. In other words, we only consider the effect of the imperfectly estimated desired signal DOA in this chapter and use the ideal interference-plus-noise covariance matrix in the beamforming weight vector calculations. The results presented, then, can be viewed as upper bounds to actual system performance.

4.3 Identical Users Scenario

In this section we consider the *Identical Users* scenario, where all users have the same incident power at the antenna array. In the first subsection, we discuss the distributions of the expected power pass through factors (PPTF) and system capacities. In the second subsection, we use the expected PPTF values to calculate and compare the user capacities of the arrays. Finally in the third subsection, we consider the relationship between the system capacity and the DOA estimation variance.

4.3.1 Distribution of the Expected Power Pass-Through Factors and System Capacities

The expressions for the expected power pass-through factor are identical to those defined in the last chapter, except that the DOAs are now random variables, and this

results in probability distributions of the power pass-through factors and the system capacities.

Recall that the energy-per-bit-to-noise ratio has the following expression:

$$\frac{E_b}{N_o} = \frac{E[\phi^{desired}]P_{signal}/R_{data}}{(E[\phi_k^{int}](M-1)P_{signal})/BW + N_A\sigma_n^2} \tag{4.12}$$

The distributions of the expected power pass-through factors (PPTF) $E[\phi^{desired}]$, $E[\phi_k^{int}]$ and the system capacities are approximated numerically based on assumed Gaussian distribution of the θ random variable. First we generate 1000 Gaussian distributed random θ values with variance equal to the CRB, then the corresponding $E[\phi^{desired}]$, $E[\phi_k^{int}]$ and capacity values are calculated for each trial.

As an example we calculate the $E[\phi^{desired}]$, $E[\phi_k^{int}]$ and capacity distributions when the true desired DOA is at 60 degrees and the coverage is omni-directional. The results are tabulated in histograms to indicate their approximate distributions, as shown in Figures (4.6), (4.7)and (4.8).

The distribution for the desired signal power pass-through factor $E[\phi^{desired}]$ shown in Figure (4.6) is one-sided because $E[\phi^{desired}]$ has an upper bound of 36 for arrays with 6 elements. Intuitively, the linear arrays, which has narrower beams, should have wider desired signal PPTF distributions due to DOA errors. But this is off-set by the lower CRB of the linear arrays.

The interfering signal PPTF $E[\phi_k^{int}]$ is determined by the beampattern sidelobe levels of each array. The linear arrays have lower sidelobe levels compare to the circular and triangular arrays, and this is confirmed by Figure (4.7).

Incorporating both $E[\phi^{desired}]$ and $E[\phi_k^{int}]$, we obtain capacity histograms in Figure (4.8). We observe that the linear arrays have higher capacities than the circular and triangular arrays, due to narrower beams in their beampatterns along the broad side. The linear arrays also produce narrower capacity distributions, due to lower DOA estimation variances.

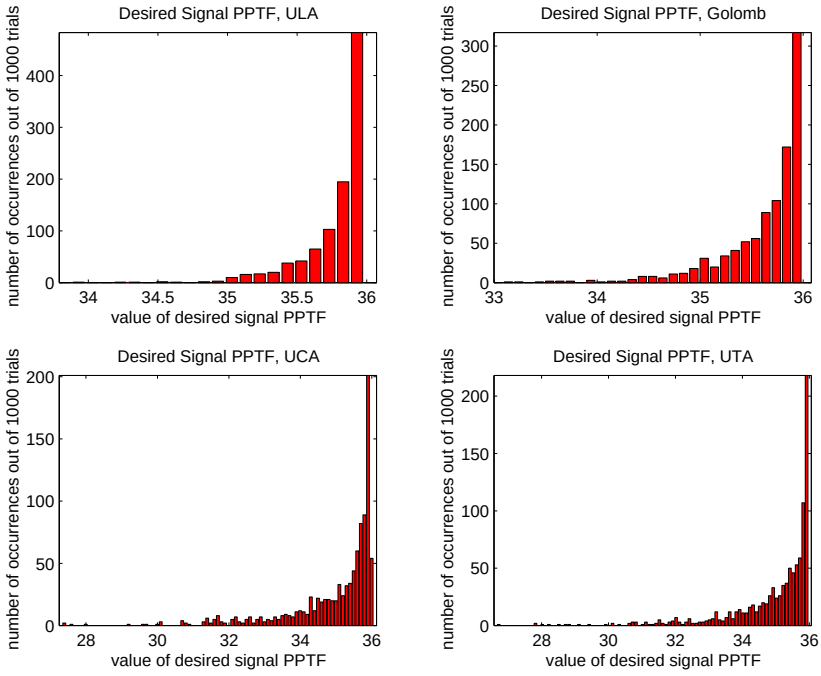

Figure 4.6: $E[\phi^{desired}]$ histogram with true desired DOA at 60 degrees

4.3.2 System Capacity Calculations

In this subsection, we calculate the average mean capacities over the angle range of coverage for the four arrays. For any given desired user DOA, we generate 1000 Monte Carlo trials, each with the estimated DOA represented by a Gaussian distributed

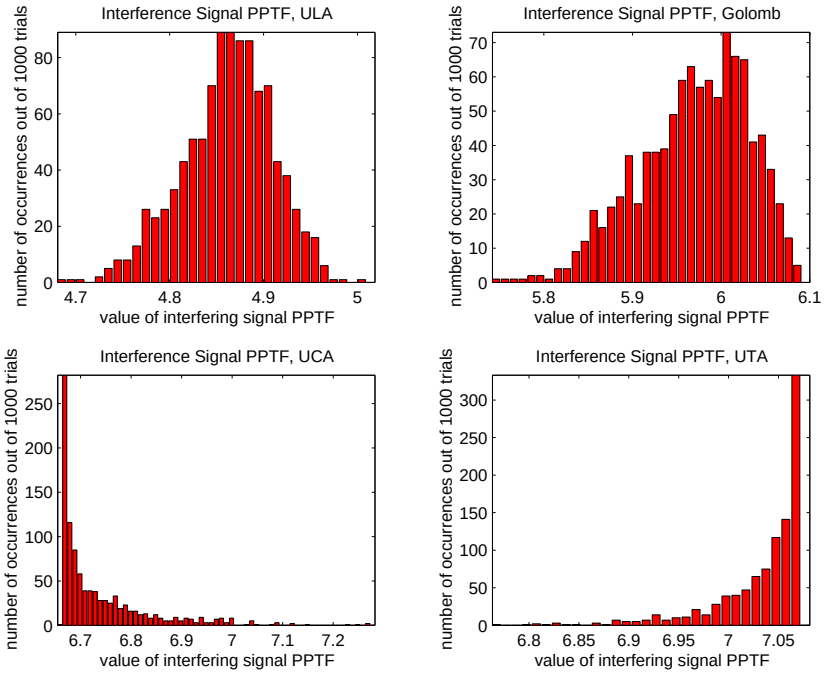

Figure 4.7: $E[\phi_k^{int}]$ histogram with true desired DOA at 60 degrees

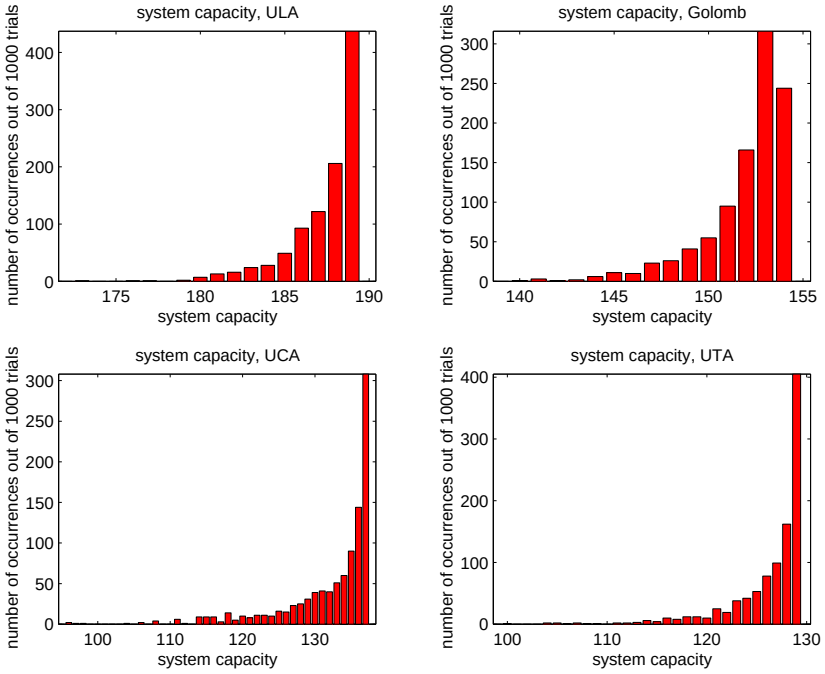

Figure 4.8: User Capacity histogram with true desired DOA at 60 degrees

random variable with variance given by the CRB. These DOAs are then used to calculate the beamforming weight vectors and the corresponding PPTF factors for the desired and interfering signal sources. The PPTF factors are then substituted into the Equation (4.13) to obtain the system capacity values.

$$\frac{E_b}{N_o} = \frac{E[\phi^{desired}]P_{signal}/R_{data}}{E[\phi_k^{int}](M-1)P_{signal}/BW + N_A\sigma_n^2} \tag{4.13}$$

The mean capacity for a given desired signal DOA is the mean capacity values over the 1000 trials. By repeating this process for all possible true desired DOAs, we can calculate the average of the mean capacities over the range of desired DOAs.

Recall that in order to calculate the user capacities we need the CRB values, but the CRB is a function of the incident SNR, which is a function of the number of interfering signals. We again tackle this problem by iterative calculation of the capacities. First we compute the mean capacities based on the capacities for the case of known DOAs as shown in Chapter Three, then we repeat the calculations using the capacity values obtained in the first calculation. The results are tabulated in Tables (4.1) and (4.2).

The two iterations of capacity calculations yield very similar results as shown in Tables (4.1) and (4.2). Thus we can conclude that the values in Table (4.2) are quite accurate.

To compare the estimated DOA results with the known DOA results, we compute the ratio of the capacities using estimated DOAs over the capacities using known DOAs, and the ratios are given in Table (4.3).

Array	ULA	Golomb	UCA	UTA
Capacity(120/120)	144.67	147.59	71.46	62.94
Capacity(120/360)	180.52	156.82	122.11	131.72
Capacity(360/360)	145.46	142.09	122.21	131.67

Table 4.1: The capacities for the Identical Users scenario based on known DOA Identical Users scenario capacities

Array	ULA	Golomb	UCA	UTA
Capacity(120/120)	144.69	147.60	71.47	62.95
Capacity(120/360)	180.51	156.83	122.11	131.71
Capacity(360/360)	145.47	142.06	122.20	131.67

Table 4.2: The iterated capacities for the Identical Users scenario based on previous Identical Users scenario capacities

From Table (4.2) we observe that the ULA has the highest capacities in the 120/360 case, and are roughly equal to the Golomb array in 120/120 and 360/360 cases. The circular and triangular arrays have poor performances for the 120/120 case as usual, but have fairly good performances in the 360/360 case. From Table (4.3) we observe that there is no significant capacity reduction due to DOA estimation for any of the arrays, but we note that this is a comparison using theoretical bounds, and practical signal processing algorithms may yield significantly different results.

Array	ULA	Golomb	UCA	UTA
Capacity(120/120)	99.69%	99.34%	99.59%	99.76%
Capacity(120/360)	99.49%	99.30%	98.43%	98.36%
Capacity(360/360)	99.31%	99.04%	98.43%	98.36%

Table 4.3: The ratio of capacities using estimated DOAs to the capacities using known DOAs

4.3.3 Relationship between System Capacities and the DOA Estimation Variance

Finally, we want to consider the relationship between the user capacities for the four arrays and the variances of the estimated DOAs. We repeat the calculations for the average capacity values across the whole range of DOA θ for cases where the DOA standard deviations equal 0.0316, 0.1, 0.316, 1, 3.16, 10, 31.6 and 100 degrees. The results are shown in Figures (4.9), (4.10) and (4.11).

In Figures (4.9), (4.10) and (4.11), we observe that the ULA has the best performance in all cases and DOA variance ranges, except at the very low variance values for the 120/120 case. Also, the capacities for the linear arrays start to decrease earlier than the circular and triangular arrays due to their narrower main beams and thus greater sensitivity to DOA estimation errors. The capacities of the Golomb array start to drop first due to its greatest sensitivity to DOA errors.

We also note that as the DOA variance increases, the capacities for all four arrays

approach 26, the system capacity without beamforming. This is intuitive since as the DOA variance increases, the effective beampattern approaches the omni-directional antenna pattern. Although the capacity curve for the Golomb array drops below those for the circular and triangular arrays for a significant range of DOA variance values , we note that for a fair comparison, the greater DOA resolution ability of the Golomb array need to be taken into account as well.

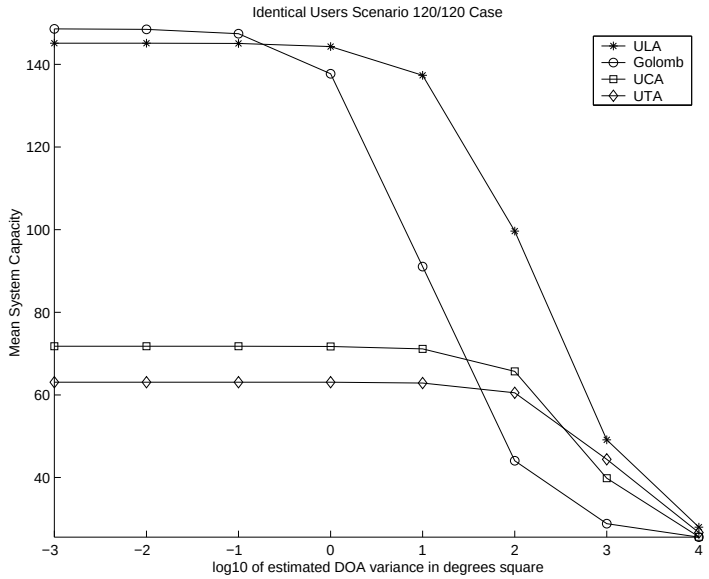

Figure 4.9: Average Capacity versus DOA variance for the Identical Users scenario 120/120 case

4.4 Multi-Rate Users Scenario

In this section we consider the *Multi-Rate Users* scenario, where some users have higher incident power at the antenna array due to higher data rate requirements. We

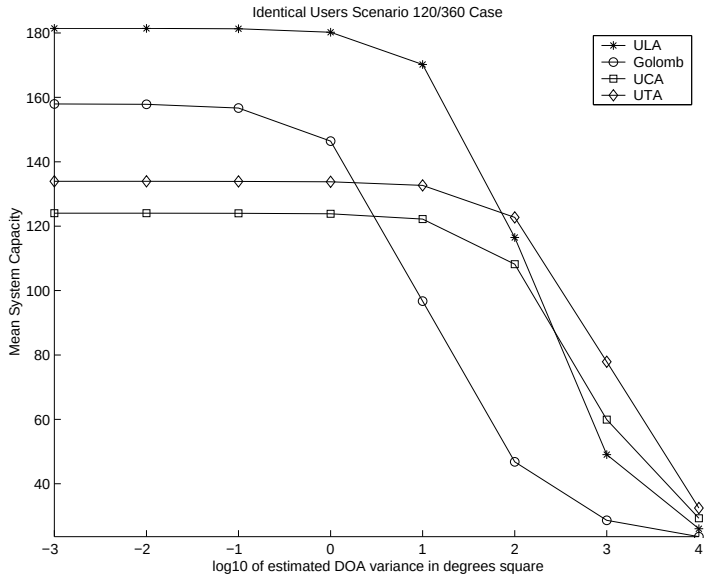

Figure 4.10: Average Capacity versus DOA variance for the Identical Users scenario 120/360 case

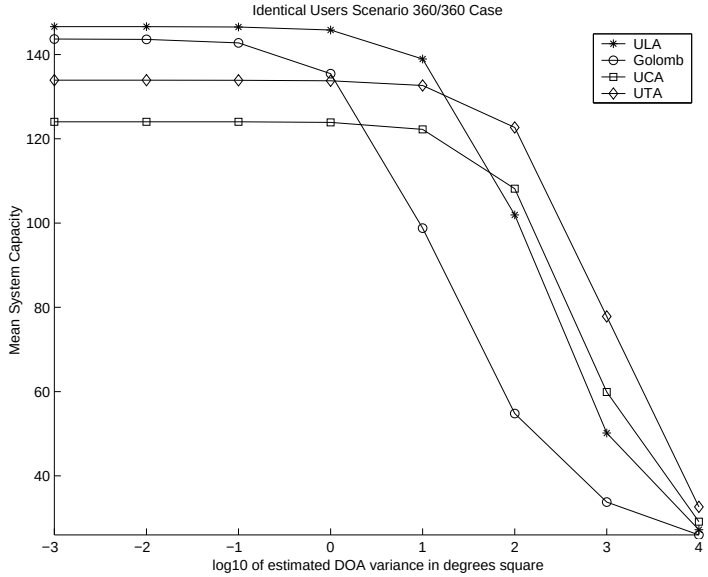

Figure 4.11: Average Capacity versus DOA variance for the Identical Users scenario 360/360 case

consider the cases where there is one or two high power interfering signals present in the system. We repeat the procedures shown in the previous section, first generate 100 Gaussian distributed DOA estimates with variances given by the CRB, and then calculate the corresponding expected power pass-through factor distributions $E[\phi^{desired}]$, $E[\phi_k^{int}]$ and $E[\phi_{hp}^{int}]$ as well as the system capacity distributions.

4.4.1 Distribution of the Expected Power Pass-Through Factors and System Capacities

As an example we calculate the $E[\phi^{desired}]$, $E[\phi_k^{int}]$, $E[\phi_{hp}^{int}]$ and capacity values using 1000 Monte Carlo trials for the case where the true desired DOA is at 60 degrees and the one high power interfering signal is at 120 degrees off the reference axis. The resulting 1000 $E[\phi^{desired}]$, $E[\phi_k^{int}]$, $E[\phi_{hp}^{int}]$ and capacity values are tabulated in histograms to indicate their approximate distributions, as shown in Figures (4.12), (4.13), (4.14) and (4.15).

Due to the interference-plus-noise covariance matrix factor in the calculation of the beamforming weight vector, the values of $E[\phi^{desired}]$ no longer have an upper bound of 36 as were the case for the *Identical Users* scenario. The resulting capacity distributions, however, show similar properties to the Identical Users scenario. The narrower beams of the linear arrays translate into higher capacities, and their lower CRBs on variances of estimated DOAs translate into narrower capacity distributions.

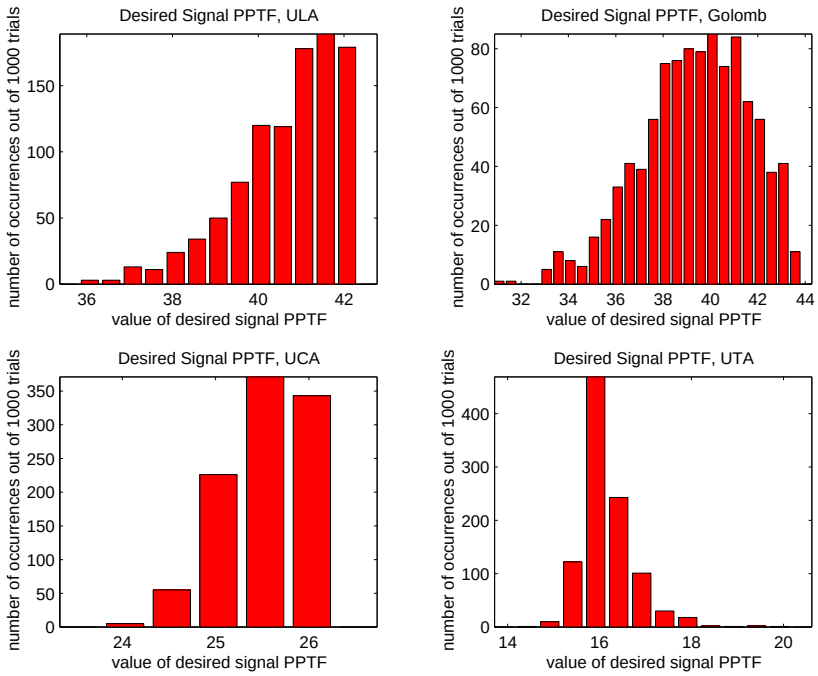

Figure 4.12: $E[\phi^{desired}]$ histogram with true desired DOA at 60 degrees

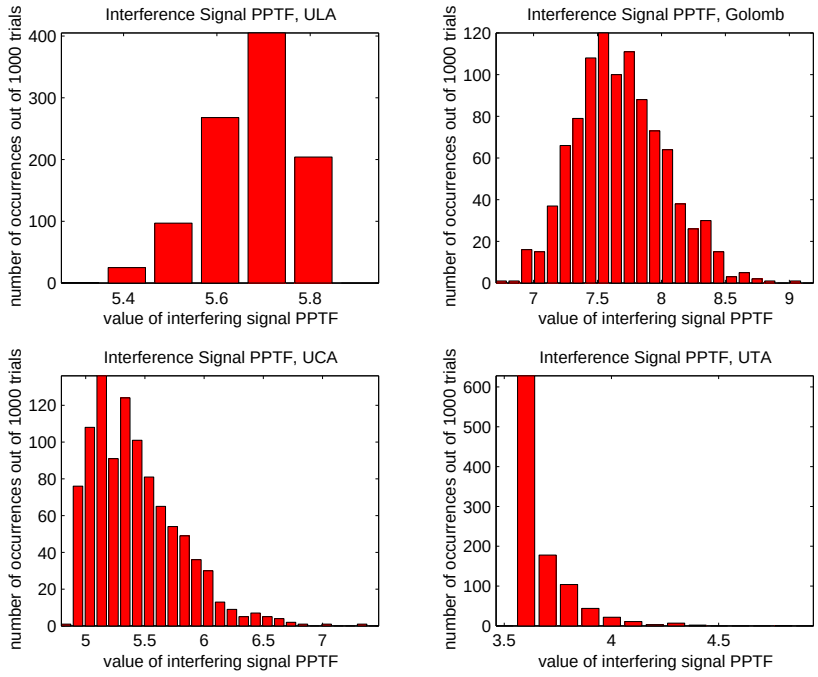

Figure 4.13: $E[\phi_k^{int}]$ histogram with true desired DOA at 60 degrees

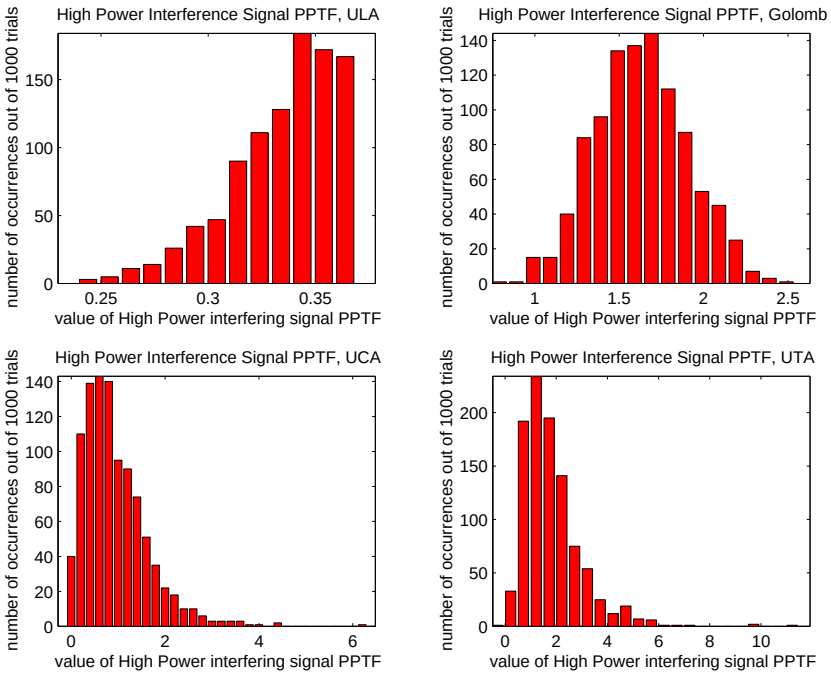

Figure 4.14: $E[\phi_{hp}^{int}]$ histogram with true desired DOA at 60 degrees

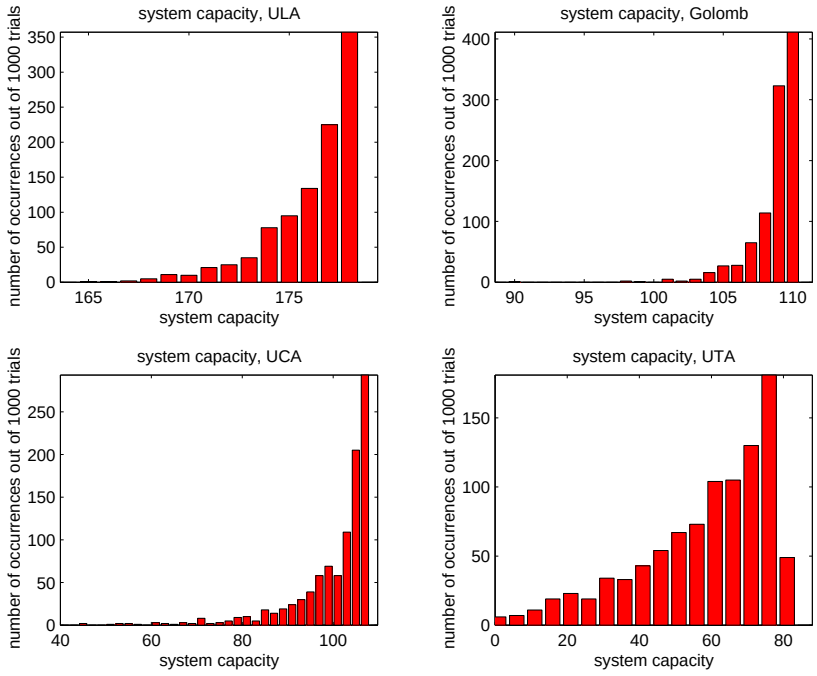

Figure 4.15: Capacity histogram with true desired DOA at 60 degrees

4.4.2 System Capacity Calculations

The calculation process is repeated for all permutations of desired signal and high power interfering signal DOAs. We first consider the case of a single high power interfering signal and calculate the PPTF factors and capacities at one-degree intervals. Again we calculate the user capacities in two iterations, first based on the multi-rate user capacities when the DOAs are known as shown in Section 3.3, then repeat the calculations using the capacities from the first iteration. The resulting capacity values are shown in Tables (4.4) and (4.5).

To compare the estimated DOA results with the known DOA results, we compute the ratio of the capacities using estimated DOAs over the capacities using known DOAs, and the ratios are given in Table (4.6).

As shown in Table (4.6), the capacity reductions due to estimated DOA are not significant. Recall that only 100 estimated DOAs are generated for each desired and interfering signal DOA combination, instead of 1000 trials each as in the identical-users case. This reduces the accuracy of the capacity calculations and this is evident for certain cases in Table (4.6).

When there are two high-power interfering signals present, the calculations for the PPTF factors and the system capacities are repeated for each DOA vector $[\theta_{desired}, \Theta_{highpower}]$. Due to time and memory constraints, we only calculate the PPTF factors and the capacities at ten degree intervals instead of one degree intervals as

Array	ULA	Golomb	UCA	UTA
Capacity(120/120)	118.90	113.45	53.58	42.21
Capacity(120/360)	152.08	123.46	100.75	103.95
Capacity(360/360)	119.10	110.42	100.94	104.61

Table 4.4: The capacities for the Multi-Rate users scenario based on known DOA Multi-Rate users scenario capacities

Array	ULA	Golomb	UCA	UTA
Capacity(120/120)	118.91	113.47	53.60	42.21
Capacity(120/360)	152.12	123.48	100.82	104.01
Capacity(360/360)	119.11	110.42	101.00	104.66

Table 4.5: The iterated capacities for the Multi-Rate users scenario based on previous Multi-Rate user scenario capacities

Array	ULA	Golomb	UCA	UTA
Capacity(120/120)	99.16%	99.32%	100.78%	101.55%
Capacity(120/360)	97.86%	99.54%	100.00%	98.93%
Capacity(360/360)	97.96%	99.34%	100.05%	99.57%

Table 4.6: The ratio of capacities using estimated DOAs to the capacities with known DOAs, when a single high power interfering signal is present

was done previously. For comparison purposes, we repeat the single high power interfering signal case at ten degree intervals. The results are tabulated in Tables (4.7) and (4.8).

From Table (4.7), we observe that the differences in the average capacities when using 10 degree and 1 degree intervals for calculation can be up to about 9%, this is for the triangular array in the 120/120 scenario. Thus the results in Table (4.8) can only be taken as rough estimates of the actual capacities of the four arrays.

Data in Table (4.8) indicate that the Golomb array has lower capacities than the ULA, and is only better than the circular and the triangular arrays in the 120/120 scenario. More importantly, the percentage drop values of the capacities from the one high power user capacities indicate that the Golomb array is the worst of the four in dealing with additional high power interfering signals.

4.4.3 Relationship between System Capacities and the DOA Estimation Variance

Finally, we want to consider the relationship between the average capacities for the four arrays across all angles and the variance of the estimated DOA when there is one high power interfering signal present. We repeat the calculations for the average capacity values across the whole range of DOA θ for cases where the DOA standard deviations equal 0.0316, 0.1, 0.316, 1, 3.16, 10, 31.6 and 100 degrees. The results are shown in Figures (4.16), (4.17) and (4.18).

Array	ULA	Golomb	UCA	UTA
Capacity(120/120)	123.28	106.91	56.47	46.17
Δ from 1 degree intervals	3.7%	-5.8%	5.4%	9.4%
Capacity(120/360)	146.19	114.63	96.99	102.80
Δ from 1 degree intervals	-3.9%	-7.2%	-3.8%	-1.2%
Capacity(360/360)	118.37	102.52	99.61	103.79
Δ from 1 degree intervals	-0.6%	-7.2%	-1.4%	-0.8%

Table 4.7: The capacities for the Multi-Rate users scenario when one high power interfering signals is present, calculated at 10 degree intervals, and the capacity variations compare to the one degree interval case

Array	ULA	Golomb	UCA	UTA
Capacity(120/120)	96.46	66.72	34.79	30.66
Δ from 1 HP case	-21.8%	-37.6%	-38.4%	-33.6%
Capacity(120/360)	117.90	73.79	70.74	74.31
Δ from 1 HP case	-19.4%	-35.6%	-27.1%	-27.7%
Capacity(360/360)	93.46	67.57	73.46	75.00
Δ from 1 HP case	-21.0%	-34.1%	-26.2%	-27.7%

Table 4.8: The capacities for the Multi-Rate users scenario when two high power interfering signals are present, calculated at 10 degree intervals, and the capacity reductions compare to the one high power interfering signal case

The capacity-vs-variance plots show exactly the same general trend as the identical-users scenario capacity-vs-variance plots, where the capacities for the linear arrays start to decrease at lower desired signal DOA variance values than the planar arrays. We observe that compare to the Identical-Users scenarios, the Multi-rate Users scenarios have higher capacities at large desired signal DOA variance values. This can be explained by noting that for large desired signal DOA variance values, the effective beampatterns for the Identical-Users scenarios are roughly uniform across all directions, resulting in no suppression for any low power interfering signals. For the Multi-rate Users scenarios, the high power interfering signals, whose DOAs are assumed to be known exactly, are suppressed along with low power interfering signals in their vicinity, resulting in higher capacities than the Identical Users scenario.

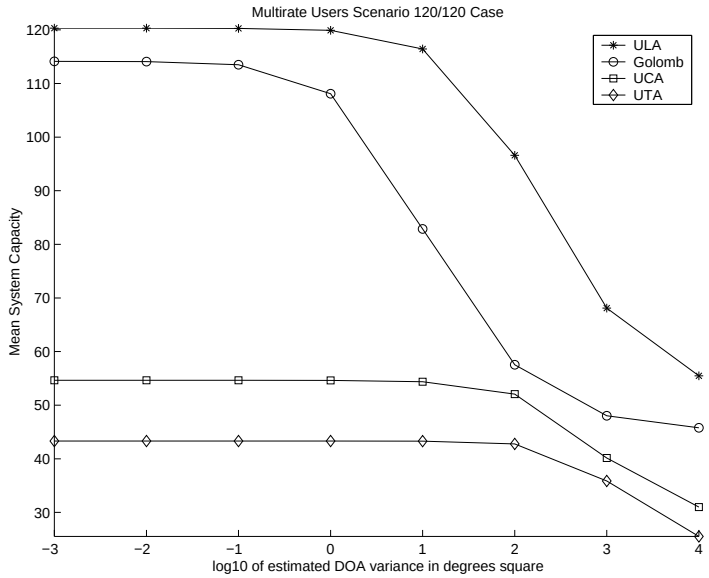

Figure 4.16: Average Capacity versus DOA variance for the Multi-Rate users scenario 120/120 case

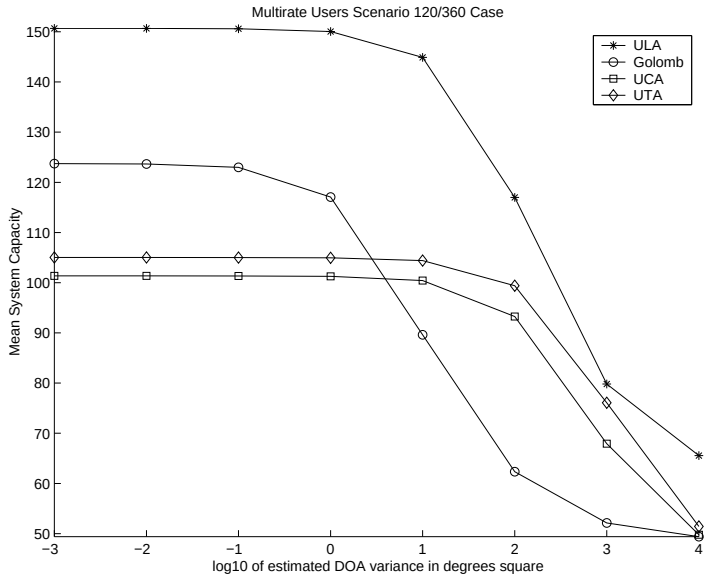

Figure 4.17: Average Capacity versus DOA variance for the Multi-Rate users scenario 120/360 case

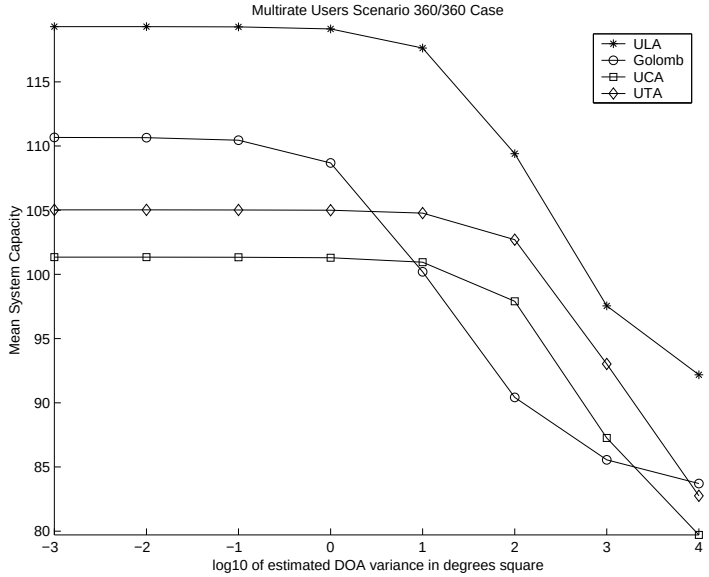

Figure 4.18: Average Capacity versus DOA variance for the Multi-Rate users scenario 360/360 case

4.5 Chapter Summary and Discussion

In this chapter we investigated the effects of several base-station antenna array geometries on the performance of a wireless communication system, with the assumption that the estimated desired signal direction of arrival has Gaussian distribution with known variance. The variances of the DOA distributions were determined by the Cramer Rao Lower Bound based on the various array geometries.

In the *Identical Users* scenario, we considered the desired signal DOA as a Gaussian distributed random variable, and the resulting average user capacities are tabulated in Table (4.2). Based on the results shown in Table (4.3) we conclude that beamforming with slightly perturbed desired signal DOAs does not significantly reduce the user capacities for the four arrays under consideration, and the effects are in the one to two percent range. At the same time, we recognize that this result is based on the lower bound on the estimated DOA variance, and actual array performances using available spatial processing algorithms will yield larger reductions in user capacities.

In the *Multi-Rate Users* scenario, we considered the desired signal DOA as a Gaussian distributed random variable, but the interference signal DOAs are assumed to be perfectly known. We again calculated the expected power pass-through factors and the corresponding system capacities for the different array geometries, and the results are tabulated in Table (4.5). Due to time and memory constraints, only 100 samples were generated to approximate the Gaussian distributed estimated DOAs, and this

results in some reduction in calculation accuracy. Nevertheless, we observe that as in the identical-users scenario, the effect of beamforming using slightly perturbed DOAs is small, resulting in roughly one to two percent reduction in user capacities.

We then consider the case where there are two high power interfering signals in the system. Base on the results shown in Table (4.8), we conclude that the Golomb array does not provide higher user capacities when there are two high power interfering signals in the system. In fact the results indicate that the Golomb array suffers the most capacity reduction when the number of high power interfering signals is increased from one to two.

Base on the results obtained in this chapter, we conclude that when the desired user DOA needs to be estimated, we can expect one to two percent reduction in user capacities in the best circumstances. Among the four antenna arrays under consideration, the uniform linear array has the best all around performance, being surpassed by the Golomb array only in a select few circumstances. The circular and the triangular arrays are particularly unsuitable to sector coverage; in omni-directional coverage situations they have better performances but still trail behind the linear arrays. The Golomb array, while having superior ability in distinguishing two closely located users, does not have performance advantage over the ULA. It might, however, find application where the angle range of coverage is small and the users are all fairly close to each other.

Chapter 5

The Perturbed Output SINR Approach and Further Array Comparisons

5.1 Introduction

In the previous chapters, we have adapted a brute force approach to the problem of estimating system capacities of different arrays in various scenarios. While this approach can yield accurate approximations to the expected system capacities, it is quite computationally intensive, and thus restricts the scope of the performance comparison possible. In this chapter, we consider the perturbed output SINR approach to system capacity estimation, as well as the effects of increasing number of high power interfering signals on the capacities.

5.1.1 Chapter Outline

This chapter has two sections. In the first section, we consider the perturbed output SINR approach and its application to system capacity estimation. In the second section, we consider the effect of increasing number of high power interfering signals in the system on the system capacities.

The first section is separated into four subsections, first we outline the perturbed output SINR results assuming independent incident signals at the array elements as obtained by T. Luo [32], then we derive the perturbed output SINR expression while taking correlations between the incident signals at the array elements into account, thirdly we compare the capacity results yielded by both models to the values obtained in Chapter Four, and finally we consider the relationship between the system capacities and the desired signal DOA variance.

In the second section we consider the effect of increasing number of high power interfering signals. This section is separated into two subsections, first we present the relationship between the system capacity and the desired signal DOA, then we consider the relationship between the system capacity and the number of high power interfering signals.

5.2 Perturbed Output SINR Due to Desired Signal ARV Perturbations

Approximating system user capacities for the arrays using the Monte Carlo method as described in the last chapter is quite computationally expensive, and we want to reduce the computational requirement of system capacity approximation through analysis. One way to do this is to extend known perturbed output SINR expressions and relate the output SINR to user capacities. In this section, we extend the work of T. Luo [32] to include considerations for correlated ARV perturbations. This is desirable since our signal model, which is a function of the desired signal DOA, yields correlated ARV elements.

5.2.1 The Uncorrelated ARV Perturbation Model

In the course of his investigations, T. Luo considered the effects of perturbations in ARV $\mathbf{a}(\theta)$ and the interference-plus-noise covariance matrix $\mathbf{Q}_{in}$ on the output SINR of a beamformer [32]. The perturbation of $\mathbf{a}(\theta)$ is modeled as $\hat{\mathbf{a}}(\theta) = \mathbf{a}(\theta) + \eta$ where $E[\eta] = 0$ and $E[\eta_i \eta_i^H] = \sigma_a^2 \delta_i \delta_j$, which means $E\{\eta\eta^H\} = \sigma_a^2 \mathbf{I}$ where $\mathbf{I}$ is the identity matrix. The perturbation of $\mathbf{Q}_{in}$ is modeled as $\hat{\mathbf{Q}}_{in} = \mathbf{Q}_{in} + \varepsilon$ where $\varepsilon = \varepsilon^H$, $E[\varepsilon] = 0$ and $E[\varepsilon_{i,j} \varepsilon_{k,l}^H] = \sigma_\omega^2 \delta_{i,k} \delta_{j,l}$, which means $E\{\varepsilon\varepsilon^H\} = N_A \sigma_\omega^2 \mathbf{I}$, where N_A is the number of antenna elements. Further more, it was assumed that the perturbation of $\mathbf{a}(\theta)$ is independent of the perturbation of $\mathbf{Q}_{in}$.

The resulting perturbed output SINR expression is given by the following expression [32]:

$$\widehat{SINR} = \frac{E\{\|\hat{\mathbf{w}}^H\mathbf{a}\|^2\}}{E\{\hat{\mathbf{w}}^H\mathbf{Q}_{in}\hat{\mathbf{w}}\}} = \frac{(\mathbf{a}^H\mathbf{Q}_{in}^{-1}\mathbf{a})^2 + \sigma_a^2\|\mathbf{Q}_{in}^{-1}\mathbf{a}\|^a + \sigma_\omega^2\|\mathbf{Q}^{-1}\mathbf{a}\|^4}{\mathbf{a}^H\mathbf{Q}_{in}^{-1}\mathbf{a} + \sigma_a^2 Tr\{\mathbf{Q}_{in}^{-1}\} + \sigma_\omega^2\|\mathbf{Q}_{in}^{-1}\mathbf{a}\|^2 Tr\{\mathbf{Q}_{in}^{-1}\}} \quad (5.1)$$

For the multi-rate users case, we assume the the high power interfering signal DOAs are known and thus $\mathbf{Q}_{in}$ is unperturbed. The Equation (5.1) is then simplified into:

$$\widehat{SINR} = \frac{(\mathbf{a}^H\mathbf{Q}_{in}^{-1}\mathbf{a})^2 + \sigma_a^2\|\mathbf{Q}_{in}^{-1}\mathbf{a}\|^2}{\mathbf{a}^H\mathbf{Q}_{in}^{-1}\mathbf{a} + \sigma_a^2 Tr\{\mathbf{Q}^{-1}\}} \quad (5.2)$$

For the identical-users case, we treat all interfering signals as noise and thus $\mathbf{Q}_{in}$ is a scalar multiple of the identity matrix $\mathbf{I}$. The Equation (5.1) is then simplified into [32]:

$$\widehat{SINR} = SINR_{unperturbed}\frac{1 + \frac{1}{N_A}\sigma_a^2}{1 + \sigma_a^2} \quad (5.3)$$

5.2.2 The Correlated ARV Perturbation Model

In Luo's perturbation model, it was assumed that the perturbations of the ARV elements are uncorrelated and thus the perturbed ARV can be represented by $\hat{\mathbf{a}}(\theta) = \mathbf{a}(\theta) + \eta$ where $E\{\eta\eta^H\} = \sigma_a^2\mathbf{I}$. But for the line-of-sight beamforming system we are considering, the perturbations in ARV elements are functions of the perturbation in DOA, resulting in correlated perturbations for the ARV elements. In this case, the correlated ARV perturbations can be represented by the expression $\hat{\mathbf{a}}(\theta) = \mathbf{a}(\theta) + \eta$ where $E\{\eta\eta^H\} = \mathbf{C}_\eta$.

Recall the expression of the output Signal to Interference and Noise Ratio:

$$\widehat{SINR} = \frac{P^{out}_{desiredsignal}}{P^{out}_{interferencesignal} + P^{out}_{noise}} = \frac{E\{\|\hat{\mathbf{w}}^H \mathbf{a}\|^2\}}{E\{\hat{\mathbf{w}}^H \mathbf{Q} \hat{\mathbf{w}}\}} \tag{5.4}$$

where $\hat{\mathbf{w}}$ is the maximum SINR beamforming weight base on the estimated array response vector $\hat{\mathbf{a}}$, $\mathbf{Q}$ is the true interference plus noise covariance matrix, and $\mathbf{a}$ is the true array response vector.

We want to derive the expression for the perturbed $\widehat{SINR}$ due to perturbations in both $\mathbf{a}$ and $\mathbf{Q}$. The perturbation in $\mathbf{Q}$ is still modeled as $\hat{\mathbf{Q}} = \mathbf{Q} + \varepsilon$, where $\varepsilon = \varepsilon^H$, $E[\varepsilon] = 0$ and $E[\varepsilon_{i,j}\varepsilon^H_{k,l}] = \sigma^2_\omega \delta_{i,j}\delta_{k,l}$, which means $E\{\varepsilon\varepsilon^H\} = M\sigma^2_\omega \mathbf{I}$, and $\hat{\mathbf{Q}}^{-1} \simeq \mathbf{Q}^{-1} - \mathbf{Q}^{-1}\varepsilon\mathbf{Q}^{-1}$. The perturbation in $\mathbf{a}$ is modeled as $\hat{\mathbf{a}} = \mathbf{a} + \eta$, and $E\{\eta\eta^H\} = E\{\hat{\mathbf{a}}\hat{\mathbf{a}}^H\} - E\{\mathbf{a}\mathbf{a}^H\} = \mathbf{C}_\eta$.

Since the beamforming weights that maximizes the output SINR has the expression $\hat{\mathbf{w}} = \hat{\mathbf{Q}}^{-1}\hat{\mathbf{a}}$, thus

$$\hat{\mathbf{w}}^H \mathbf{a} = \hat{\mathbf{a}}^H \hat{\mathbf{Q}}^{-1}\mathbf{a} = \hat{\mathbf{a}}^H \mathbf{Q}\mathbf{a} - \hat{\mathbf{a}}^H \mathbf{Q}^{-1}\varepsilon\mathbf{Q}^{-1}\mathbf{a} \tag{5.5}$$

and

$$(\hat{\mathbf{w}}^H \mathbf{a})^H = \mathbf{a}^H \hat{\mathbf{Q}}^{-1}\hat{\mathbf{a}} = \mathbf{a}^H \mathbf{Q}\hat{\mathbf{a}} - \hat{\mathbf{a}}^H \mathbf{Q}^{-1}\varepsilon\mathbf{Q}^{-1}\hat{\mathbf{a}} \tag{5.6}$$

thus

$$\begin{aligned} \|\hat{\mathbf{w}}^H \mathbf{a}\|^2 &= (\hat{\mathbf{w}}^H \mathbf{a})^H (\hat{\mathbf{w}}^H \mathbf{a}) \\ &= \mathbf{a}^H \mathbf{Q}^{-1}\hat{\mathbf{a}}\hat{\mathbf{a}}^H \mathbf{Q}^{-1}\mathbf{a} - \mathbf{a}\mathbf{Q}^{-1}\varepsilon\mathbf{Q}^{-1}\hat{\mathbf{a}}\hat{\mathbf{a}}^H \mathbf{Q}^{-1}\mathbf{a} \\ &- \mathbf{a}^H \mathbf{Q}^{-1}\hat{\mathbf{a}}\hat{\mathbf{a}}^H \mathbf{Q}^{-1}\varepsilon\mathbf{Q}^{-1}\mathbf{a} + \mathbf{a}^H \mathbf{Q}^{-1}\varepsilon\mathbf{Q}^{-1}\hat{\mathbf{a}}\hat{\mathbf{a}}^H \mathbf{Q}^{-1}\varepsilon\mathbf{Q}^{-1}\mathbf{a} \end{aligned} \tag{5.7}$$

so the numerator of the $\widehat{SINR}$ expression becomes

$$
\begin{aligned}
& E\{\|\hat{\mathbf{w}}^H\mathbf{a}\|^2\} = E\{(\hat{\mathbf{w}}^H\mathbf{a})^H(\hat{\mathbf{w}}^H\mathbf{a})\} \\
= \; & E\{\mathbf{a}^H\mathbf{Q}^{-1}\hat{\mathbf{a}}\hat{\mathbf{a}}^H\mathbf{Q}^{-1}\mathbf{a}\} - \underbrace{E\{\mathbf{a}\mathbf{Q}^{-1}\varepsilon\mathbf{Q}^{-1}\hat{\mathbf{a}}\hat{\mathbf{a}}^H\mathbf{Q}^{-1}\mathbf{a}\}}_{\to 0} \\
- \; & \underbrace{E\{\mathbf{a}^H\mathbf{Q}^{-1}\hat{\mathbf{a}}\hat{\mathbf{a}}^H\mathbf{Q}^{-1}\varepsilon\mathbf{Q}^{-1}\mathbf{a}\}}_{\to 0} + E\{\mathbf{a}^H\mathbf{Q}^{-1}\varepsilon\mathbf{Q}^{-1}\hat{\mathbf{a}}\hat{\mathbf{a}}^H\mathbf{Q}^{-1}\varepsilon\mathbf{Q}^{-1}\mathbf{a}\} \\
= \; & \mathbf{a}^H\mathbf{Q}^{-1}(\mathbf{a}\mathbf{a}^H + \mathbf{C}_\eta)\mathbf{Q}^{-1}\mathbf{a} + \underbrace{E\{\mathbf{a}^H\mathbf{Q}^{-1}\varepsilon\mathbf{Q}^{-1}(\mathbf{a}\mathbf{a}^H + \mathbf{C}_\eta)\mathbf{Q}^{-1}\varepsilon\mathbf{Q}^{-1}\mathbf{a}\}}_{expression1} \qquad (5.8)
\end{aligned}
$$

noting that $E\{\varepsilon\} = 0$. At this point, we refer to lemma (4.21) in [32]

$$E\{(\varepsilon\mathbf{Q}^{-1}\mathbf{a})(\varepsilon\mathbf{Q}^{-1}\mathbf{a})^H\} = \sigma_\omega^2\|\mathbf{Q}^{-1}\mathbf{a}\|^2\mathbf{I} \qquad (5.9)$$

and the second term in the previous expression becomes:

$$
\begin{aligned}
expression1 \; &= \; E\{\mathbf{a}^H\mathbf{Q}^{-1}\varepsilon\mathbf{Q}^{-1}\mathbf{a}\mathbf{a}^H\mathbf{Q}^{-1}\varepsilon\mathbf{Q}^{-1}\mathbf{a}\} + E\{\mathbf{a}^H\mathbf{Q}^{-1}\varepsilon\mathbf{Q}^{-1}\mathbf{C}_\eta\mathbf{Q}^{-1}\varepsilon\mathbf{Q}^{-1}\mathbf{a}\} \\
&= \; E\{(\varepsilon\mathbf{Q}^{-1}\mathbf{a})^H\mathbf{Q}^{-1}\mathbf{a}\mathbf{a}^H\mathbf{Q}^{-1}(\varepsilon\mathbf{Q}^{-1}\mathbf{a})\} + E\{(\varepsilon\mathbf{Q}^{-1}\mathbf{a})^H\mathbf{Q}^{-1}\mathbf{C}_\eta\mathbf{Q}^{-1}(\varepsilon\mathbf{Q}^{-1}\mathbf{a})\} \\
&= \; \sigma_\omega^2\|\mathbf{Q}^{-1}\mathbf{a}\|^4 + \underbrace{\mathbf{C}_\eta\sigma_\omega^2}_{\to 0}\|\mathbf{Q}^{-1}\mathbf{a}\|^2 Tr(\mathbf{Q}^{-1}\mathbf{Q}^{-1}) \qquad (5.10)
\end{aligned}
$$

where the second order perturbation term is approximately zero. Substitute this expression into equation (5.8):

$$
\begin{aligned}
E\{\|\hat{\mathbf{w}}^H\mathbf{a}\|^2\} &= \mathbf{a}^H\mathbf{Q}^{-1}(\mathbf{a}\mathbf{a}^H + \mathbf{C}_\eta)\mathbf{Q}^{-1}\mathbf{a} + \sigma_\omega^2\|\mathbf{Q}^{-1}\mathbf{a}\|^4 \\
&= (\mathbf{a}^H\mathbf{Q}^{-1}\mathbf{a})^2 + \mathbf{a}^H\mathbf{Q}^{-1}\mathbf{C}_\eta\mathbf{Q}^{-1}\mathbf{a} + \sigma_\omega^2\|\mathbf{Q}^{-1}\mathbf{a}\|^4 \qquad (5.11)
\end{aligned}
$$

For the expression of the output SINR, we also need the expression for the denominator:

$$
\begin{aligned}
\hat{\mathbf{w}}^H\mathbf{Q}\hat{\mathbf{w}} &= \hat{\mathbf{a}}^H\hat{\mathbf{Q}}^{-1}\mathbf{Q}\hat{\mathbf{Q}}^{-1}\hat{\mathbf{a}} \\
&= \hat{\mathbf{a}}^H(\mathbf{Q}^{-1} - \mathbf{Q}^{-1}\varepsilon\mathbf{Q}^{-1})\mathbf{Q}(\mathbf{Q}^{-1} - \mathbf{Q}^{-1}\varepsilon\mathbf{Q}^{-1})\hat{\mathbf{a}} \\
&= \hat{\mathbf{a}}^H\mathbf{Q}^{-1}\hat{\mathbf{a}} - 2\hat{\mathbf{a}}^H\mathbf{Q}^{-1}\varepsilon\mathbf{Q}^{-1}\hat{\mathbf{a}} + \hat{\mathbf{a}}^H\mathbf{Q}^{-1}\varepsilon\mathbf{Q}^{-1}\varepsilon\mathbf{Q}^{-1}\hat{\mathbf{a}} \qquad (5.12)
\end{aligned}
$$

taking the expected value

$$\begin{aligned} E\{\hat{\mathbf{w}}^H\mathbf{Q}\hat{\mathbf{w}}\} &= E\{\hat{\mathbf{a}}^H\mathbf{Q}^{-1}\hat{\mathbf{a}}\} - \underbrace{2E\{\hat{\mathbf{a}}^H\mathbf{Q}^{-1}\varepsilon\mathbf{Q}^{-1}\hat{\mathbf{a}}\}}_{\to 0} + E\{\hat{\mathbf{a}}^H\mathbf{Q}^{-1}\varepsilon\mathbf{Q}^{-1}\varepsilon\mathbf{Q}^{-1}\hat{\mathbf{a}}\} \\ &= Tr\{(\mathbf{a}\mathbf{a}^H + \mathbf{C}_\eta)\mathbf{Q}^{-1}\} + Tr\{(\mathbf{a}\mathbf{a}^H + \mathbf{C}_\eta)E\{\mathbf{Q}^{-1}\varepsilon\mathbf{Q}^{-1}\varepsilon\mathbf{Q}^{-1}\}\} \\ &= \mathbf{a}^H\mathbf{Q}^{-1}\mathbf{a} + Tr\{\mathbf{C}_\eta\mathbf{Q}^{-1}\} + Tr\{\mathbf{a}\mathbf{a}^H E\{\mathbf{Q}^{-1}\varepsilon\mathbf{Q}^{-1}\varepsilon\mathbf{Q}^{-1}\}\} \\ &+ Tr\{\mathbf{C}_\eta E\{\mathbf{Q}^{-1}\varepsilon\mathbf{Q}^{-1}\varepsilon\mathbf{Q}^{-1}\}\} \end{aligned} \tag{5.13}$$

notice that the expectation value of ε is zero. By ignoring the last term which includes the product of two perturbation terms $\mathbf{C}_\eta$ and ε, and referring to equation (4.52) in [32], we obtain:

$$E\{\hat{\mathbf{w}}^H\mathbf{Q}\hat{\mathbf{w}}\} = \mathbf{a}^H\mathbf{Q}^{-1}\mathbf{a} + Tr\{\mathbf{C}_\eta\mathbf{Q}^{-1}\} + \sigma_\omega^2\|\mathbf{Q}^{-1}\mathbf{a}\|^2 Tr\{\mathbf{Q}^{-1}\} \tag{5.14}$$

so the perturbed output SINR becomes

$$\widehat{SINR} = \frac{E\{\|\hat{\mathbf{w}}^H\mathbf{a}\|^2\}}{E\{\hat{\mathbf{w}}^H\mathbf{Q}_{in}\hat{\mathbf{w}}\}} = \frac{(\mathbf{a}^H\mathbf{Q}_{in}^{-1}\mathbf{a})^2 + \mathbf{a}^H\mathbf{Q}_{in}^{-1}\mathbf{C}_\eta\mathbf{Q}_{in}^{-1}\mathbf{a} + \sigma_\omega^2\|\mathbf{Q}_{in}^{-1}\mathbf{a}\|^4}{\mathbf{a}^H\mathbf{Q}_{in}^{-1}\mathbf{a} + Tr\{\mathbf{C}_\eta\mathbf{Q}^{-1}\} + \sigma_\omega^2\|\mathbf{Q}_{in}^{-1}\mathbf{a}\|^2 Tr\{\mathbf{Q}_{in}^{-1}\}} \tag{5.15}$$

where $\mathbf{C}_\eta$ is given by Equation (B.7) in Appendix B.

For the multi-rate users case, we assume the the high power interfering signal DOAs are known and that $\mathbf{Q}_{in}$ is unperturbed. The Equation (5.15) is then simplified into:

$$\widehat{SINR} = \frac{(\mathbf{a}^H\mathbf{Q}_{in}^{-1}\mathbf{a})^2 + \mathbf{a}^H\mathbf{Q}_{in}^{-1}\mathbf{C}_\eta\mathbf{Q}_{in}^{-1}\mathbf{a}}{\mathbf{a}^H\mathbf{Q}_{in}^{-1}\mathbf{a} + Tr\{\mathbf{C}_\eta\mathbf{Q}_{in}^{-1}\}} \tag{5.16}$$

For the identical-users case, we treat all interfering signals as noise and thus $\mathbf{Q}_{in} = \sigma^2\mathbf{I}$. The Equation (5.15) can be simplified as:

$$\widehat{SINR} = \frac{(\mathbf{a}^H\mathbf{Q}_{in}^{-1}\mathbf{a})^2 + \mathbf{a}^H\mathbf{Q}_{in}^{-1}\mathbf{C}_\eta\mathbf{Q}_{in}^{-1}\mathbf{a}}{\mathbf{a}^H\mathbf{Q}_{in}^{-1}\mathbf{a} + Tr\{\mathbf{C}_\eta\mathbf{Q}^{-1}\}} = \frac{\frac{1}{\sigma^4}N_A^2 + \frac{1}{\sigma^4}\mathbf{a}^H\mathbf{C}_\eta\mathbf{a}}{\frac{1}{\sigma^2}N_A + \frac{1}{\sigma^2}Tr\{\mathbf{C}_\eta\}} \tag{5.17}$$

because $\mathbf{a}^H\mathbf{a} = \|\mathbf{a}\|^2 = N_A$ and $SINR_{unperturbed} = \frac{(\mathbf{a}^H\mathbf{Q}_{in}^{-1}\mathbf{a})^2}{\mathbf{a}^H\mathbf{Q}_{in}^{-1}\mathbf{a}} = \mathbf{a}^H\mathbf{Q}^{-1}\mathbf{a} = \frac{N_A}{\sigma^2}$,

$$\widehat{SINR} = \frac{N_A}{\sigma^2}\frac{\frac{N_A}{\sigma^2} + \frac{1}{N_A\sigma^2}\mathbf{a}^H\mathbf{C}_\eta\mathbf{a}}{\frac{N_A}{\sigma^2} + \frac{1}{\sigma^2}Tr\{\mathbf{C}_\eta\}} = SINR_{unperturbed}\frac{1 + \frac{1}{N_A^2}\mathbf{a}^H\mathbf{C}_\eta\mathbf{a}}{1 + \frac{1}{N_A}Tr\{\mathbf{C}_\eta\}} \tag{5.18}$$

5.2.3 Perturbed User Capacities

In the previous section we obtained the expression of the perturbed output SINR when the perturbations of the ARV elements are correlated. Now we want to relate the output SINR to the system user capacity.

Recall the system capacities are calculated base on the energy-per-bit-to-noise-ratio expression:

$$\frac{E_b}{N_o} = \frac{E[\phi^{desired}]P_{signal}/R_{data}}{\left(\underbrace{E[\phi_k^{int}](M-1-M_{high-power})P_{signal}}_{low-power-interference} + \underbrace{\sum_{hp=1}^{M_{high-power}} E[\phi_{hp}^{int}]P_{hp}}_{high-power-interference}\right)/BW + N_A\sigma_n^2} \tag{5.19}$$

and

$$\frac{E_b}{N_o} = \frac{128E[\phi^{desired}]P_{signal}}{\underbrace{\sum_{k=1}^{M_{low-power}} E[\phi_k^{int}]P_{signal}}_{low-power-interference} + \underbrace{\sum_{hp=1}^{M_{high-power}} E[\phi_{hp}^{int}]P_{hp}}_{high-power-interference} + N_A\sigma_n^2 BW} \propto \frac{E\{\|\hat{\mathbf{w}}^H\mathbf{a}\|^2\}}{E\{\hat{\mathbf{w}}^H\mathbf{Q}_{in}\hat{\mathbf{w}}\}} = \widehat{SINR} \tag{5.20}$$

for the IS-95 CDMA system, the ratio between $\frac{E_b}{N_o}$ and $\widehat{SINR}$ is given by the de-spreading gain $BW/R_{data} = 128$.

Recall the perturbed output SINR has the expression $\widehat{SINR} = SINR_{unperturbed}K$, where K is the SINR reduction factor. The energy-per-bit-to-noise-ratio $\frac{E_b}{N_o}$ would be

reduced by the same factor K if all other parameters remain the same. In order to maintain the same required $\frac{E_b}{N_o}$, $M_{low-power}^{perturbed}$ must be reduced from the value of $M_{low-power}^{unperturbed}$.

Base on the expressions for the SINR reduction factor K obtained earlier, we calculate the corresponding system user capacities and tabulate them in Tables (5.1) and (5.2). We observe that the capacity results yielded by the correlated ARV perturbation model are in closer agreement to the Monte Carlo capacity results obtained in Chapter Four, validating the correlated ARV perturbation model.

5.2.4 Relationship between System Capacities and the DOA Estimation Variance

In this section we consider the relationship between the average capacities across all angles for the four arrays and the variance of the estimated desired signal DOA using the perturbed output SINR approach. We repeat the calculations for the average capacity values across the range of DOA θ for seven cases where the DOA standard deviations equal 0.0316, 0.1, 0.316, 1, 3.16, 10, 31.6 and 100 degrees.

In Figures (5.1), (5.2), and (5.3), we plot the average system capacities vs the DOA estimation variance using the perturbed output SINR approach for the Identical Users scenario, as well as the results of the Monte Carlo approach as obtained in Chapter Four.

In Figures (5.4), (5.5), and (5.6), we plot the average system capacities vs the

Array	ULA	Golomb	UCA	UTA
$Capacity(120/120)_{uncorrelated}$	139.99	141.83	70.80	61.89
$Capacity(120/360)_{uncorrelated}$	172.74	150.26	121.20	128.62
$Capacity(360/360)_{uncorrelated}$	139.37	136.16	121.26	128.59
$Capacity(120/120)_{correlated}$	144.59	147.63	71.25	62.72
$Capacity(120/360)_{correlated}$	180.55	156.79	122.11	131.62
$Capacity(360/360)_{correlated}$	145.86	142.49	122.20	131.58
$Capacity(120/120)_{Chapter4}$	144.69	147.60	71.47	62.95
$Capacity(120/360)_{Chapter4}$	180.51	156.83	122.11	131.71
$Capacity(360/360)_{Chapter4}$	145.47	142.06	122.20	131.67

Table 5.1: Identical-Users scenario system capacities for the four different array geometries base on perturbed output SINR expression, first for uncorrelated Equation (5.3) then for correlated ARV perturbations Equation (5.18), and compare with results from Chapter Four

Array	ULA	Golomb	UCA	UTA
$Capacity(120/120)_{uncorrelated}$	119.91	114.24	53.18	41.57
$Capacity(120/360)_{uncorrelated}$	148.46	118.36	98.38	101.24
$Capacity(360/360)_{uncorrelated}$	116.65	106.35	98.86	101.69
$Capacity(120/120)_{correlated}$	119.92	114.24	53.18	41.57
$Capacity(120/360)_{correlated}$	154.78	123.20	99.42	103.70
$Capacity(360/360)_{correlated}$	121.15	110.50	99.75	103.86
$Capacity(120/120)_{Chapter4}$	118.91	113.47	53.60	42.21
$Capacity(120/360)_{Chapter4}$	152.12	123.48	100.82	104.01
$Capacity(360/360)_{Chapter4}$	119.11	110.42	101.00	104.66

Table 5.2: Multi-Rate Users scenario system capacities for the four different array geometries base on perturbed output SINR expression, first for uncorrelated Equation (5.2) then for correlated ARV perturbations Equation (5.16), and compare with results from Chapter Four

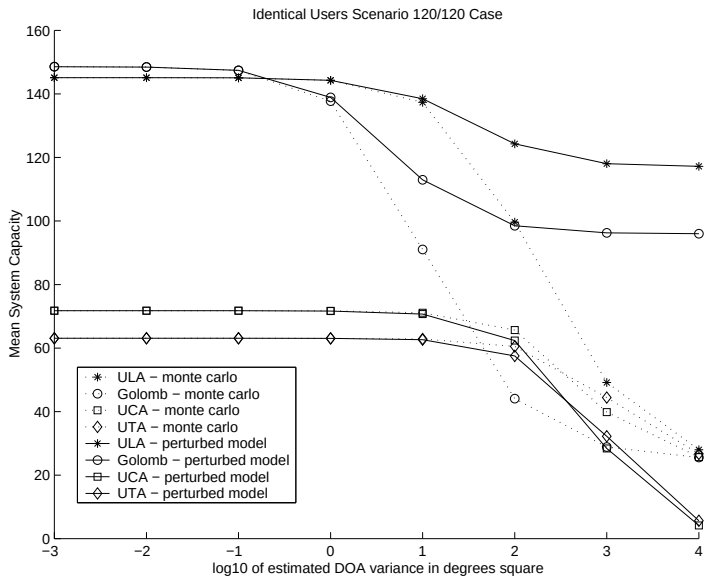

Figure 5.1: Average Capacity versus DOA variance for the Identical Users scenario 120/120 case

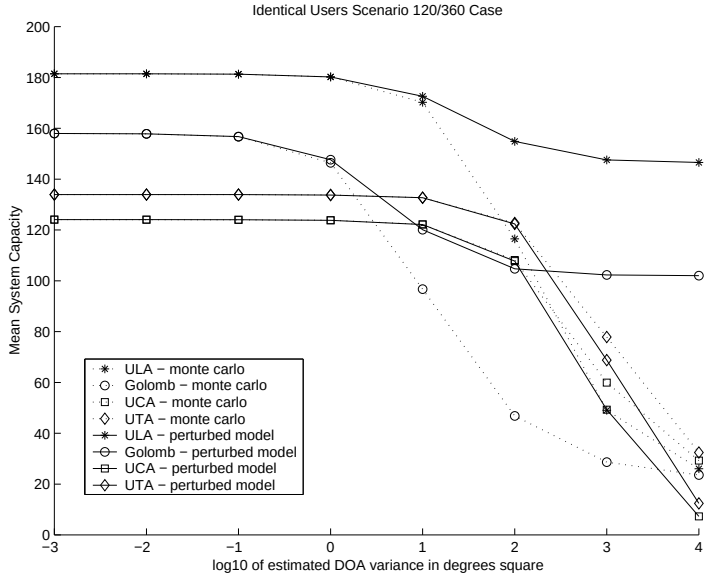

Figure 5.2: Average Capacity versus DOA variance for the Identical Users scenario 120/360 case

DOA estimation variance using the perturbed output SINR approach for the Multi-rate Users scenario, along with the results of the Monte Carlo approach as obtained in Chapter Four.

Note that in Figures (5.1), (5.2), (5.3), (5.4), (5.5), and (5.6), the capacities yielded by the perturbation model are plotted in solid lines. The Monte Carlo results obtained in Chapter Four are drawn as dashed lines here for comparison purposes. We note that the perturbation model breaks down at different points for the different arrays. For the Golomb array, the capacities given by the perturbation model start to deviate from the capacities given by the Monte Carlo method around the point of DOA standard deviation equals 3.16 degrees; for the ULA, this happens around 10 degrees and for the UCA and the UTA, around 31.6 degrees. We also note that the capacities for the linear arrays given by the perturbation model seem to have an asymptotic behavior as the desired signal DOA variance goes to infinity, which is significantly different from the results obtained in Chapter Four.

5.3 Effects of Increasing Number of High Power Interfering Signals

The perturbed output SINR approach enabled relatively fast determination of the effect of desired signal DOA estimation errors on system capacities. Base on this approach, we now consider the relationship between the capacities for the four arrays

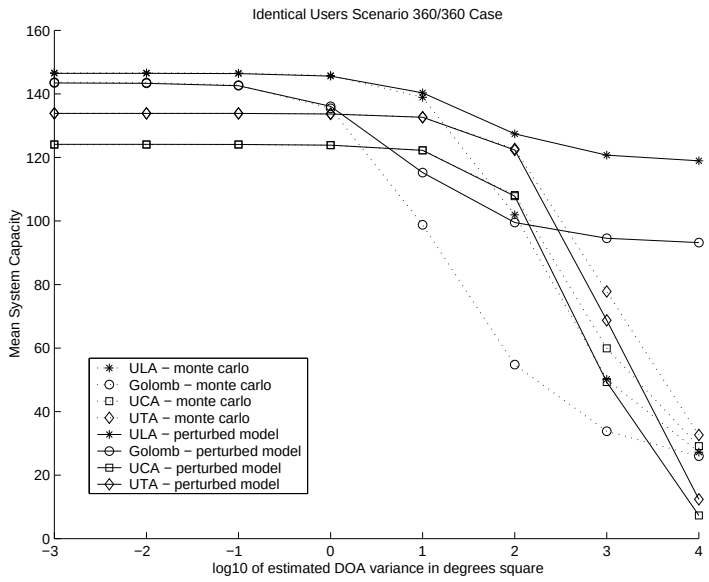

Figure 5.3: Average Capacity versus DOA variance for the Identical Users scenario 360/360 case

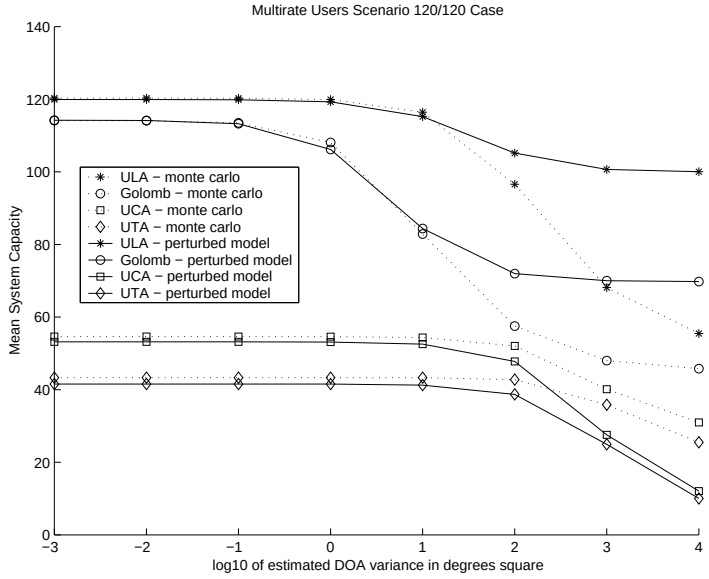

Figure 5.4: Average Capacity versus DOA variance for the Multi-Rate Users scenario 120/120 case

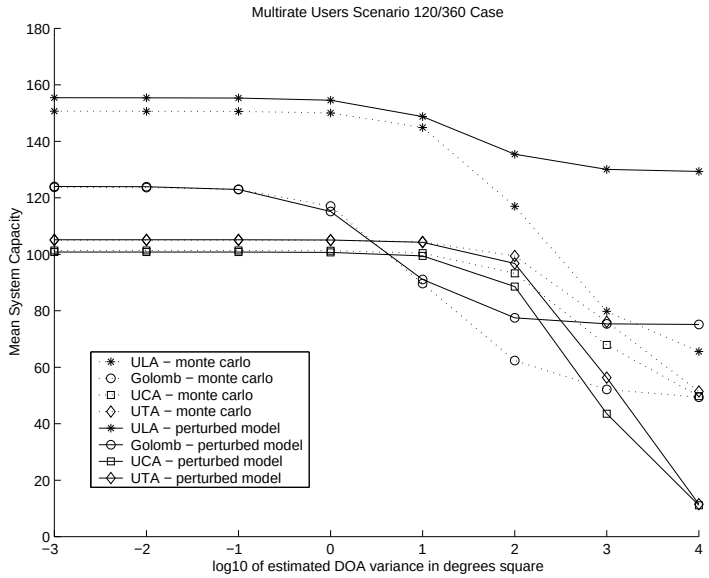

Figure 5.5: Average Capacity versus DOA variance for the Multi-Rate Users scenario 120/360 case

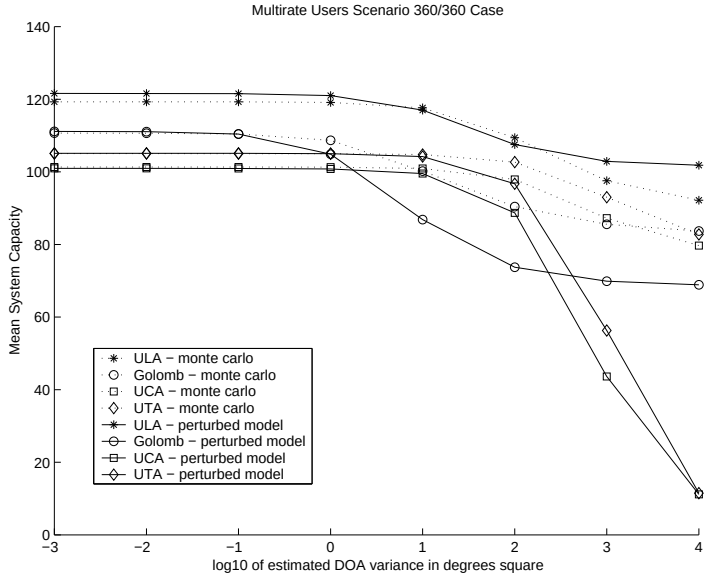

Figure 5.6: Average Capacity versus DOA variance for the Multi-Rate Users scenario 360/360 case

and the number of high power interfering signals present in the system.

In this section we calculate the capacity values for cases where the number of high power interfering signals increases from 2 to 10. We present the results in two ways, the capacities as functions of the desired signal DOA, and the average capacities over all desired signal DOAs as functions of the number of high power interfering signals.

5.3.1 Capacities as Functions of the DOA

To approximate the expected system capacities with high power interfering signals present, it is necessary to account for all possible high power interfering signal DOA combinations. The number of cases becomes very large as the number of high power interfering signals increases; for instance, when there are 6 high power interfering signals present inside a 120 degree range, the number of different DOA combinations at 1 degree intervals is $\frac{120!}{6!114!} = \frac{115\times116\times117\times118\times119\times120}{6!} = \frac{2.629976\times10^{12}}{720} = 3652745460.$ Thus averaging the capacities for all high power interfering DOA combinations is impractical.

Instead we use the Monte Carlo simulation approach, where we randomly generate 1000 sets of high power interfering signal DOA combinations for each desired signal DOA taken at 10 degree intervals. The mean capacity of these trials are then taken as estimates of the expected system capacity for a particular desired signal DOA. In Figures (5.7), (5.8), (5.9), and (5.10), we plot the mean capacities vs the desired signal DOA for the four arrays ULA, Golomb, UCA and UTA respectively.

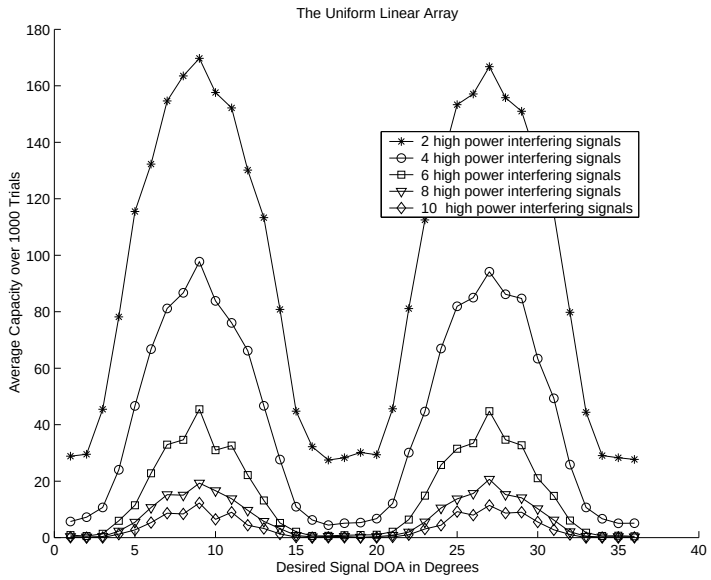

Figure 5.7: Mean Capacity versus DOA for the ULA when 2, 4, 6, 8, or 10 high power interfering signals are present

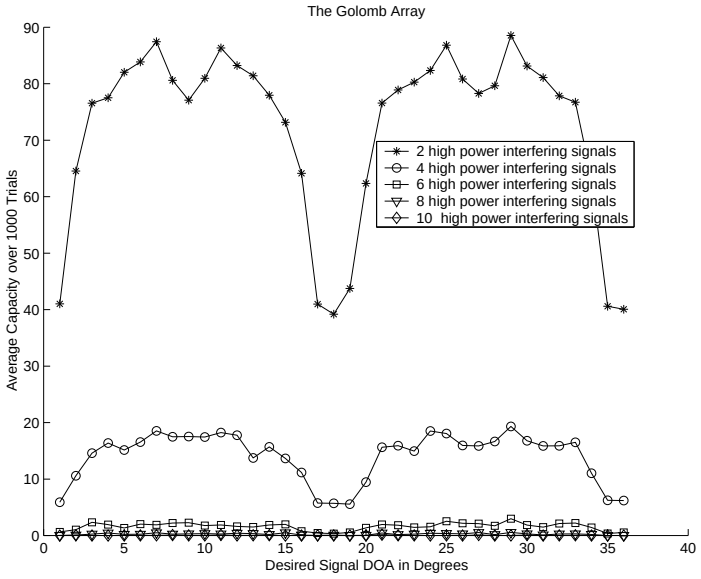

Figure 5.8: Mean Capacity versus DOA for the Golomb Array when 2, 4, 6, 8, or 10 high power interfering signals are present

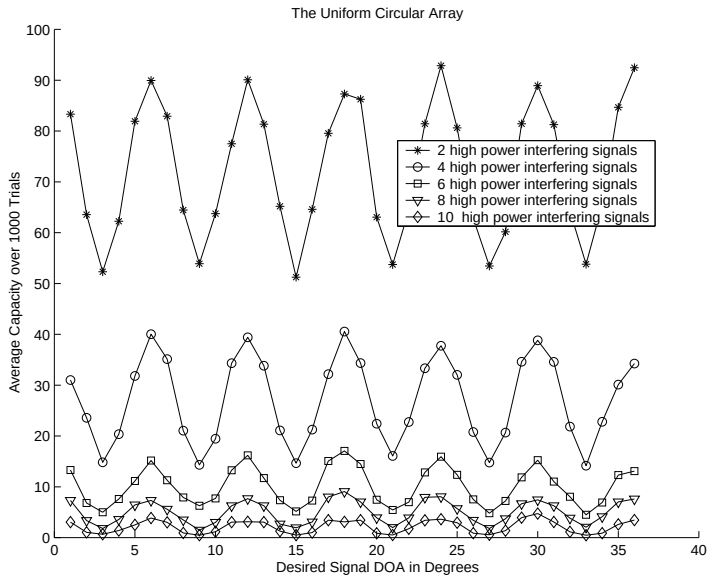

Figure 5.9: Mean Capacity versus DOA for the UCA when 2, 4, 6, 8, or 10 high power interfering signals are present

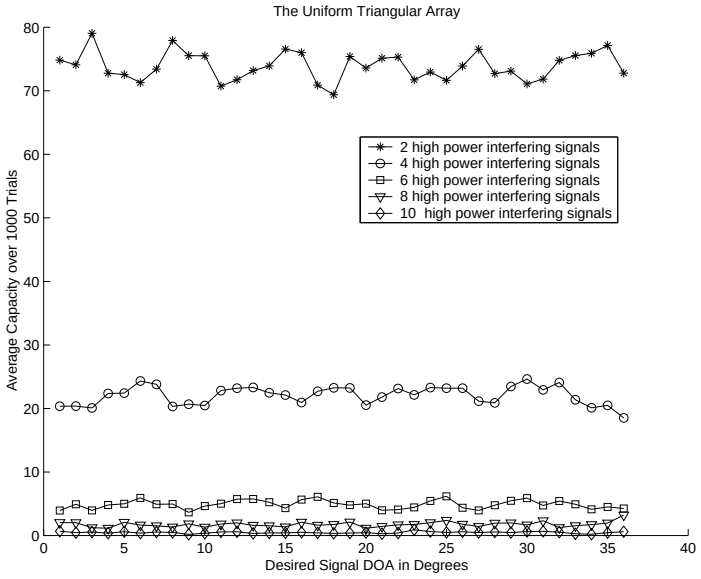

Figure 5.10: Mean Capacity versus DOA for the UTA when 2, 4, 6, 8, or 10 high power interfering signals are present

In Figures (5.7) and (5.8), we observe that, typical of linear arrays, the ULA and the Golomb array have performance peaks along the broadside of the array and valleys near the endfire directions. In Figures (5.9) and (5.10), we observe performances that are more uniform across the whole range of angles. The capacities for the uniform circular array, in particular, has a clearly cyclic behavior with 6 peaks and 6 valleys. For all arrays, the capacity decreases with increasing number of high power interfering signals.

In Figures (5.11), (5.12), (5.13), and (5.14), we plot the capacity variances vs the desired signal DOA for the four arrays ULA, Golomb, UCA and UTA respectively. We observe that the Golomb array has the lowest capacity variance over 1000 trials, this is due to the high DOA resolution ability of the Golomb array, which allows adequate suppression for any combinations of high power interfering signal DOAs. On the other hand, arrays with lower DOA resolution can have good performances when the interfering DOAs are far from the desired signal DOA, but will have very bad performances when they are close, resulting in large capacity variations from trial to trial.

We also observe that the capacity variance decreases with increasing number of high power interfering signals. This is due to lower system capacities possible when the number of high power interfering signals is large. Thus although the ratio between the variance and the mean increases with the number of high power interfering signals, the variance values actually decrease. This difference in average capacities should also be taken into account when comparing variances between the arrays.

Finally, we note that the capacity variance is a function of the array geometry rather than the number of trials, thus increases in the number of Monte Carlo trials would not reduce the capacity variance. Increase in the number of Monte Carlo trials reduces the error between the estimated capacity variance and the true capacity variance.

5.3.2 Capacities as Functions of the Number of High Power Interfering Signals

In this section we consider the capacities as functions of the number of high power interfering signals in the system. In Figures (5.15), (5.16) and (5.17), we plot the average capacities over all desired signal DOAs vs the number of high power interfering signals for the four arrays in the 120/120, 120/360 and 360/360 coverage scenarios respectively.

Base on Figures (5.15), (5.16) and (5.17), we make several observations. First, the system capacities decrease monotonically with increasing number of high power interfering signals for all arrays. Second, the Golomb array suffers the worst capacity reduction due to increase in number of high power interfering signals, as shown by the smallest slope of all curves. The capacity of the Golomb array drops below those of the UCA and UTA for some cases after the number of high power interfering signals reaches a certain point. For the 120/360 scenario, this number is 3; for the 360/360 scenario, this number is roughly 2. Finally, we note that the linear array has the best

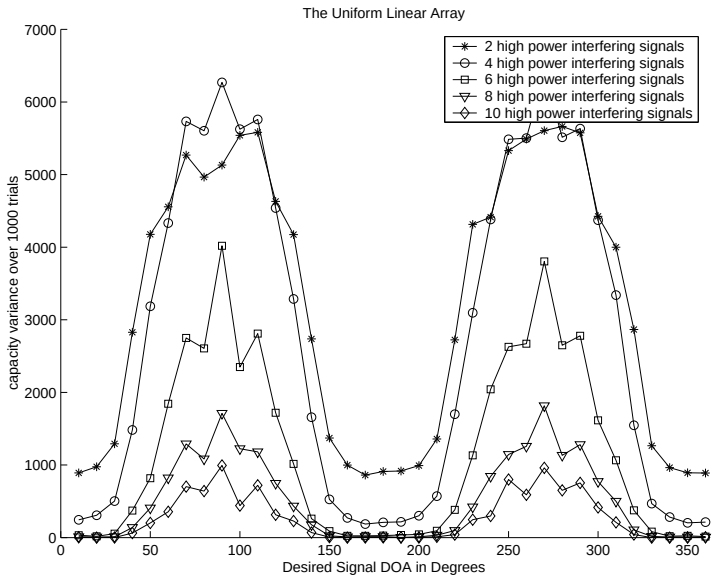

Figure 5.11: Capacity Variance versus DOA for the ULA when 2, 4, 6, 8, or 10 high power interfering signals are present

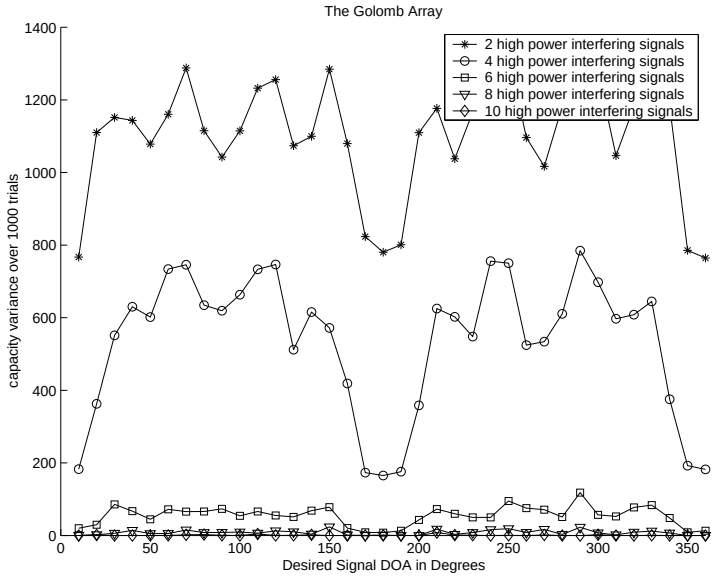

Figure 5.12: Capacity Variance versus DOA for the Golomb Array when 2, 4, 6, 8, or 10 high power interfering signals are present

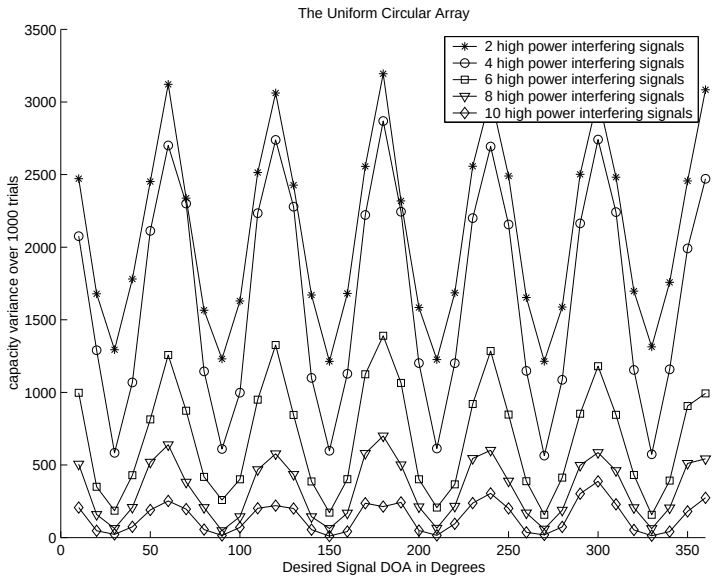

Figure 5.13: Capacity Variance versus DOA for the UCA when 2, 4, 6, 8, or 10 high power interfering signals are present

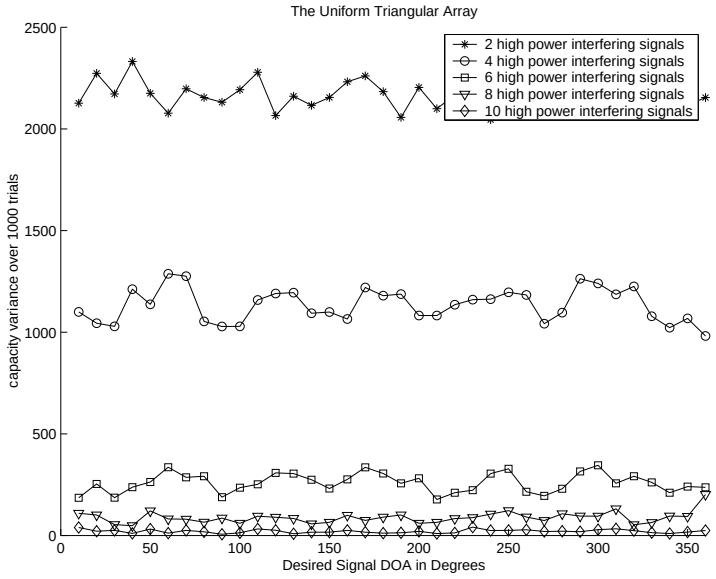

Figure 5.14: Capacity Variance versus DOA for the UTA when 2, 4, 6, 8, or 10 high power interfering signals are present

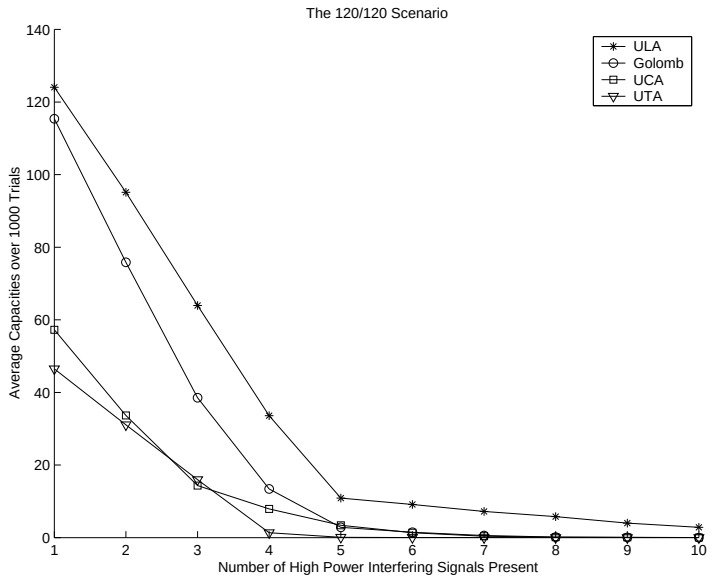

Figure 5.15: Average Capacity versus the number of high power interfering signals, 120/120 scenario

capacity performance at all times.

5.4 Chapter Summary and Discussion

In this chapter we investigated the perturbed output SINR approach to system capacity estimation, as well as the effects of increasing number of high power interfering signals on the capacities using Monte Carlo methods.

In the second section, we extended existing perturbed output SINR results to take correlations between desired signal ARV elements into account, and then applied the new expression to system capacity calculation. Compared to the Monte Carlo

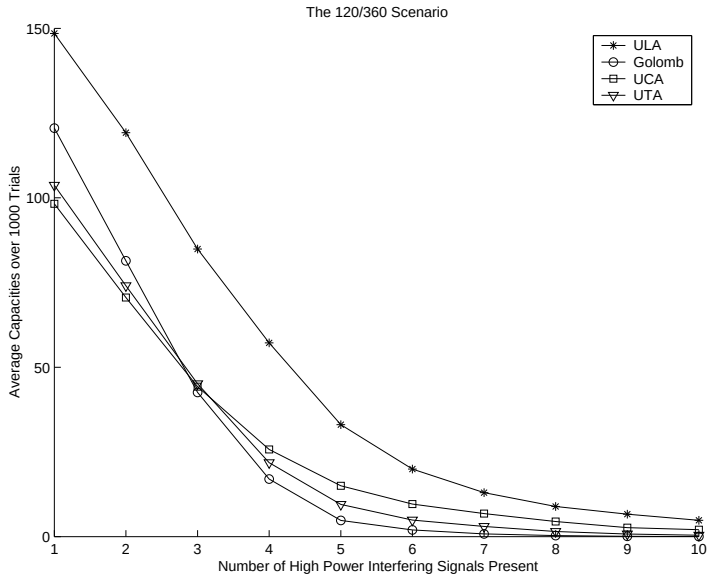

Figure 5.16: Average Capacity versus the number of high power interfering signals, 120/360 scenario

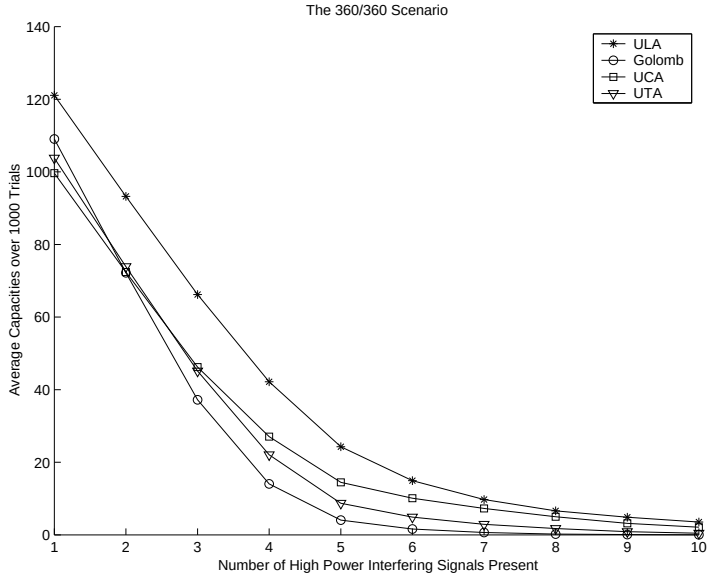

Figure 5.17: Average Capacity versus the number of high power interfering signals, 360/360 scenario

method used in Chapter Four, the perturbed output SINR approach requires orders of magnitude less computational time. And the correlated ARV perturbation model proved to be superior than the uncorrelated ARV perturbation model, yielding closer values to the Monte Carlo results obtained in Chapter Four.

We then consider the relationship between system capacity and desired signal DOA variance using the perturbation approach. By comparing with the results obtained in Chapter Four, we observe that the perturbation model breaks down at different points for the different arrays. The capacities given by the perturbation model and Monte Carlo simulations start to differ significantly when the DOA standard deviation is about 3.16 degrees for the Golomb array, about 10 degrees for the ULA and roughly 31.6 degrees for the UCA and UTA.

In the third section we considered the effects of increasing number of high power interfering signals on the system capacities. We used the Monte Carlo approach when considering high power interfering signal DOAs since the number of different DOA combinations is too large to be taken into account individually. We consider the cases where the number of high power interfering signals increases from 2 to 10, and we present the results in two ways: average capacities over the Monte Carlo trials as functions of the desired signal DOA, and average capacities over desired signal DOAs as functions of the number of high power interfering signals.

Based on the results obtained, we conclude that system capacities decrease monotonically with increasing number of high power interfering signals for all arrays; the

Golomb array suffers the worst capacity reduction due to increase in number of high power interfering signals, its capacity drops below those of the UCA and UTA after the number of high power interfering signals reaches 3 in the 120/360 scenario and 2 in the 360/360 scenario. We also note that the linear array has the best performance in all circumstances.

Finally, we note that we have assumed perfectly known high power interfering signal DOAs. Practical systems need to estimate these DOAs as well, and the uncertainties due to estimation will further reduce the capacities of the different arrays differently. But based on the results of estimated desired signal DOA considerations, we predict that the capacities obtained while taking high power interfering signal DOA uncertainties into account will not differ significantly to the capacity values that we have obtained.

Chapter 6

Conclusions and Future Directions

6.1 Summary of Thesis

In this thesis we compared the user capacities for four common antenna array geometries in a beamforming system, and it can be separated into four main parts: the background information from which our investigation builds on, the performance comparisons between four simple antenna array geometries assuming that the user DOAs are known, performance comparisons of the same four array geometries when their respective DOA estimation capabilities are taken into account, and the perturbed output SINR approach to user capacity estimation.

In Chapter Two, we reviewed the necessary background information of our investigation, including an overview of the wireless communication system structure, various DOA estimation techniques including both conventional and sub-space methods, fundamentals of antenna signal processing including the maximum SNR/SINR

beamformers, the different antenna geometries being investigated in this thesis, and the expression of DOA estimation Cramer-Rao Lower Bound expression for arbitrary three-dimensional array geometry.

In Chapter Three, we compared each antenna array in two situations: the *Identical Users* scenario where all users have the same data rate, modeling the second generation voice-only communication systems, and the *Multi-Rate Users* scenario where some users have a higher data rate and thus higher incident power on the array, modeling the contemporary mobile communication systems in transition between 2G voice-only systems and 2.5G/3G multi-media systems.

Our user capacity comparisons show that the uniform linear array has the highest mean capacity in the scenarios that we considered. The Golomb array, while having the highest DOA resolution, has lower user capacities due to the relatively high side-lobe levels of the Golomb array beampattern. We also found that the Golomb array does not perform well when there are more than one high power interfering signals present in the system.

In Chapter Four, we compared the user capacities of the four arrays while taking into account the different DOA resolution abilities of the different arrays. Based on the results obtained in Chapter Four, we conclude that when the user DOAs are estimated, we can expect one to two percent reduction in user capacities in the best circumstances. Among the four antenna arrays under consideration, the uniform linear array has the best all around performance, being surpassed by the Golomb array

only in a select few circumstances. The circular and the triangular arrays are particularly unsuitable to 120-degree sector coverage, in omni-directional coverage situations they have fair performances in all directions, unlike the linear arrays. The Golomb array, while having superior ability in distinguishing two closely located users, does not have performance advantage over the ULA. This is due to its greater sensitivity to errors in DOA, since it produces narrower main beams.

Also in Chapter Four, we considered performance comparisons using practical DOA estimation algorithms where the DOA estimation variance does not coincide with the CRB, the results were presented by the mean capacity vs DOA variance curves.

In Chapter Five, we presented the expressions of the perturbed output SINR due to perturbations in the array response vector, which is then used to calculate the user capacities. We extended T. Luo's work for un-correlated ARV perturbations to include correlated ARV perturbation. The results based on analytical derivations are then compared to the results obtained through Monte Carlo calculations. Capacity values based on correlated ARV perturbation model are shown to be in closer agreement to the Monte Carlo capacity values.

We also considered the impacts of increasing number of high power interfering signals on the capacities of the four arrays. The results show that contrary to intuition, the non-uniform Golomb array actually has rather poor performances when the number of high power interfering signals is increased.

6.2 Future Directions

Further studies on the maximization of user capacity using base station antenna arrays in practical wireless communication systems require the optimization of three-dimensional antenna array geometries while taking the following considerations into account:

Other Spatial Channel Models In this thesis we have assumed that line-of-sight channel exists for all users, and we have ignored all channel effects including shadowing, scattering and multi-path fading. Most mobile wireless systems are deployed in an urban environment where line-of-sight conditions are very rare while scattering and fading effects are pronounced.

For example, local-to-the-mobile scattering effects have been modeled as having either uniform or Gaussian power distribution inside a range of DOAs around the mobile DOA called the *angle spread* [60]. Guideline ranges are available for typical communication environments and they are determined by empirical measurements.

This model can be incorporated into our framework by rewriting the general Power Pass-Through Factor expression given by Equation (3.3). By replacing the user DOA distribution $f(\Theta)$ by an angular signal power distribution $g(\Theta)$, which is a function of $f(\Theta)$ and the scattering power distribution, we can obtain

the total interference power given a desired DOA:

$$E[\mathbf{phi}_k^{int}(\Theta_{desired})] = \int_{range-of-\Theta} g(\Theta) \left|\mathbf{w}^H(\Theta_{desired})\mathbf{a}(\Theta)\right|^2 d\Theta \tag{6.1}$$

$$g(\Theta) = \int_{\Theta_k} P(\Theta;\Theta_k) f(\Theta_k) d\Theta_k \tag{6.2}$$

where $P(\Theta;\Theta_k)$ is the angular pdf of incident signal power for the k-th mobile, and Θ is the three dimensional DOA vector. In other words, summing or integrating the scattered power distributions of all mobile users gives us the total angular incident power distribution $g(\Theta)$. Weighting this incident power distribution by the beamforming weight $\mathbf{w}$ gives the PPTF for scattered interfering signals.

Performance Comparison for Diversity Systems In our investigation we have assumed line-of-sight communication and exact cross-correlation between the received signals of the array elements in order to facilitate beamforming. For current wireless deployments, the base station antenna is usually high above ground, thus most of the multi-path scatterers are located close to the mobile user, resulting in high cross correlations between the received signal envelopes. Thus our assumption of high cross-correlation between the incident signals at the array elements is valid. But for systems where the cross-correlation between incident signals at the array elements are low, it is necessary to utilize diversity techniques.

Two applications which may find antenna array diversity techniques useful are indoor wireless systems and future generation street level antenna arrays. In

an indoor wireless environment, multi-path scatterers are often located close to the base station, reducing the cross-correlation of the received signals. In future generation wireless systems, where the carrier frequencies will be high, the coverage area for each base station will be small due to larger path loss. More base stations that are closer to the users need to be deployed, resulting in street level antenna arrays rather than the tower installations that are common today. The cross correlations between the received signals of the antenna elements will be reduced due to vicinity of the scatterers.

Forward Link Performance Comparisons In this thesis our focus is on the reverse link system performance, but practical systems need to provide forward link services as well. It has been shown that a CDMA system is a forward link limited system [22], thus antenna array geometry optimization taking forward link capacity maximization into account is an important future study.

Virtual Array Considerations The use of virtual arrays to facilitate antenna signal processing [11] [26] is another aspect that may be considered in antenna array design. Due to changing channel environments, base stations may need to employ dynamic virtual array schemes in response. Thus the suitability of different physical array geometries to create potential virtual array geometries should be studied.

Mutual Coupling Effects Mutual coupling effects between antenna array elements

impedes the array performance [60] [34]. This effect is different for arrays of different geometries due to the different inter-elemental distances for the different arrays.

Performances of Existing Algorithms The main focus when designing practical systems is on what is actually achievable rather than what is the theoretical limit on performance. Thus studies comparing array geometries or optimization of array geometry when taking existing signal processing algorithms in account would be a worthwhile study.

6.3 Conclusions

In this thesis we compared several antenna array geometries using practical performance requirements of a wireless communication system, and we draw three main conclusions base on the results obtained. First, we found that the intrinsic effects of DOA estimation on the system capacities based on the CRB is small for all arrays considered, although we note that practical DOA estimation algorithms whose estimation variance differs from the CRB may yield significantly different results.

Second, we found that the array with the highest DOA resolution does not have the highest user capacity, due to its greater sensitivity to DOA errors. On the other hand, arrays with low DOA resolutions do not have satisfactory user capacities either, thus we conclude that there is no simple relationship between DOA resolution and user capacity.

And finally, we found that contrary to the intuition that arrays with high DOA resolution can better suppress dominant interfering signals, the Golomb array actually has very poor performance in dealing with increasing number of high power interfering signals.

By considering DOA estimation performance bounds, we were able to compare the performances of four array geometries in a general and algorithm-independent way. We hope that this investigation has laid down a good foundation and provided a viable starting point onto future studies in the area of array geometry optimization.

Appendix A

CRB for the Azimuth and Elevation DOA Estimates

In this appendix we present the derivation of the CRB expression for the DOA estimates given arbitrary three-dimensional array geometry as derived by Chambers et al [8]. In this derivation we use the results of the vector parameter and general Gaussian CRB which were discussed in Chapter Two, where the data is the received signal samples, and the parameters to be estimated are the azimuth and elevation angles θ and ϕ.

Assuming that the array elements are identical and omni-directional, the normalized array response vector can be written as:

$$\mathbf{a}(\theta,\phi) = \frac{1}{\sqrt{N}}[e^{-j\mathbf{k}^T\mathbf{x}_1}e^{-j\mathbf{k}^T\mathbf{x}_2}...e^{-j\mathbf{k}^T\mathbf{x}_N}]^T \tag{A.1}$$

where we recall from equation (2.1) that $\mathbf{x}_i = [x_i, y_i, z_i]^T$ are the coordinates of the i-th element in the array with respect to a reference element; $\mathbf{k}$ is the vector wave

number of the plane wave coming from the signal source, written as:

$$\mathbf{k}(\theta,\phi,\lambda) = \frac{2\pi}{\lambda}\begin{bmatrix} \sin(\theta)\cos(\phi) \\ \cos(\theta)\cos(\phi) \\ \sin(\phi) \end{bmatrix} \tag{A.2}$$

We assume, without loss of generality, that $\sum_{i=1}^{N}\mathbf{x}_i = 0$, in effect moving the reference point to the centroid of the array. Recalling the Fisher information matrix expression for the general Gaussian case, and noting that the mean μ is not a function of $\underline{\theta}$, the first term in the expression is zero. So to evaluate the Fisher information matrix (2.14), we only need the inverse and the derivatives of the data covariance matrix.

The covariance matrix for received signal vector $\mathbf{y}$ when there is only one signal present is represented by the expression [25] :

$$\mathbf{C} = E[\mathbf{y}\mathbf{y}^H] = NP\mathbf{a}\mathbf{a}^H + \sigma^2\mathbf{I} \tag{A.3}$$

where N is the number of elements in the array, and P is the received signal power. Using Woodbury's identity [48]:

$$R = R_0 + \gamma^2 uu^T \longrightarrow R^{-1} = R_0^{-1} - \frac{\gamma^2}{1+\gamma^2 u^T R_0^{-1} u} R_0^{-1} uu^T R_0^{-1} \tag{A.4}$$

and some algebra gives:

$$\mathbf{C}^{-1} = \frac{1}{\sigma^2}[\mathbf{I} - \frac{NP\mathbf{a}\mathbf{a}^H}{\sigma^2 + NP}] \tag{A.5}$$

The derivatives of the covariance matrix are then calculated as:

$$\begin{aligned} \frac{\partial \mathbf{C}}{\partial \theta} &= NP(\frac{\partial \mathbf{a}}{\partial \theta}\mathbf{a}^H + \mathbf{a}\frac{\partial \mathbf{a}^H}{\partial \theta}) \\ \frac{\partial \mathbf{C}}{\partial \phi} &= NP(\frac{\partial \mathbf{a}}{\partial \phi}\mathbf{a}^H + \mathbf{a}\frac{\partial \mathbf{a}^H}{\partial \phi}) \end{aligned} \tag{A.6}$$

since $\mathbf{k}_i^T\mathbf{x}_l = \frac{2\pi}{\lambda}(\sin\theta_i\cos\phi_i x_l + \cos\theta_i\cos\phi_i y_l + \sin\phi_i z_l)$, by taking the l-th components of the array response vectors of the i-th signal source we obtain:

$$\begin{aligned}\frac{\partial[\mathbf{a}_i]_l}{\partial\theta} &= \frac{\partial}{\partial\theta}\left(\frac{1}{\sqrt{N}}\exp(-j\mathbf{k}_i\mathbf{x}_l)\right) = \frac{1}{\sqrt{N}}\exp(-j\mathbf{k}_i\mathbf{x}_l)\frac{\partial(-j\mathbf{k}_i\mathbf{x}_l)}{\partial\theta} \\ &= \frac{1}{\sqrt{N}}\exp(-j\mathbf{k}_i\mathbf{x}_l)[-j\frac{2\pi}{\lambda}(\cos\theta_i\cos\phi_i x_l - \sin\theta_i\cos\phi_i y_l)] \\ &= [-j\frac{2\pi}{\lambda}(\cos\theta_i\cos\phi_i x_l - \sin\theta_i\cos\phi_i y_l)][\mathbf{a}_i]_l \equiv -jG_l(\theta_i,\phi_i)[\mathbf{a}_i]_l \quad \text{(A.7)}\end{aligned}$$

and similarly,

$$\begin{aligned}\frac{\partial[\mathbf{a}_i]_l}{\partial\phi} &= [-j\frac{2\pi}{\lambda}(-\sin\theta_i\sin\phi_i x_l - \cos\theta_i\sin\phi_i y_l + \cos\phi_i z_l)][\mathbf{a}_i]_l \equiv -jH_l(\theta_i,\phi_i)[\mathbf{a}_i]_l \\ \frac{\partial[\mathbf{a}_i^H]_l}{\partial\theta} &= [j\frac{2\pi}{\lambda}(\cos\theta_i\cos\phi_i x_l - \sin\theta_i\cos\phi_i y_l)][\mathbf{a}_i^H]_l \equiv jG_l(\theta_i,\phi_i)[\mathbf{a}_i^H]_l \\ \frac{\partial[\mathbf{a}_i^H]_l}{\partial\phi} &= [j\frac{2\pi}{\lambda}(-\sin\theta_i\sin\phi_i x_l - \cos\theta_i\sin\phi_i y_l + \cos\phi_i z_l)][\mathbf{a}_i^H]_l \equiv jH_l(\theta_i,\phi_i)[\mathbf{a}_i^H]_l\end{aligned}$$

so in general, the trace of the matrix of partial derivatives has the expression:

$$tr[\frac{\partial\mathbf{a}^H}{\partial\theta}\frac{\partial\mathbf{a}}{\partial\phi}] = \frac{\partial\mathbf{a}^H}{\partial\theta}\frac{\partial\mathbf{a}}{\partial\phi} = \sum_{k=1}^{N}\frac{\partial[\mathbf{a}^H]_k}{\partial\theta}\frac{\partial[\mathbf{a}]_k}{\partial\phi} = \sum_{k=1}^{N}G_k(\theta,\phi)H_k(\theta,\phi)[\mathbf{a}]_k^2 = tr[\frac{\partial\mathbf{a}}{\partial\theta}\frac{\partial\mathbf{a}^H}{\partial\phi}] \quad \text{(A.8)}$$

The Fisher information matrix, when M snapshots of data are taken into account, has the following expression [25]:

$$\mathbf{I}_{ij} = Mtr\left[\mathbf{C}^{-1}\frac{\partial\mathbf{C}}{\partial\underline{\theta}_i}\mathbf{C}^{-1}\frac{\partial\mathbf{C}}{\partial\underline{\theta}_j}\right] = \begin{bmatrix}\mathbf{I}_{\theta\theta} & \mathbf{I}_{\theta\phi} \\ \mathbf{I}_{\phi\theta} & \mathbf{I}_{\phi\phi}\end{bmatrix} \quad \text{(A.9)}$$

note that $\underline{\theta} = [\theta,\phi]$. Evaluating the cross term $\mathbf{I}_{\theta\phi}$ in Equation (A.9) first:

$$\begin{aligned}\mathbf{I}_{\theta\phi} &= Mtr\left[\mathbf{C}^{-1}\frac{\partial\mathbf{C}}{\partial\theta}\mathbf{C}^{-1}\frac{\partial\mathbf{C}}{\partial\phi}\right] \\ &= \frac{N^2P^2M}{\sigma^4}tr\left[(\mathbf{I} - \frac{NP\mathbf{a}\mathbf{a}^H}{\sigma^2+NP})(\frac{\partial\mathbf{a}}{\partial\theta}\mathbf{a}^H + \mathbf{a}\frac{\partial\mathbf{a}^H}{\partial\theta})(\mathbf{I} - \frac{NP\mathbf{a}\mathbf{a}^H}{\sigma^2+NP})(\frac{\partial\mathbf{a}}{\partial\phi}\mathbf{a}^H + \mathbf{a}\frac{\partial\mathbf{a}^H}{\partial\phi})\right] \\ &= \frac{N^2P^2M}{\sigma^4}\mathbf{A} \quad \text{(A.10)}\end{aligned}$$

We then expand and simplify the expression for $\mathbf{A}$ using the trace rule of rotation *tr(ABC) = tr(BCA)* and the following property:

Proposition:

$$\frac{\partial \mathbf{a}^H}{\partial \theta}\mathbf{a} = 0 = \mathbf{a}^H\frac{\partial \mathbf{a}}{\partial \theta} = \frac{\partial \mathbf{a}^H}{\partial \phi}\mathbf{a} = \mathbf{a}^H\frac{\partial \mathbf{a}}{\partial \phi} \tag{A.11}$$

Proof:

$$\begin{aligned}\frac{\partial \mathbf{a}^H}{\partial \theta}\mathbf{a} &= \sum_{k=1}^{N}\frac{\partial [\mathbf{a}^H]_k}{\partial \theta}[\mathbf{a}]_k \\ &= \sum_{k=1}^{N} j\frac{2\pi}{\lambda}(x_k\cos\theta\cos\phi - y_k\sin\theta\cos\phi)\underbrace{[\mathbf{a}^H]_k[\mathbf{a}]_k}_{1} \\ &= j\frac{2\pi}{\lambda}\cos\theta\cos\phi\underbrace{\sum_{k=1}^{N}x_k}_{0} - j\frac{2\pi}{\lambda}\sin\theta\cos\phi\underbrace{\sum_{k=1}^{N}y_k}_{0} = 0\end{aligned} \tag{A.12}$$

due to normalization of the array response vector and the centroid reference point assumption. Q.E.D. Similarly for the other terms in the proposition.

Using Equations (A.8) and (A.11), the expression of $\mathbf{A}$ can be simplified into:

$$\begin{aligned}\mathbf{A} &= (1-\frac{NP}{\sigma^2+NP})tr[\frac{\partial \mathbf{a}^H}{\partial \theta}\frac{\partial \mathbf{a}}{\partial \phi} + \frac{\partial \mathbf{a}}{\partial \theta}\frac{\partial \mathbf{a}^H}{\partial \phi}] = (1-\frac{NP}{\sigma^2+NP})2tr[\frac{\partial \mathbf{a}^H}{\partial \theta}\frac{\partial \mathbf{a}}{\partial \phi}] \\ &= (1-\frac{NP}{\sigma^2+NP})2[\frac{\partial \mathbf{a}^H}{\partial \theta}\frac{\partial \mathbf{a}}{\partial \phi}]\end{aligned} \tag{A.13}$$

thus

$$\mathbf{I}_{\theta\phi} = \frac{N^2P^2M}{\sigma^4}\frac{2\sigma^2}{\sigma^2+NP}tr[\frac{\partial \mathbf{a}^H}{\partial \theta}\frac{\partial \mathbf{a}}{\partial \phi}] = \frac{2M(ASNR)^2}{1+(ASNR)}[\frac{\partial \mathbf{a}^H}{\partial \theta}\frac{\partial \mathbf{a}}{\partial \phi}] = \frac{2M(ASNR)^2}{1+(ASNR)}\mathbf{AV}_{xz} \tag{A.14}$$

Where we denote $ASNR = \frac{NP}{\sigma^2}$ as the received *Antenna Signal to Noise Ratio.* The quantity $\mathbf{AV}$ is referred to as the *Array Variance.* Similarly,

$$\mathbf{I}_{\theta\theta} = \frac{2M(ASNR)^2}{1+ASNR}\mathbf{AV}_{xx}$$

$$\mathbf{I}_{\phi\phi} = \frac{2M(ASNR)^2}{1+ASNR}\mathbf{AV}_{zz} \tag{A.15}$$

Note that $\mathbf{AV}_{xz} = \mathbf{AV}_{zx} = \frac{\partial \mathbf{a}^H}{\partial \theta}\frac{\partial \mathbf{a}}{\partial \phi}$, $\mathbf{AV}_{xx} = \frac{\partial \mathbf{a}^H}{\partial \theta}\frac{\partial \mathbf{a}}{\partial \theta}$ and $\mathbf{AV}_{zz} = \frac{\partial \mathbf{a}^H}{\partial \phi}\frac{\partial \mathbf{a}}{\partial \phi}$. The above give the complete expression for the two-element by two-element Fisher information matrix, and the diagonal elements of its inverse gives the Cramer Rao Lower Bound of the angle estimates:

$$\begin{aligned}\mathbf{CRB} &= \mathbf{I}^{-1} = \left\{ \frac{2M(ASNR)^2}{1+ASNR} \begin{bmatrix} AV_{xx} & AV_{xz} \\ AV_{xz} & AV_{zz} \end{bmatrix} \right\}^{-1} \\ &= \frac{1+ASNR}{2M(ASNR)^2} \frac{1}{AV_{xx}AV_{zz} - AV_{xz}^2} \begin{bmatrix} AV_{zz} & -AV_{xz} \\ -AV_{xz} & AV_{xx} \end{bmatrix} \end{aligned} \tag{A.16}$$

Taking the two diagonal elements, we obtain the Cramer Rao Lower Bound for the azimuth and elevation DOA estimates:

$$\begin{aligned}\mathbf{CRB}(\theta) &= \frac{1+ASNR}{2M(ASNR)^2} \frac{AV_{zz}}{AV_{xx}AV_{zz} - AV_{xz}^2} \\ \mathbf{CRB}(\phi) &= \frac{1+ASNR}{2M(ASNR)^2} \frac{AV_{xx}}{AV_{xx}AV_{zz} - AV_{xz}^2} \end{aligned} \tag{A.17}$$

which agrees with the expressions found in [8].

Appendix B

Desired Signal ARV Error Correlation Matrix

In this appendix we present the expression of the correlation matrix for the error vector of the desired signal array response vector.

We make the assumption that the perturbation in the array response vector $\mathbf{a}$ is a zero mean random variable. Given that assumption, the expected value of the perturbed desired signal correlation matrix has the following expression:

$$E\{\hat{\mathbf{Q}}_{desired}\} = P_s E\{\hat{\mathbf{a}}\hat{\mathbf{a}}^H\} = P_s[\mathbf{a}\mathbf{a}^H + \mathbf{C}_\eta] = P_s[\mathbf{Q}_{desired} + \mathbf{C}_\eta] \tag{B.1}$$

where the (m,m)th element of $\mathbf{C}_\eta$ is $\mathbf{C}_\eta^{m,m} = E\{(\hat{\mathbf{a}}_m - \mathbf{a}_m)(\hat{\mathbf{a}}_m - \mathbf{a}_m)^H\} = var\{\mathbf{a}_m\}$, and $\mathbf{C}_\eta^{m,n} = E\{(\hat{\mathbf{a}}_m - \mathbf{a}_m)(\hat{\mathbf{a}}_n - \mathbf{a}_n)^H\}$.

Since the array response vector $\mathbf{a}$ is defined by:

$$\begin{aligned} \mathbf{a} &= \left[e^{-j\pi(x_1\cos\theta + y_1\sin\theta)}, e^{-j\pi(x_2\cos\theta + y_2\sin\theta)}, \ldots, e^{-j\pi(x_M\cos\theta + y_M\sin\theta)}\right]^T \\ &= \left[\mathcal{F}_1(x_1, y_1, \theta), \mathcal{F}_2(x_2, y_2, \theta), \ldots, \mathcal{F}_M(x_M, y_M, \theta)\right]^T \end{aligned} \tag{B.2}$$

taking the Taylor series expansion of the m-th element of the estimated array response vector:

$$\begin{aligned}\hat{\mathbf{a}}_m &= \mathcal{F}_m\left(x_m, y_m, \hat{\theta}\right) \\ &= \underbrace{\mathcal{F}_m\left(x_m, y_m, \theta\right)}_{\mathbf{a}_m} + \underbrace{\left(\hat{\theta}-\theta\right)\frac{\partial}{\partial\theta}\mathcal{F}_m\left(x_m, y_m, \theta\right) + \ldots\ldots}_{\eta_m} \end{aligned} \tag{B.3}$$

where the higher order terms are omitted. If we write $\mathcal{F}\left(x, y, \theta\right)$ as $\mathcal{F}\left(\theta\right)$ then the (m,n)th elements of $\mathbf{C}_\eta$ has the following expression:

$$\begin{aligned}\mathbf{C}_\eta^{m,n} &= E\left\{(\hat{\mathbf{a}}_m - E\left\{\hat{\mathbf{a}}_m\right\})(\hat{\mathbf{a}}_n - E\left\{\hat{\mathbf{a}}_n\right\})^H\right\} \\ &\approx E\left\{(\mathcal{F}_m(\hat{\theta}) - \mathcal{F}_m(\theta))(\mathcal{F}_n(\hat{\theta}) - \mathcal{F}_n(\theta))^H\right\} \\ &\approx E\left\{\left((\hat{\theta}-\theta)\frac{\partial}{\partial\theta}\mathcal{F}_m(\theta)\right)\left((\hat{\theta}-\theta)\frac{\partial}{\partial\theta}\mathcal{F}_n(\theta)\right)^H\right\} \\ &= \frac{\partial}{\partial\theta}\mathcal{F}_m(\theta)\left(\frac{\partial}{\partial\theta}\mathcal{F}_n(\theta)\right)^H E\left\{(\hat{\theta}-\theta)^2\right\} \\ &\geq \frac{\partial}{\partial\theta}\mathcal{F}_m(\theta)\left(\frac{\partial}{\partial\theta}\mathcal{F}_n(\theta)\right)^H CRB(\theta) \end{aligned} \tag{B.4}$$

since the expression for $\mathcal{F}_k$ is:

$$\mathcal{F}_k(\theta) = e^{-j\pi(x_k\cos\theta + y_k\sin\theta)} \tag{B.5}$$

taking the derivative $\frac{\partial}{\partial\theta}\mathcal{F}_k$ gives:

$$\begin{aligned}\frac{\partial}{\partial\theta}\mathcal{F}_k\left(\theta\right) &= e^{-j\pi(x_k\cos\theta + y_k\sin\theta)}\left(-j\pi(-x_k\sin\theta + y_k\cos\theta)\right) \\ &= \mathcal{F}_k\left(\theta\right)\left(j\pi(x_k\sin\theta - y_k\cos\theta)\right) \end{aligned} \tag{B.6}$$

so the (m,n)th element of the expected value of perturbation of the covariance matrix for the desired signal Q_d has the following expression:

$$\mathbf{C}_\eta^{mn} = \frac{\partial}{\partial\theta}\mathcal{F}_m\left(\theta\right)\left(\frac{\partial}{\partial\theta}\mathcal{F}_n\left(\theta\right)\right)^H CRB(\theta)$$

$$
\begin{aligned}
&= \mathcal{F}_m(\theta)\,\mathcal{F}_n^H(\theta)\,\pi^2(x_m\sin\theta - y_m\cos\theta)(x_n\sin\theta - y_n\cos\theta)CRB(\theta) \\
&= \pi^2(x_m\sin\theta - y_m\cos\theta)(x_n\sin\theta - y_n\cos\theta)e^{-j\pi[(x_m-x_n)\cos\theta+(y_m-y_n)\sin\theta]}CRB(\theta)
\end{aligned}
\tag{B.7}
$$

Bibliography

[1] Y.I. Abramovich and N.K. Spencer Design of nonuniform linear antenna array geometry and signal processing algorithm for DOA estimation, *Digital signal processing - a review journal*, vol 10, no 4, October 2000

[2] R.P. Aldridge and R. Steele Strategies for combatting base station failure in highway cicrocellular clusters, *Electronic Letters*, vol 24, no 21, October 1988

[3] I.F. Akyildiz J. McNair, L. R. Martorell, R. Puigjaner and Y. Yesha Medium access control protocols for multimedia traffic in wireless networks, *IEEE Network*, vol 13, no 4, July-August 1999

[4] C.W. Ang, C.M. See and A.C. Kot Optimization of array geometry for identifiable high resolution parameter estimation in sensor array signal processing, *Proceedings of the 1997 1st international conference on information, communications and signal processing*, vol 3, 1997

[5] M. Austin, A. Buckley, C. Coursey, P. Hartman and R. Kobylinski Service and system enhencement for TDMA digital cellular systems, *IEEE Personal Communications*, vol 6, no 3, 1999

[6] W.P. Ballance and A.G. Jaffer Explicit analytic Cramer-Rao bound on angle estimation, *Conference record of Asilomar conference on circuits, systems and computers*, vol 1, 1989

[7] A. Bhuyan and P.M. Schultheiss Estimation of source separation with an array of arbitrary shape, *Proceedings of the ICASSP*, vol 5, 1990

[8] C. Chambers, T.C. Tozer, K.C. Sharman and T.S. Durrani Temporal and Spatial Sampling Influence on the Estimates of Superimposed Narrowband Signals: When Less Can Mean More, *IEEE Transactions on Signal Processing*, Vol. 44, No. 12, December 1996

[9] H. Chen, Y.L. Wang and S. Wan Performance improvement of estimation direction of arrival via array geometry arrangement, *Proceedings of the 1999 IEEE international antennas and propagation symposium*, vol 3, 1999

[10] Y.H. Chen, A.C. Chang and H.T. Lee Array calibration methods for sensor position and pointing errors, *Microwave and optical technology letters*, vol 26, no 2, 2000

[11] P. Chevalier and A. Ferreol On the virtual array concept for the fourth-order direction finding problem, *IEEE transaction on signal processing*, vol 47, no 9, 1999

[12] G. Colman *An investigation into the capacity of cellular CDMA communication systems with beamforming in environments of scatter*, Master's thesis, Queen's University, 1998

[13] Leon W. Couch II *Digital and Analog Communication Systems*, Macmillan Publishing, 1993

[14] A. Dogandzic, A. Nehorai Cramer-Rao bound for estimating range, velocity and direction with an active array, *IEEE transaction on signal processing*, vol 49, no 6, June 2001

[15] N. Dowlut and A. Manikas Polynomial rooting approach to super-resolution array design, *IEEE transaction on signal processing*, vol 48, no 6, 2000

[16] R.B. Ertel, P. Cardieri, K.W. Sowerby, T.S. Rappaport and J.H. Reed Overview of Spatial Channel Models for Antenna Array Communication Systems, *IEEE personal communications*, February 1998

[17] M.H. Er and S.K. Hui Array pattern synthesis in the presence of faulty elements, *Signal Processing*, vol 29, no 1, October 1992

[18] T.L. Galgon and W.D. Jemison Mobile antenna characterization and optimization for UHF satellite communications, *Journal of the Franklin Institute*, vol 336, no 1, January 1999

[19] K.S. Gilhousen, I.M. Jacobs, R. Padovani, A.J. Viterbi, L.A. Weaver and C.E. Wheatley III On the capacity of a cellular CDMA system, *IEEE transactions on vehicular technology*, Vol 40, no 2, May 1991

[20] J. Goldberg and H. Messer Inherent limitations in the localization of a coherently scattered source, *IEEE transactions on signal processing*, vol 46, no 2, December 1998

[21] J.S. Hammerschmidt and A.A. Hutter Spatio- temporal channel models for the mobile station: concept, parameters, and canonical implementation, *IEEE vehicular technology conference*, vol 3, 2000

[22] D.C. Hastings and H.M. Kwon Soft handoffs in code division multiple access systems with smart antenna arrays, *IEEE Vehicular Technology Conference*, vol 1, no 52, 2000

[23] N. Hew and N. Zein Space-time estimation techniques for UTRA systems, *IEE conference publication, 1st international conference on 3G communication technologies*, no 471, 2000

[24] H.R. Karimi and A. Manikas Manifold of a planar array and its effects on the accuray of direction finding systems, *IEE proceedings on Radar, sonar and navigation*, vol 143, no 6, December 1996

[25] S.M. Kay *Fundamentals of Statistical Signal Processing Volume 2 - Estimation Theory*, Prentice Hall PTR, 1998

[26] Y.S. Kim and Y.S. Kim Improved resolution capability via virtual expansion of array, *Electronics letters*, vol 35, no 19, 1999

[27] A. D. Kucar Mobile radio: an overview, *IEEE Communications Magazine*, vol 29, no 11, November 1991

[28] L. Landesa, F. Obelleiro and J.L. Rodriquez Practical improvement of array antennas in the presence of environmental objects using genetic algorithms, *Microwave and optical technology letters*, vol 23, no 5, 1999

[29] K.C. Lee Optimization of a finite dipole array with genetic algorithm including mutual coupling effects, *International journal of RF and microwave computer aided engineering*, vol 10, no 6, November 2000

[30] C.S. Lee Robust algorithm for passive angle tracking of multiple moving targets, *Proceedings of IEEE international conference on communication systems*, vol 3, 1994

[31] J.C. Liberti and T.S. Rappaport *Smart Antennas for Wireless Communications: IS-95 and Third Generation CDMA Applications*, Prentice Hall PTR, 1999

[32] T. Luo *Beamforming in the Uplink and Downlink Channels of a Cellular CDMA Communication System*, Master's thesis, Queen's University, 1998

[33] R.J. Mailloux and W.F. Brandow Array element failure correction for signals with wide angular distribution, *Proceedings of the IEEE Antennas and Propagation International Symposium*, vol 1, 1994

[34] A. Manikas and N. Fistas Modelling and estimation of mutual coupling between array elements, *ICASSP Proceedings*, vol 4, 1994

[35] A. Manikas, A. Sleiman and I. Dacos Manifold studies of nonlinear antenna array geometries, *IEEE transactions on signal processing*, vol 49, no 3, March 2001

[36] J.E. Miller and S.L. Miller DS-SS-CDMA uplink performance with imperfect power control and a base station antenna array, *Proceedings of the IEEE Vehicular Technology Conference*, vol 1, 1996

[37] H. Messer, Y. Rockah and P.M. Schultheiss Localization in the presence of coherent interference, *IEEE transaction on acoustics, speech and signal processing*, vol 38, no 2, December 1990

[38] A.N. Mirkin and L.H. Sibul Cramer-Rao bounds on angle estimation with a two-dimensional array, *IEEE transactions on signal processing*, vol 39, no 2, February 1991

[39] R. Nielsen Estimation of azimuth and elevation angles for a plane wave sine wave with a 3-D array, *IEEE transactions on Signal Processing*, November 1994

[40] A. Papoulis *Probability, Random Variables, and Stochastic Processes*, Third Edition, McGraw-Hill, 1991

[41] A. Paulraj, B. Ottersten, R. Roy, A. Swindlehurst, G. Xu and T. Kailath Subspace Methods for Direction of Arrival Estimatiion, *Handbook of Statistics*, Vol. 10, 1993

[42] R. Prasad, T. Ojanpera Survey on CDMA: Evolution towards wideband CDMA, *Proceedings of the 1998 IEEE 5th International Symposium on Spread Spectrum Techinques and Applications*, vol. 1, 1998

[43] R. Prasad, T. Ojanpera Overview of air interface multiple access for IMT-2000/UMTS, *IEEE Communications Magazine*, vol 36, no 9, Septermber 1998

[44] K.B. Preetham and G.R. Branner Design of low sidelobe circular ring arrays by element radius optimization, *Proceedings of 1999 IEEE international antennas and propagation symposium*, vol 3, 1999

[45] J.G. Proakis *Digital Communications-third ed*, McGraw-Hill, 1995

[46] G. Raleigh, S.N. Diggavi, A.F. Naguib and A. Paulraj Characterization of fast fading vector channels for multi-antenna communication systems, *Proceedings of the 28th Asilomar conference on signals, systems and computers*, vol 2, 1994

[47] T.S. Rappaport *Wireless Communications - principles and practice*, IEEE press, Prentice Hall, 1996

[48] L.L. Scharf *Statistical Signal Processing - Detection, Estimation, and Time Series Analysis*, Addison-Wesley, 1991

[49] S.V. Schell and W.A. Gardner High-Resolution Direction Finding, *Handbook of Statistics*, Vol. 10, 1993

[50] R.O. Schmidt *A Signal Subspace Approach to Multiple Emitter Location and Spectral Estimation*, PhD thesis, Stanford University, 1981

[51] C.E. Shannon A Mathematical Theory and Communication, *Bell System Technical Journal*, Vol 27, July, October 1948

[52] C.E. Shannon Communication in the Presence of Noise, *Proceedings of the IRE*, vol 37, January 1949

[53] W.Y. Shiu *Noniterative Digital Beamforming in CDMA Cellular Communication Systems*, Master's Thesis, Queen's University, 1998

[54] A. Sleiman and A. Manikas Antenna array manifold: a simplified representation, *Proceedings of ICASSP*, vol 5, 2000

[55] H. Steyskal and R.J. Mailloux Generalization of an array failure correction method, *IEE Proceedings on microwaves, antennas and propagation*, vol 145, no 4, August 1998

[56] H. Tsuji, H. Ogawa and M. Hirakawa Alternative high-speed wireless access system with mobile tracking technology, *Proceedings of Asia-Pacific microwave conference*, 2000

[57] B.D. Van Veen and K.M. Buckley Beamforming: A Versatile Approach to Spatial Filtering, *IEEE ASSP Magazine*, April 1988

[58] A.J. Viterbi *CDMA: Principles of Spread Spectrum Communication*, Addison Wesley, 1995

[59] E.J. Vertatschitsch and S. Haykin Impact of linear array geometry on direction of arrival estimation for a single source, *IEEE transactions on antennas and propagation*, vol 39, no 5, May 1991

[60] A. Wyglinski *Performance of CDMA systems using digital beamforming with mutual coupling and scattering effects*, Master's thesis, Queen's University, 2000

Vita

Joseph Yi-Lin Chou

EDUCATION

M.Sc.	Electrical and Computer Engineering, Queen's University	1996–2002
B.Sc(Eng).	Engineering Physics (Elec), University of British Columbia	1991–1996

EXPERIENCE

Research Assistant (1996–2000),
Image Processing and Communications Laboratory, Queen's University

Teaching Assistant (1996–1998),
Electrical and Computer Engineering, Queen's University

Defence Research Assistant (summer 1996),
Defence Research Establishment Ottawa